Bimetallic Catalysts for Multi-Step Reactions

A thesis submitted in partial fulfillment of the requirements for the degree of Masters of Research

By

Joshua Tompsett

Department of Molecular Sciences

Macquarie University

Supervisors: Prof. Barbara Messerle and Dr. Roy McBurney

9th October 2017

Declaration of Originality

I, Joshua Tompsett, declare that this work contains no material which has been accepted for the award of any other degree or diploma in any university or other tertiary institution and, to the best of my knowledge, contains no material previously published or written by another person, except where due reference has been made in the text.

Acknowledgments

This year in the MRes program has been challenging beyond anything I have experienced previously, yet I have learnt more this year about research, chemistry and myself than I ever could have predicted. In completing this thesis, I have achieved what, at many times through the year, I believed I could not achieve. This is due in no small part to the overwhelming support of a number of people, the following of whom I would like to thank.

First and foremost, I would like to thank my excellent supervisors, Prof. Barbara Messerle and Dr. Roy McBurney for your support and dedication in guiding me towards my goals in this research project. Obviously, without everything you have taught me this year, and especially without your patience and belief in me, none of this would have been possible.

Thank you to our post-doctoral researcher Dr. Indrek Pernik and former post-doctoral researcher Dr. Mark Gatus. Your indispensable knowledge and advice made understanding all of the chemistry and NMR results possible. Thank you especially to Mark for having done a lot of the previous work that this project is built upon.

I would also like to thank the staff at Macquarie University, in particular, Dr. Erika Davies for her excellent guidance in all things NMR, and Dr. Louise Brown and A/Prof. Bridget Mabbutt for doing their best to ensure that the MRes program was a successful and enjoyable experience.

To the past and present members of the BAM group: Matt, Ralph, Shelly, Danfeng, Masahiro, Ashwin, Sam, and our adopted group member Marco, for the great fun we have in the lab and outside the lab, you've made this year that much more enjoyable. A big thank you also goes to Matt for running mass spectroscopy samples for me, helping me attempt to grow crystals, and putting up with my never-ending torrent of questions and requests for guidance in the lab.

Lastly, I would like to thank my friends and family for their support and understanding throughout the year. My parents especially for everything they do for me, and my three best friends Stephen, Donny, and Steve for keeping me sane, if not providing a major source of distraction, though I can't complain. I would not have made it through any of this without you all, so for that I am eternally grateful.

Josh Tompsett

October 2017

List of Abbreviations

$[BAr^F{}_4]^-$	*tetrakis*[3,5-bis(trifluoromethyl)phenyl]borate anion
Bn	benzyl
$[BPh_4]^-$	*tetra*phenylborate anion
bpm	*bis*(1-pyrazolyl)methane
br	broad (NMR)
Bu	Butyl
cat.	Catalyst
COD	1,5-cyclooctadiene
Conv.	Conversion
COSY	Correlation Spectroscopy
δ	chemical shift (ppm)
d	deutero
DCM	Dichloromethane
D	Deuterium
equiv.	Equivalent
ESI-MS	Electrospray Ionisation Mass Spectrometry
FTIR	Fourier Transform Infrared
h	hour(s)
HMBC	Heteronuclear Multiple Bond Correlation
HSQC	Heteronuclear Single Quantum Coherence
Hz	Hertz
i	ipso (NMR)
i-Bu	*iso*-Butyl
IR	Infrared
J	scalar coupling constant (NMR)
L	Ligand
LC	Liquid Chromatography
m	multiplet (NMR)
m	Meta
m/z	mass to charge ratio
Me	Methyl
MeOH	Methanol
Mesityl	1,3,5-trimethylphenyl
mim	(1-methylimidazolyl)imine
mmol	Millimoles
mol	Moles
n-Bu	*n*-Butyl
Na_2[EDTA]	Disodium ethylenediaminotetraacetic acid
NHC	*N*-Heterocyclic Carbene
NMR	Nuclear Magnetic Spectroscopy
nOe	nuclear Overhauser effect (NMR)
NOESY	Nuclear Overhauser Effect Spectroscopy
v(CO)	Carbon monoxide IR stretching frequency
o	Ortho
o.n.	Overnight
p	Para
Ph	Phenyl
ppm	parts per million
q	quartet (NMR)

r.t.	room temperature
s	singlet (NMR) or strong (FTIR)
t	triplet (NMR)
t-Bu	*tert*-Butyl
TCE-d_2	Deuterated 1,1,2,2,-tetrachloroethane
TOF	Turnover Frequency
Tol	Toluene
^{t}Xan	2,7-Di-*tert*-butyl-9,9-dimethyl-9H-xanthene

Table of Contents

List of Figures

List of Schemes

List of Tables

Abstract

The synthesis of pro-ligands containing pairs of *N*-heterocyclic carbene (NHC) substituents on organic scaffolds was explored. These ligands were used to develop homobimetallic Ir(I) complexes containing 1,8-cyclooctadiene (COD) and carbonyl co-ligands. The catalytic activity of a bimetallic complex was investigated and compared against related monometallic complexes to determine the extent of bimetallic cooperativity present.

A novel ligand, 1,1'-(2,7-di-*tert*-butyl-9,9-dimethyl-9H-xanthene-4,5-diyl)bis(3-methyl-1H-imidazol-3-ium) iodide, was synthesised by an Ullman coupling reaction of imidazole onto a 4,5-dibromo-2,7-bis(1,1-dimethylethyl)-9,9-dimethylxanthene scaffold. A subsequent methylation with iodomethane generated the bis-imidazolium salt. A novel bimetallic Ir(I) catalyst containing this ligand was synthesised *via* deprotonation using potassium carbonate and complexation with $[Ir(COD)Cl]_2$, followed by a carbonylation of both metal centres using carbon monoxide.

The catalytic activity of these bimetallic systems was explored in the following multi-step alkyne activation reactions and compared to the reactivity of two analogous monometallic Ir(I) catalysts: (i) the hydroamination of alkynyl amines; and (ii) the tandem dihydroalkoxylation of alkyne diols to form spiroketals. For all catalytic transformations, the bimetallic complex was found to be an efficient catalyst with excellent turnover frequencies. Bimetallic cooperative enhancement was observed in the catalytic activity of the bimetallic Ir(I) catalyst in comparison to the activity of one of the analogous monometallic Ir(I) catalysts.

Chapter 1 : Introduction

1.1. Catalysis

Catalysis is a vital technology for the major chemical industries that are relied upon in today's society. Catalysis was first described by Ostwald in 1894 as the addition of a substance to a chemical reaction that would increase the rate of the reaction without consuming the added substance.[1] This added substance is known as a catalyst. A catalyst is able to speed up the rate of a reaction by providing an alternate energetic pathway that bypasses the rate-determining step of the uncatalysed mechanism, thus lowering the activation energy for the reaction.[2] Although a catalyst will undergo transformations during catalysis, it will be regenerated by the end of the catalytic cycle, allowing it to be used in substoichiometric quantities. Catalysis not only speeds up the rate of a reaction, but may also initiate a reaction where one may not have occurred at all without a catalyst. Catalysts can also introduce selectivity for a single product in a reaction where two or more products may be formed. This is particularly useful in the synthesis of biologically active molecules that are chiral, using optically active catalysts to achieve enantioselectivity.[3]

The major goals for researchers is to design and develop new and better catalysts that promote the reduction of waste, improved atom economy, more efficient use of resources, and a reduction in energy usage. The challenges for this are in tailoring catalysts for specific reactions with excellent selectivity and the ability to catalyse tandem processes, thus simplifying the synthetic process. Catalysts are generally described as either homogeneous or heterogeneous, that is, either operating in the same phase as the substrate(s) or in a different phase to the substrate(s) respectively. Whilst heterogeneous catalysis has been employed more extensively in industry to date, there have been many advancements in the field of homogeneous catalyst design that have led to the increased use of homogeneous catalysis in industry.

1.2. Organometallic Complexes as Catalysts

Organometallic complexes are a class of compound that are commonly used as homogeneous catalysts for a large variety of organic synthetic reactions.[4,5] Organometallic complexes are defined as having at least one carbon of an organic ligand bound directly to a metal atom, or alternatively, having at least one largely covalent bond between a metal atom and an element in an organic ligand.[6,7] A metal atom may also be bound to a heteroatom (such as nitrogen, phosphorous or oxygen) of a ligand *via* a coordination bond. However, compounds of this type are known as coordination compounds, not organometallic compounds despite containing both organic ligands and metal nuclei. Examples of these coordination compounds are porphyrin containing compounds such as myoglobin,

haemoglobin and chlorophyll.[5,7] For the purpose of this review, we will not discuss coordination compounds further, and will focus solely on organometallic complexes.

The first organometallic complex to be synthesised was Zeise's salt in 1827, a platinum complex with an ethylene co-ligand, $K[PtCl_3(\eta^2\text{-}C_2H_4)]$. A landmark discovery was that of the Grignard reagent, for which François Grignard won the Nobel Prize in 1912. It is still used today as an important reagent for the alkylation of carbonyls.[8,9] Organometallic complexes have since received a lot of attention and many compounds containing various types of ligands and metal centres have been synthesised and put to use as catalysts. Organometallic complexes are promising as catalysts due to the ability of their electronic and steric properties to be "tuned" by making changes to either the ligand or the metal centre of the complex.[10] As homogeneous catalysts they are particularly useful because the reaction mechanism is easily studied using non-invasive spectroscopic techniques such as nuclear magnetic resonance (NMR) spectroscopy, infrared (IR) spectroscopy, and ultraviolet/visible (UV/Vis) spectroscopy. Both the intermediates of the reaction being catalysed and the catalyst itself can be characterised using these techniques which leads to a much deeper understanding of how the catalyst works, and consequently the design of cheaper, more efficient and selective catalysts.[3,11]

Homogeneous organometallic catalysts are used in a vast array of industrial processes and reactions. The most notable are reactions such as the Ziegler-Natta catalysis for polymer production, the Wacker oxidation of alkenes to aldehydes (Scheme 1.1), the Cativa process and Monsanto process for the production of acetic acid using iridium or rhodium catalysts (Scheme 1.1), and hydroformylation in the plasticiser, fragrances and pharmaceutical industries.[5,12] Organometallic catalysts are also used in industrial organic transformations such as olefin metathesis,[5,13-16] hydrogenation,[5,17] hydroamination,[18-20] and hydrosilylation.[5,21] Despite this widespread use, much work is still needed to develop efficient organometallic catalysts for industrial processes that can introduce better selectivity, reduce energy cost and also facilitate the replacement of dangerous reactants for safer and greener alternatives.

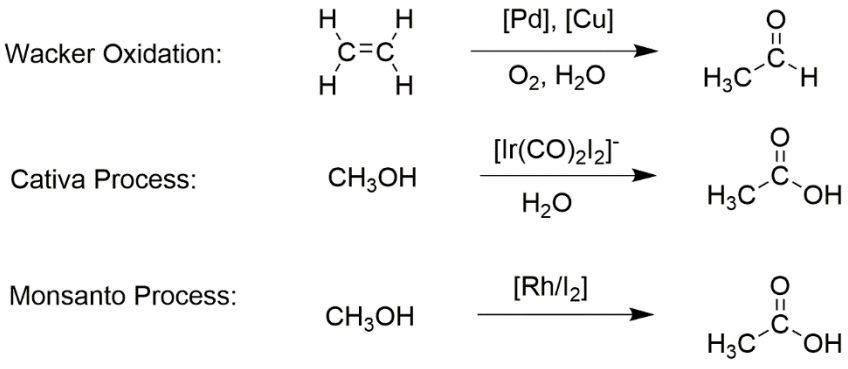

Scheme 1.1: Industrial processes using homogeneous organometallic catalysts.

Homogeneous catalysis is of particular interest in the pharmaceutical industry for the synthesis of asymmetric, biologically-active compounds.[22] The synthesis of chiral and optically active organometallic complexes for homogeneous catalysis is a growing area of research as these catalysts have the potential to provide a high level of enantioselectivity. Examples of asymmetrical catalysis in industry include the synthesis of Metolachlor using an iridium catalysed hydrogenation and a rhodium catalysed transfer hydrogenation in the synthesis of (-)-menthol (Scheme 1.2).[23,24]

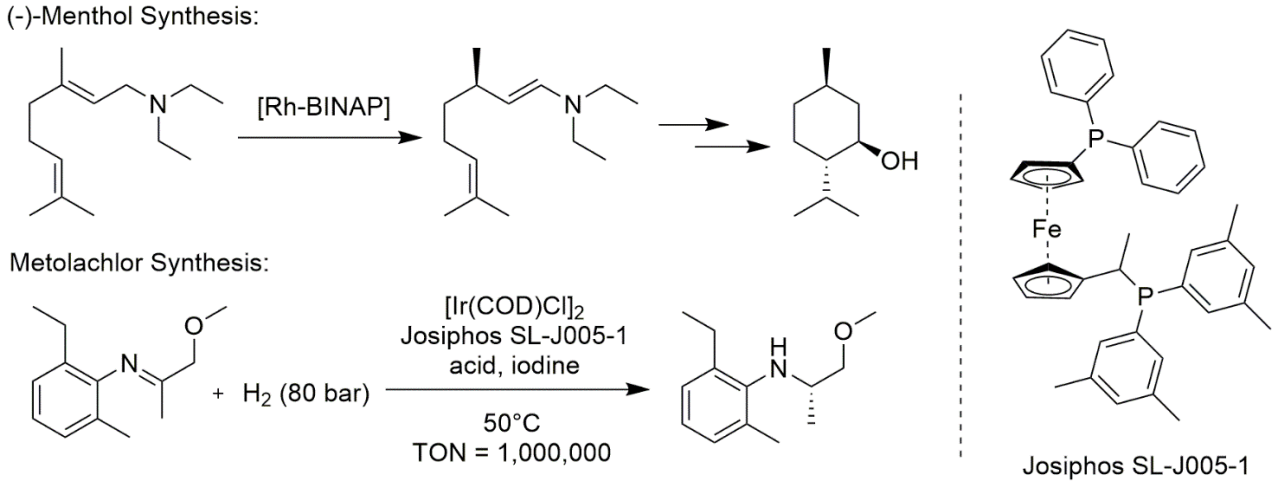

Scheme 1.2: Synthesis of (-)-Menthol and Metolachlor.

Biologically active molecules often contain C-X bonds where X is a heteroatom (usually nitrogen or oxygen). Therefore, there is a growing interest in the development of efficient organometallic catalysts for C-X bond forming reactions. The goal is to significantly reduce the number of synthesis and purification steps that are necessary for the synthesis of biologically active molecules by performing catalysed multi-step reactions in a one-pot synthesis.[25,26] Not only should this reduce the length of the synthesis of these molecules, it will improve the overall atom economy and, with careful design of the catalyst, selectivity as well.

1.3. Organometallic Catalyst Design

1.3.1. Monometallic Catalysts

Traditionally, using monometallic catalysts, the ability to "tune" reactivity of the catalyst was restricted to varying one of two parameters within the catalyst, either the metal or the ligand(s).[3] The identity of the metal atom could be changed, thus changing the type of reaction that the catalyst may be successfully employed in. For example, complexes containing ruthenium are known to be useful for hydrogenation reactions of esters and ketones, whereas iridium complexes may be used to catalyse the alkylation of amines using an alcohol.[27] The electronic and steric properties of the catalyst can be "tuned" by modification of the ligand. Changes to the ligand will affect the ability of the catalyst to

perform certain functions within the reaction, such as activation of the substrate, adoption of the necessary coordination geometries for the reaction, and the release of the product from the active site upon completion of the reaction.[28] Changes to the ligand are also generally determinate of the selectivity in the reaction being catalysed, as in the case of a complex containing a chiral ligand being used to catalyse the formation of a specific enantiomer.[3,23,24]

1.3.2. Bimetallic Catalysts

An area of intense growing interest is the use of two metal centres held in close proximity to one another in a single catalyst, known as a bimetallic catalyst. The use of a bimetallic catalyst introduces additional parameters that can be used to optimise the efficiency of the catalyst.[3] There are three main types of connection between the pairs of metals in a bimetallic complex. The two metals may be bound directly to one another through a covalent bond (Figure 1.1a), the two metals may be connected by bridging donor atoms (e.g. halides, Figure 1.1b), or the metals may both be bound to two separate ligand functional groups on a scaffold (Figure 1.1c). In this project, we will focus on bimetallic complexes with metals connected *via* a bridging scaffold ligand. Bimetallic catalysts containing bridging scaffold ligands can be "tuned" by varying the rigidity of the ligand, the intermetallic distance between the two metal centres, and the spatial and geometric orientations of the metal centres relative to one another.

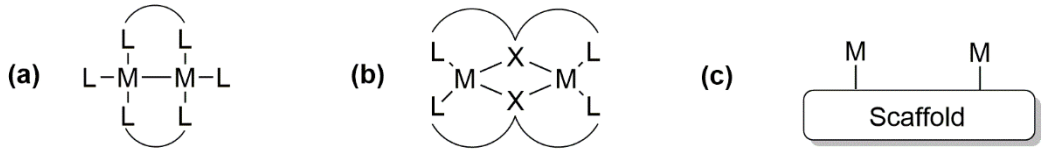

Figure 1.1: Different types of bimetallic systems where M = metal, L = ligand, and X = bridging donors. **(a)** Metals bonded directly through covalent bond. **(b)** Metals connected *via* bridging donor atoms. **(c)** Metals connected *via* a bridging scaffold ligand.

A bimetallic complex can be homobimetallic (containing two atoms of the same metal) or heterobimetallic (containing two different metals).[3] A compatible pairing of metal centres can result in stabilisation of reaction intermediates through binding of the substrate to both metal atoms simultaneously, stabilisation of the geometry of electronics of one metal ion by the second metal ion, or binding of two different substrates to the two metal centres at the same time in close proximity to facilitate catalysis (Figure 1.2).[29]

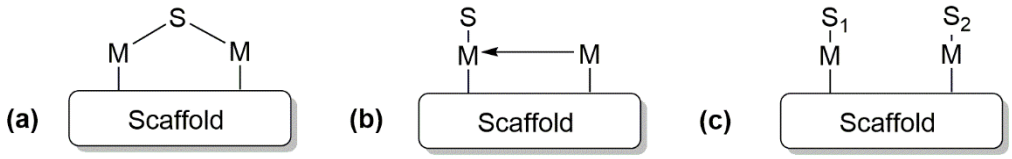

Figure 1.2: Possible substrate-metal intermediates with bimetallic complexes where M = metal and S = substrate. **(a)** Simultaneous binding of one substrate. **(b)** Electronic stabilisation. **(c)** Simultaneous binding of two different substrates.

1.3.3. Group 9 Metals – Rhodium and Iridium

Rhodium and iridium have been widely researched as metal centres for organometallic catalysts, ever since the development of Wilkinson's catalyst, $RhCl(PPh_3)_3$, for use in the hydrogenation of alkenes and alkynes.[30] Complexes of iridium and rhodium are now used extensively in industrial reactions such as the Cativa and Monsanto processes for the production of acetic acid (Scheme 1.1),[5] and in the manufacture of chiral compounds such as (-)-menthol and metolachlor (Scheme 1.3).[23,24] Late transition metals such as iridium and rhodium also exhibit far less oxophilicity than early transition metals, which makes complexes of these metals more stable in the presence of air or moisture.[28,31] Complexes of rhodium and iridium can demonstrate square planar, tetrahedral, square pyramidal, trigonal bipyramidal, or octahedral coordinate geometries based on the oxidation state of the metal centres. In the +1 oxidation state, both rhodium and iridium metal centres are extremely conducive to substrate binding due to them being coordinatively unsaturated. Thus, the multiple oxidation states rhodium and iridium may adopt are readily accessible, making complexes of the two metals excellent catalysts for C-X bond formation reactions involving oxidative addition and reductive elimination mechanisms.[32]

1.4. Cooperativity in Bimetallic Complexes

When compared to an analogous monometallic catalyst, bimetallic systems have been shown on many occasions to exhibit large enhancements in both efficiency and selectivity in catalysis. These enhancements in catalytic efficiency that have been observed in bimetallic systems are larger than the sum of two equivalents of the analogous monometallic system, and on some occasions, are seen to be orders of magnitude larger.[3,29,33-35] The general consensus is that these enhancements are due to a phenomenon known as "bimetallic cooperativity". There has been growing interest in the use of bimetallic catalysts since the seminal report by Stanley in 1993, where the authors demonstrated a significant enhancement over a commercially available monometallic rhodium complex $[Rh(acac)(CO)_2]$ in the hydroformylation of 1-hexene using a homobimetallic rhodium complex (Scheme 1.3).[36]

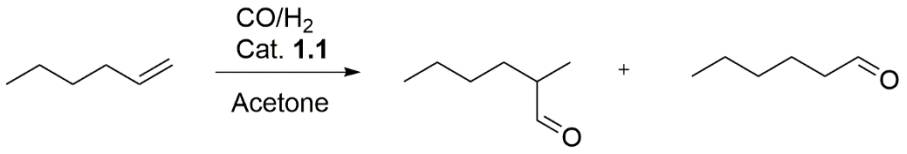

Scheme 1.3: Hydroformylation of 1-hexene to form aldehydes.

Stanley and colleagues designed and synthesised dirhodium complexes with phosphine ligand scaffolds that exhibited no metal-metal bonding between the rhodium atoms in the complex (Figure 1.3, e.g. **1.1**). The purpose of designing bimetallic catalysts that employed a bridging scaffold without any Rh-Rh bonding was to allow the synthesis of monometallic catalysts that were structurally analogous to "half" of the corresponding bimetallic complex. They found that the monometallic complexes achieved a maximum of 2% conversion of alkene to aldehyde with poor selectivity between the branched and linear isomers, whereas the bimetallic catalyst **1.1** showed excellent conversion and product selectivity, even surpassing the commercially employed monometallic catalyst by 40% in catalytic efficiency.[36]

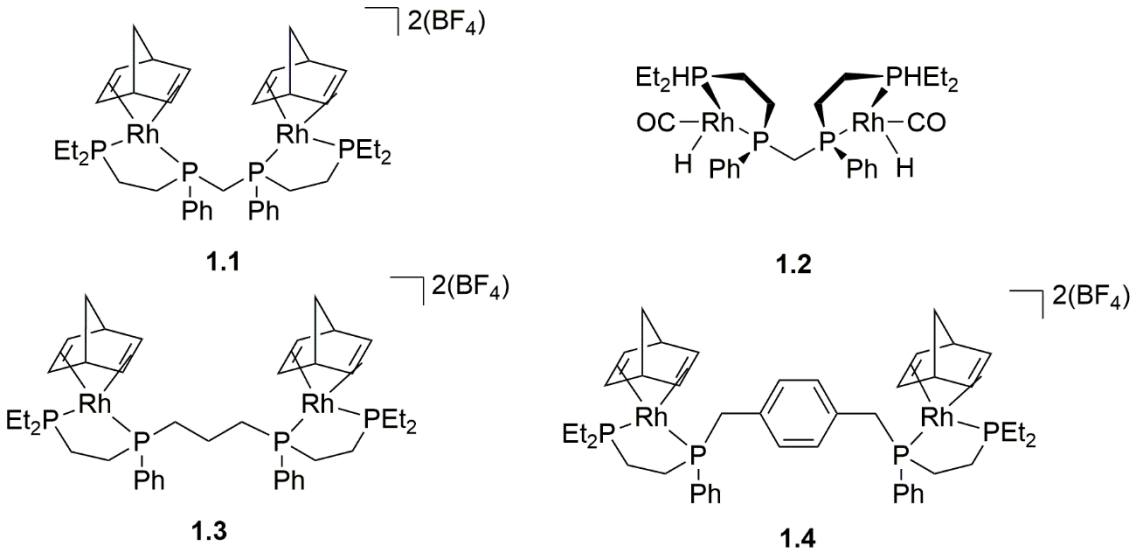

Figure 1.3: Homobimetallic rhodium catalyst **1.1**, the activated catalyst upon addition of CO/H_2 **1.2**, catalyst with increased intermetallic distance **1.3**, and catalysts with increased intermetallic distance and rigidity of the linker **1.4.**

Stanley and colleagues also hypothesised that the close proximity of the two metal centres was key to the cooperativity effect. They investigated this by synthesising two new catalysts that had a larger distance between the two metal centres than catalyst **1.1**, one with flexibility in the bridging scaffold, **1.3**, and one without flexibility **1.4** (Figure 1.3). The two bimetallic complexes with larger distances between the metals exhibited similarly poor catalytic conversion and selectivity,

comparable to the monometallic complexes. This provided evidence that the intermetallic distance is important in the cooperativity between two metals in a bimetallic catalyst.

1.4.1. Intermetallic Distance and Spatial Orientation

In many cases, a closer proximity between metal centres has been observed to increase the efficiency and selectivity of bimetallic complexes as catalysts, due to the two metals ability to cooperate in the catalysis, as was seen in the Stanley example in the previous section.[29,34,36] Feringa and colleagues proposed that there is an ideal distance between two metal centres for cooperative enhancement in a bimetallic catalyst, between 3.5 – 6 Å.[29] This observation was made in 1998 after a review of the most efficient enzymatic and synthetic catalysis utilising bimetallic complexes of late transition metals.

Marks and co-workers observed that when bimetallic zirconium catalysts featuring constrained geometries were used for olefin polymerisation reactions, there was a lack of selectivity for higher molecular weight polymers and attempted to determine whether intermetallic distance was a factor in this.[37,38] Marks and colleagues synthesised zirconium bimetallic "constrained geometry catalysts" (CGCs) which they used in ethylene homopolymerisation and ethylene/1-hexene copolymerisation reactions (Figure 1.4). The selectivity of the bimetallic catalyst with the smaller intermetallic distance **1.7a** showed significant enhancement in selectivity for higher molecular weight polymers than both the bimetallic with a larger intermetallic distance **1.6a** (≈ 70 times greater) and the related monometallic "half-unit" CGC **1.5a** (≈ 130 times greater). In the catalysis of the ethylene/1-hexene copolymerisation, catalyst **1.7** showed an approximately 40 times enhancement in selectivity for higher molecular weight and a 3 times greater enhancement in selectivity for the α-olefin enchainment than the monometallic.[37]

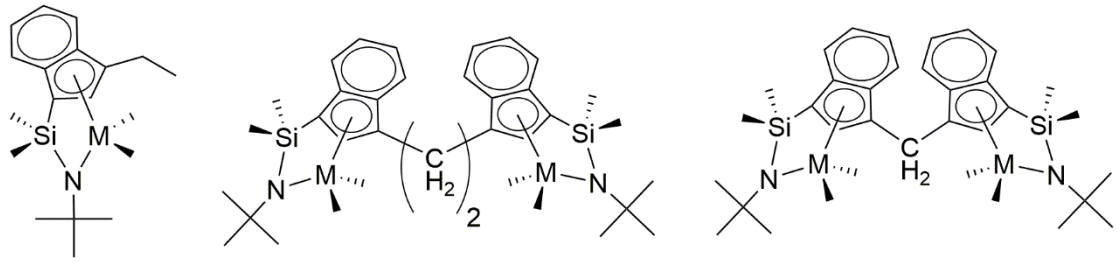

1.5a, M = Zr
1.5b, M = Ti

1.6a, M = Zr
1.6b, M = Ti

1.7a, M = Zr
1.7b, M = Ti

Figure 1.4: Bimetallic CGCs of zirconium and titanium with methylene **1.7** and ethylene **1.6** linkers and their corresponding monometallic "half-unit" **1.5**.

The crystal structure of the bimetallic **1.7a** revealed that the metal centres were located on the same side of the methylene linker of the indenyl ligand and that the energy barrier for the rotation

around the bonds of that linker were large, indicating that the energetically favoured structural conformation held the metals in well defined, close proximity.[38]

Guilard demonstrated how the metal-metal proximity and orientation in cofacial copper biscorroles could be tightly controlled by changes in the bridging scaffold ligand (Figure 1.5).[39] The authors used various bridging scaffold ligands such as anthracene, dibenzothiophene, dibenzofuran, biphenylenyl, and 9,9-dimethylxanthene, as well as a phenyl substituent on the monometallic analogue. Guilard and colleagues also showed that porphyrin-corrole dyads and bisporphyrins could be constructed with the same bridging scaffold motifs and coordinated to various metals such as cobalt, iron, manganese and nickel to form a library of homobimetallic and heterobimetallic complexes with controlled intermetallic distances.[39-41]

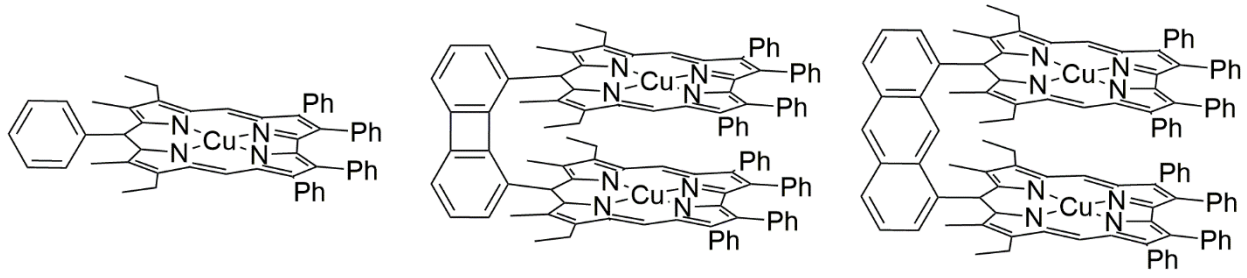

Figure 1.5: Homobimetallic copper biscorrole complex on an anthracene (right) and a biphenylenyl (middle) scaffold, and the related monometallic "half-unit" (left).

The cooperativity between the two metals in the biscorrole complexes of Guilard and colleagues was investigated using cyclic voltammetry as the ligands containing anthracene and biphenylenyl, for example, were conjugated and thus allowed for direct electronic communication between metals. They found that the bimetallic complexes exhibited two separate reversible steps in the reduction process compared to one reversible step in the monometallic species. The same was observed within the oxidation process. They also noted that the potentials of the first irreversible oxidation process in the bimetallic complexes were higher than the potential of that in the monometallic complex. This was evidence that the bimetallic complexes may exhibit greater stability as catalysts in reduction processes. Guilard and colleagues then demonstrated this in the reduction of molecular oxygen to water using biscobalt complexes as electrocatalysts.[42] They found that the biscobalt porphyrin-corrole dyad, which has mixed oxidation states of cobalt(III) and cobalt(IV), exhibited the greatest selectivity for the production of water over hydrogen peroxide.

1.4.2. Cooperative Enhancement in Multi-Step Reactions

In the synthesis of industrially important organic molecules, often those containing heterocycles, many of the known synthetic routes contain multiple steps. Many of these multi-step

syntheses require the isolation of intermediates, delayed addition of reagents, changing of reaction conditions, and work-up procedures that result in the process being atomically uneconomical, energy inefficient and laborious for the chemist(s) responsible. Therefore, the application of organometallic catalysts in these processes, with the intention of promoting multiple organic transformations to occur sequentially in the "one-pot", is of great importance. The application of metal-catalysed, multi-step, "one-pot" syntheses (often called tandem or sequential reactions) results in the reduction of reagent use, solvent use, waste generation, and labour.[43]

When considering the application of bimetallic catalysts to these reactions, the benefit is two-fold. In addition to modes of cooperativity described in section 3.2 (Figure 1.2) for bimetallic complexes as catalysts, there are two more possible modes for cooperativity in a bimetallic catalyst for a tandem reaction. In a two-step reaction, one metal of the bimetallic catalysts may catalyse the first transformation of the reactant to the intermediate which is then rapidly transferred to the second metal on the same catalyst molecule to be transformed into the product (Figure 1.6a). In either a homobimetallic or a heterobimetallic catalyst, both metals may be able to catalyse either of the two steps in the reaction, or one metal centre may specifically promote the formation of the intermediate from the reactant and the other metal centre may then catalyse the transformation of that intermediate to the product. The second additional mode of cooperativity in bimetallic catalysts for multi-step reactions involves the stabilisation of an intermediate through coordination to both metals of the bimetallic catalyst, where stabilisation using a monometallic either would not occur or would be far less effective (Figure 1.6b).

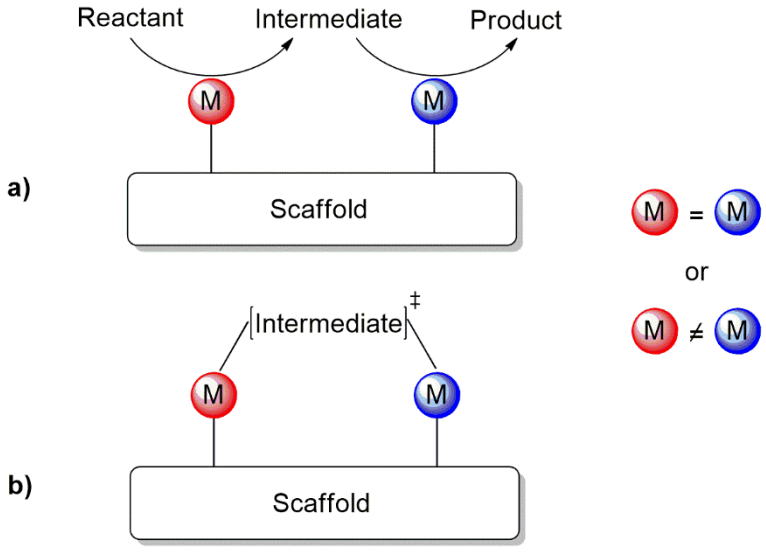

Figure 1.6: a) Mode of cooperativity in either a homobimetallic or heterobimetallic catalyst for a two-step "one-pot" reaction. **b)** Stabilisation of reactive intermediate through coordination to both metals of the bimetallic catalyst. M = metal.

It has been demonstrated that the use of two separate catalysts together in a "one-pot" synthesis is a useful endeavour as it can allow multiple steps in the reaction to proceed sequentially as each of the catalysts promote a specific transformation in the sequence. Chung and colleagues provide a good example of this in the synthesis of fenestranes from enynes and alkyne diesters.[44] Traditional synthetic methods of fenestranes involve multiple steps that have frequently been reported as having difficult separations. One of these methods is a three-step synthesis involving a Pauson-Khand reaction, followed by an allylic alkylation, followed by another Pauson-Khand reaction. The Pauson-Khand reactions are cobalt catalysed whereas the alkylation reaction is palladium catalysed. After some catalyst screening, Chung and colleagues were able to perform this synthesis in a "one-pot" procedure using a mixture of cobalt and palladium catalysts with decent yields of the fenestrane products.

Even though the use of mixtures of homometallic catalysts has been demonstrated to catalyse "one-pot" tandem reactions, this does not benefit from the modes of cooperativity that arise in bimetallic catalysts due to the metals being held in close proximity to one another within the same molecule (Figure 1.6). The enhancements that are gained from the inclusion of two separate monometallic catalysts is generally the sum of the two counterparts. The use of bimetallic complexes as catalysts can result in enhancements far greater than the sum of the contributions from two analogous monometallic catalysts due to the synergistic effects of cooperativity between the metals.

Peris demonstrated in three novel tandem processes that the use of heterobimetallic complexes of iridium and palladium as catalysts could achieve conversions far greater than a mixture of homobimetallic iridium and palladium catalysts could achieve.[45] The tandem reactions investigated were a dehalogenation/transfer hydrogenation of haloacetophenones (Scheme 1.4), a Suzuki coupling/transfer hydrogenation of *p*-bromoacetophenone, and a Suzuki coupling/α-alkylation of *p*-bromoacetophenone.

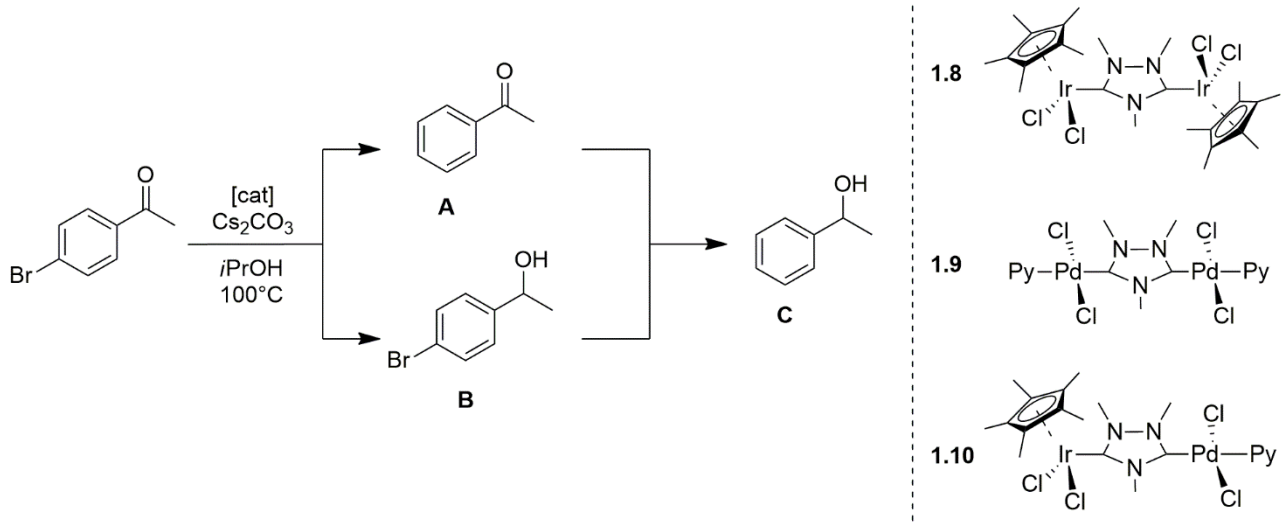

Scheme 1.4: Tandem dehalogenation/transfer hydrogenation of haloacetophenones using a homobimetallic iridium complex **1.8**, a homobimetallic palladium complex **1.9**, and a heterobimetallic iridium/palladium complex **1.10**.

Another example of a tandem catalytic process that is enhanced by the use of bimetallic catalysts is given by Messerle and colleagues in a dihydroalkoxylation of alkyne diols using rhodium and iridium complexes containing bis(pyrazolyl)methane (bpm) ligand substituents on various ligand scaffolds (Scheme 1.5).[46,47] The authors found that all of the homobimetallic species **1.12**, **1.13**, and **1.14** displayed enhanced turnover frequencies (TOF) in comparison to the corresponding monometallic species **1.11** to varying degrees. The degree of enhancement on the monometallic analogue increased with decreasing intermetallic distance and obstruction of the space between the metals. The greatest enhancement was observed in the rhodium bimetallic catalyst on the anthracene scaffold **1.14** which was approximately 34 times more efficient than the monometallic rhodium catalyst.[46] It was concluded that this is another example of spatially-dependent cooperativity between the two metals of a bimetallic catalyst.

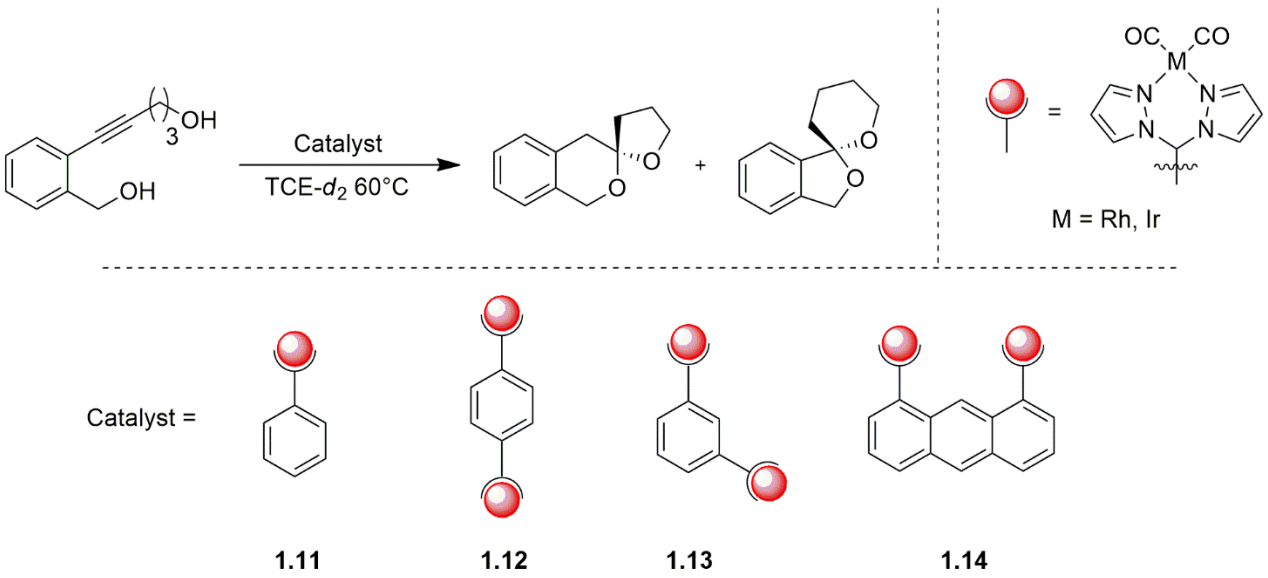

Scheme 1.5: Dihydroalkoxylation of alkyne diol to form spiroketals using mono- and homobimetallic rhodium and iridium catalysts.

Messerle and co-workers modelled the structural conformations of the rhodium catalysts in Scheme 1.5 as well as some with different ligand scaffolds such as 9,9-dimethylxanthene and dibenzofuran using density functional theory (DFT) calculations.[34] The purpose was to draw strong correlations between the catalytic enhancement and the intermetallic distance. However, this could not be achieved because of the free rotation around the bpm-arene bonds that allowed the catalysts to adopt a range of conformations with varying intermetallic distance.

To address the issue of poorly defined intermetallic distances due to flexible ligand structures, Messerle and colleagues developed a new set of catalysts that employed imidazolyl-imine (mim) ligand substituents on a benzene scaffold and also with an ethylene linker to assess the role that rigidity plays in catalytic enhancement (Scheme 1.6).[48] It was found that the *ortho* substituted bimetallic catalyst **1.17** demonstrated turnover frequencies between 500 to 1000 times greater than the bimetallic catalyst with greater intermetallic distance **1.16**, and the bimetallic catalyst with flexibility in the ligand scaffold **1.18**. Most significantly however, was that the reaction performed with catalyst **1.17** achieved an enhancement in turnover frequency that was 6800 times greater than the corresponding monometallic catalyst **1.15**.

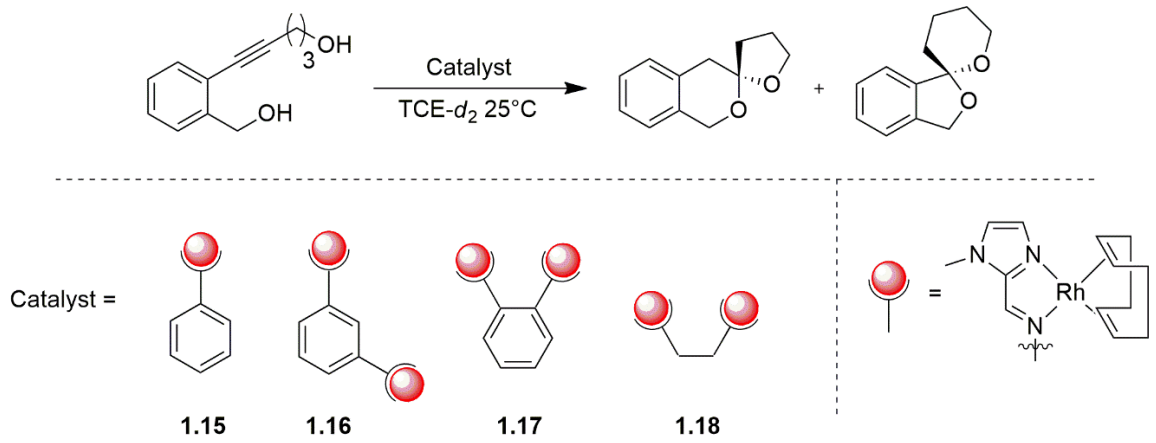

Scheme 1.6: Dihydroalkoxylation using rhodium catalysts that feature imidazolyl-imine ligand substituents.

This is a very significant enhancement; however, it is worth noting that catalyst **1.15** was not an overly efficient catalyst. Therefore, the possibility of achieving such a significant enhancement on an efficient monometallic catalyst is a very exciting prospect, and is a goal of this project.

1.5. Objectives

Unpublished work from the Messerle group has demonstrated that monometallic Ir(I) catalysts featuring a *N*-heterocyclic carbene (NHC) ligand with benzene and mesitylene substituents (**3.1** and **3.2**) are excellent catalysts for the two target multi-step reactions of this project.[49] The goal here is to develop an analogous bimetallic complex on 9,9-dimethylxanthene **3.4** that enables cooperative enhancement with structurally flat monodentate NHC ligands (Figure 1.7). The efficiency of these bimetallic complexes as catalysts will be compared with the analogous monometallic catalysts **3.1** and **3.2** to assess enhancement of an already efficient catalytic system due to cooperative effects whilst simultaneously developing excellent catalysts for important C-X bond forming tandem processes.

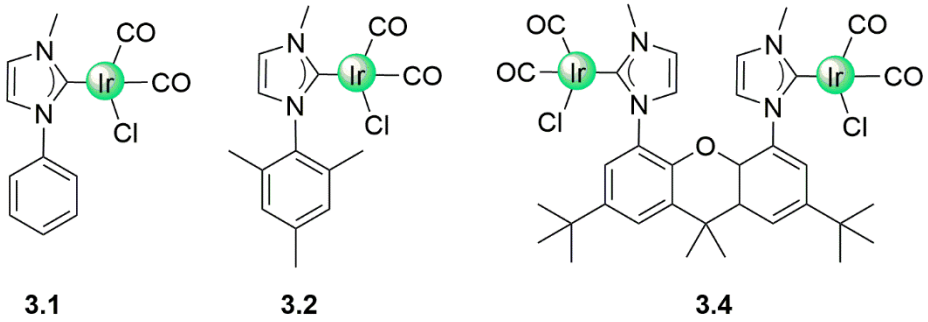

Figure 1.7: Target bimetallic catalyst of this project **3.4** and its monometallic analogues **3.1** and **3.2**.

In this project, the type of target catalytic transformations are as follows: two-step intramolecular dihydroalkoxylation of alkyne diols to form spiroketals, and the hydroamination of alkynyl amines (Scheme 1.7). In both cases, C-X bonds are formed through alkyne activation.

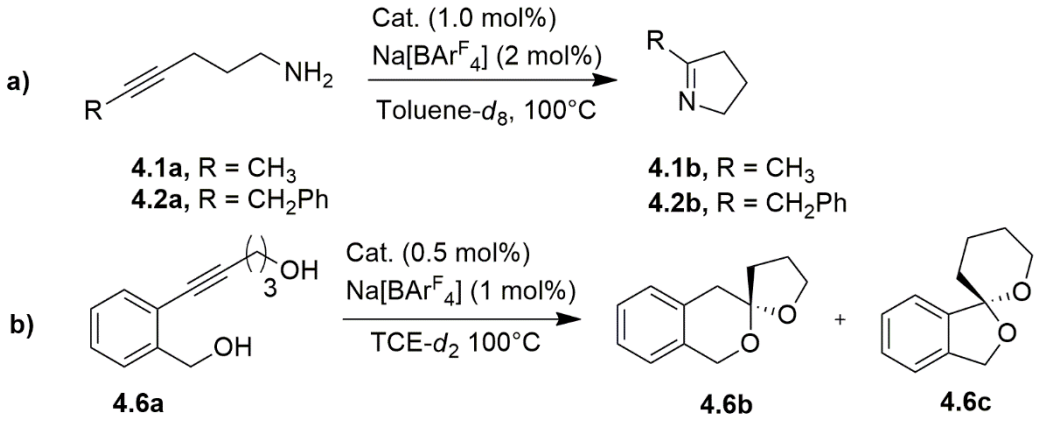

Scheme 1.7: Examples of C-X bond-forming alkyne activation reactions; **a)** intramolecular hydroamination of alkynyl amines to form cyclic imines, **b)** tandem dihydroalkoxylation of alkyne diols to form spiroketals.

(a) Hydroamination of alkynyl amines. The hydroamination reaction of an alkyne with an amine results in C-N bond formation which is useful for the synthesis of imines, enamines and *N*-heterocycles. These are functional groups that are frequently present in bulk chemicals and pharmaceuticals.[50]

(b) Dihydroalkoxylation of alkyne diols. The intramolecular dihydroalkoxylation is a one-pot, multi-step synthesis of spiroketals. Spiroketals are natural products that are used in pharmaceuticals such as anti-inflammatories and cancer-cell inhibitors.[51,52]

Chapter 2 : Ligand Synthesis

2.1. Introduction

This chapter describes the design, synthesis and characterisation of ligands containing two *N*-heterocyclic carbene (NHC) ligand substituents on a xanthene scaffold, for the purpose of generating a bimetallic iridium(I) catalyst. The aim of this work was to synthesise a highly active catalyst based on bimetallic cooperativity. In particular, a ligand providing the possibility of bringing two metals close together was required.

Xanthene was chosen as a suitable scaffold due to its planarity and geometry in combination with two NHC ligand substituents that should allow for favourable alignment of the two metal centres in a bimetallic complex of such a ligand. The *tert*-butyl groups on the scaffold were included for enhanced solubility of the pro-ligand and metal complexes of the ligand in organic solvents, as well as directing groups for the site of substitution on the scaffold. The NHC ligand substituents are strong σ-donors and weak π-acceptors, and as such are considered to be analogues of phosphine ligands.[53] Due to this strong donating character, NHCs typically form strong carbon to metal bonds, and therefore, stable organometallic complexes.

2.2. Synthesis of Binucleating NHC Pro-Ligands

This section describes the synthesis of novel binucleating pro-ligands **2.2**, **2.3**, and **2.4** *via* copper(I)-catalysed nucleophilic aromatic substitution of imidazole with the brominated scaffold precursor, followed by alkylation of the imidazole with an alkyl halide (Scheme 2.1).[54] The successful synthetic routes to 1,1'-(2,7-di-*tert*-butyl-9,9-dimethyl-9H-xanthene-4,5-diyl)bis(3-methyl-1H-imidazol-3-ium) iodide ([(MeNHC)$_2$^{t}Xan]I$_2$, **2.2**) and 1,1'-(2,7-di-*tert*-butyl-9,9-dimethyl-9H-xanthene-4,5-diyl)bis(3-benzyl-1H-imidazol-3-ium) bromide ([(BnNHC)$_2$^{t}Xan]Br$_2$, **2.4**) are summarised in Scheme 2.1.

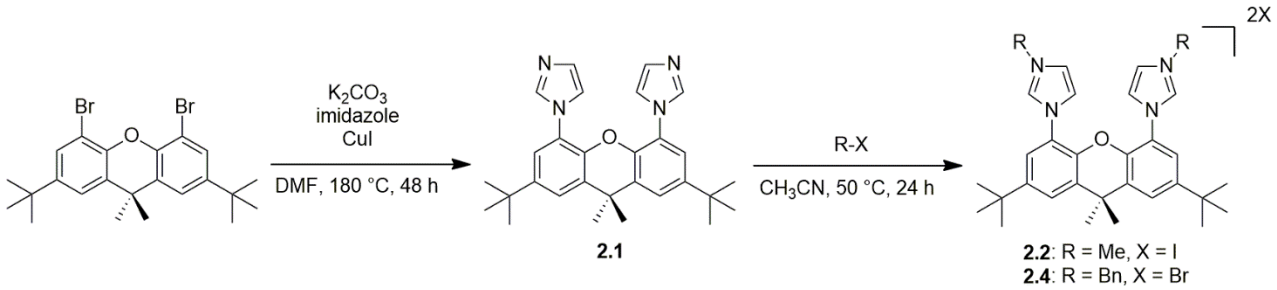

Scheme 2.1: General synthetic route toward ditopic pro-ligands [(MeNHC)$_2$^{t}Xan]I$_2$ **2.2** and [(BnNHC)$_2$^{t}Xan]Br$_2$ **2.4.**

2.2.1. Synthesis and Characterisation of 1,1'-(2,7-Di-*tert*-butyl-9,9-dimethyl-9H-xanthene-4,5-diyl)bis(1H-imidazole) (2.1)

The pro-ligand precursor 1,1'-(2,7-di-*tert*-butyl-9,9-dimethyl-9H-xanthene-4,5-diyl)bis(1H-imidazole) (**2.1**) was synthesised by an Ullman-type coupling[55,56] that involved a copper(I)-catalysed nucleophilic aromatic substitution of imidazole onto a brominated xanthene scaffold (Scheme 2.2). On the first attempt, copper(I) iodide (CuI) was used as a catalyst at 20 mol% loading, which resulted in 31% yield of the product. Subsequently, one molar equivalent (*i.e.* 100 mol%) of CuI relative to the substrate was employed as the strong affinity of copper for nitrogen donors (*i.e.* imidazole) is likely to have reduced the availability of copper in the reaction. Hence at lower loadings the copper may coordinate to the nitrogen atoms of the imidazole, preventing it from acting as a catalyst for the coupling reaction. After increasing the amount of copper(I) catalyst used, the product was obtained in 78% yield.

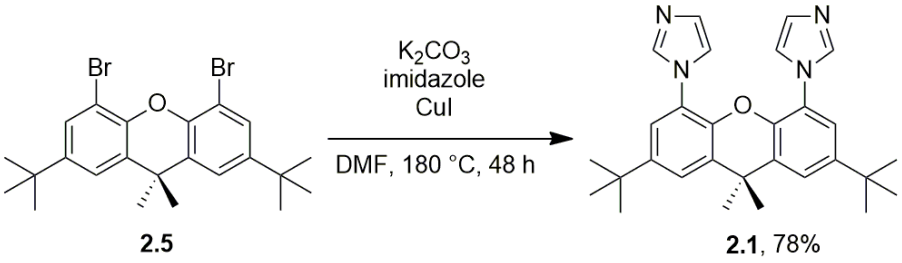

2.5 **2.1**, 78%

Scheme 2.2: Base-promoted Ullman-type coupling[56] of dibromoxanthene (**2.5**) and imidazole to form 1,1'-(2,7-di-*tert*-butyl-9,9-dimethyl-9H-xanthene-4,5-diyl)bis(1H-imidazole) (**2.1**).

The ^{1}H and ^{13}C NMR spectra of **2.1** were fully assigned. A key feature exhibited in the ^{1}H NMR spectrum is the appearance of only one singlet corresponding to the protons of the two methyl groups on the scaffold (**H**14). This equivalence is an indication that the pro-ligand precursor is symmetrical about the plane of the scaffold. Only one set of resonances that was attributed to the protons on the two imidazole rings was exhibited in the ^{1}H NMR spectrum, which also indicates a magnetic equivalence at room temperature and therefore geometrical symmetry. The ^{1}H and ^{13}C NMR spectra were in agreement with the spectra of the analogous compound (lacking the *tert*-butyl substituents) reported in the literature.[57]

2.2.2. Synthesis and Characterisation of [(MeNHC)$_2$^{t}Xan]I$_2$ (2.2)

The novel pro-ligand [(MeNHC)$_2$^{t}Xan]I$_2$ **2.2** was synthesised by alkylation of the nitrogen atom of each imidazole on **2.1** with excess iodomethane in acetonitrile at 50 °C for 24 hours to generate the imidazolium salt (Scheme 2.3). This S_N2 reaction yields the pro-ligand **2.2** in 98% yield after reprecipitation in excess *n*-hexane from a saturated solution in dichloromethane.

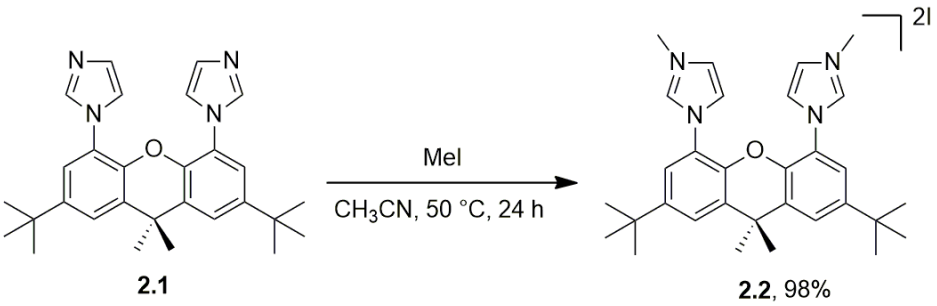

Scheme 2.3: Synthesis of **2.2**.

The ^{1}H and ^{13}C NMR spectra for **2.2** were fully assigned and were consistent with the spectra of the analogous pro-ligand reported in the literature.[57] Clear formation of the imidazolium salt was observed in the ^{1}H NMR spectrum by the down field shift to 9.65 ppm of the resonance due to the imidazolium proton (**H**2) when compared to the chemical shift of the resonance due to the equivalent proton from **2.1** which appeared at 7.02 ppm (Figure 2.1). The appearance of a sharp singlet at 4.34 ppm in the ^{1}H NMR spectrum, integrating to 6 protons is attributed to the protons of the attached methyl group on the imidazolium nitrogen (**H**1).

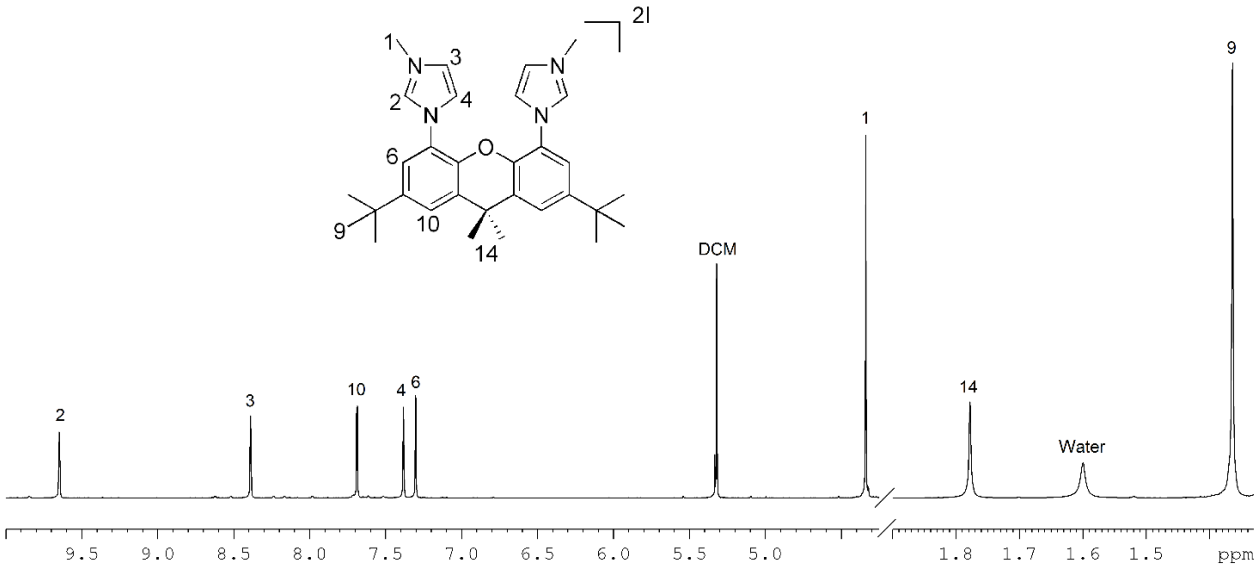

Figure 2.1: ^{1}H NMR (400 MHz, CD_2Cl_2, 25 °C) spectrum of $[(MeNHC)_2{}^{t}Xan]I_2$ **2.2**.

Assignment of the aromatic proton resonances (**H**6 and **H**10) and the imidazole backbone protons (**H**3 and **H**4) was established using a ^{1}H-^{1}H NOESY (Nuclear Overhauser Effect Spectroscopy) experiment by NMR. The aromatic proton **H**10 has a nuclear Overhauser effect (nOe) correlation to the protons of the *tert*-butyl group (**H**9) and the methyl groups on the xanthene (**H**14), whereas the aromatic proton **H**6 only correlates to **H**9 and does not correlate to **H**14. The imidazole

backbone proton **H**3 correlates to the protons on the methyl group attached to the imidazole nitrogen **H**1, whereas the other imidazole backbone proton **H**4 does not (Figure 2.2).

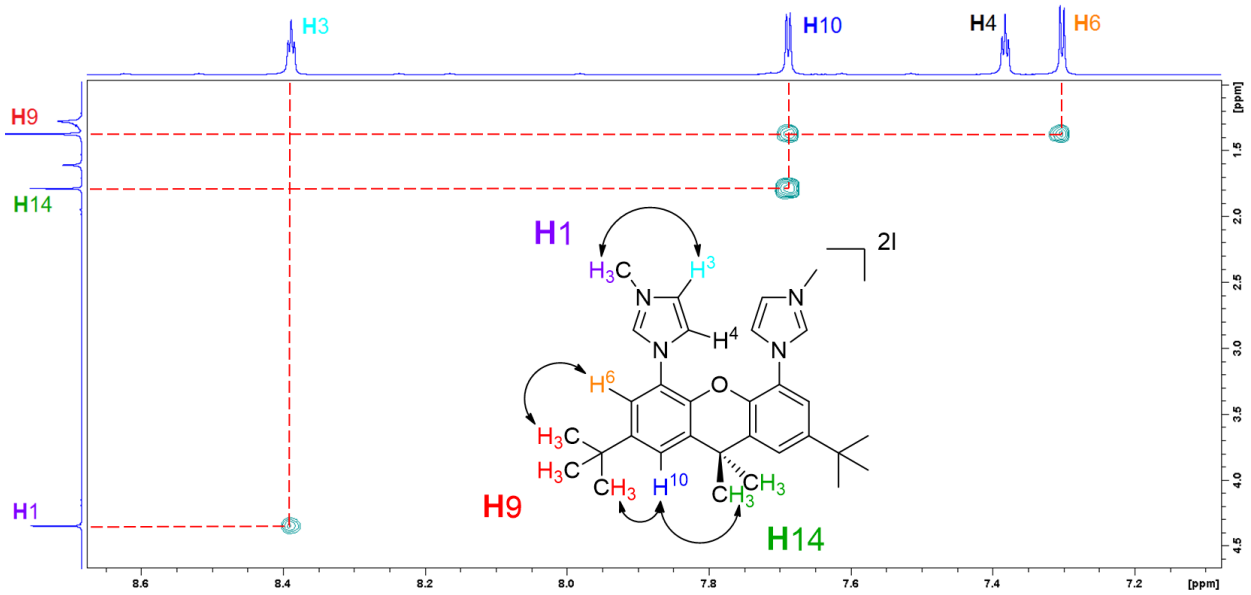

Figure 2.2: ^{1}H-^{1}H NOESY (400 MHz, CD_2Cl_2, 25 °C) spectra of $[(MeNHC)_2{}^{t}Xan]I_2$ **2.2** illustrating the nOe correlations between aromatic protons and neighbouring methyl and *tert*-butyl group protons.

In order to abstract the imidazolium proton (**H**2) and generate the carbene ligand using a base for the base-promoted complexation reaction with the Ir(I) precursor (Chapter 3), it was necessary to exchange the halide counterions for bulkier $[BPh_4]^-$ counterions, as a far more weakly coordinating counterion than iodine was needed. This was achieved by stirring pro-ligand **2.2** and $Na[BPh_4]$ in dichloromethane at room temperature (Scheme 2.4). The pro-ligand with a $[BPh_4]^-$ counterion (**2.3**) was obtained with a 72% yield.

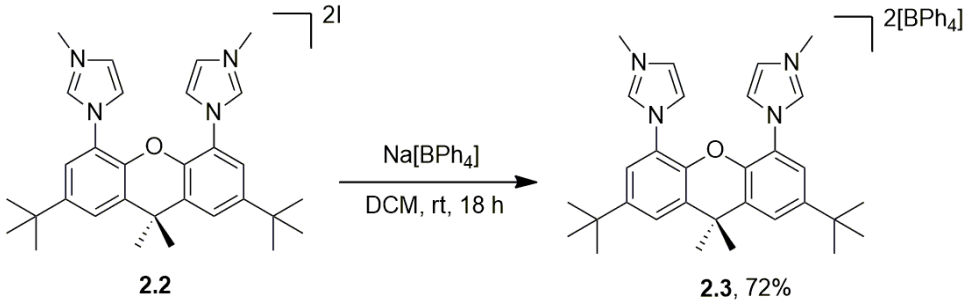

Scheme 2.4: Synthesis of $[(MeNHC)_2{}^{t}Xan][BPh_4]_2$ (**2.3**) *via* anion exchange with $Na[BPh_4]$.

The exchange of the counterion to $[BPh_4]^-$ is heralded by the significant upfield shift of the imidazolium proton resonance (**H**2) in the ^{1}H NMR spectrum, and a slightly less significant upfield shift of the imidazole backbone proton resonances (**H**3 and **H**4) from 9.65, 8.39, and 7.38 ppm for

the iodide salt to 5.86, 6.44, and 6.22 ppm in the tetraphenylborate salt respectively (Figure 2.3). The resonance for the methyl group protons on the imidazole nitrogen (**H**1) also shift significantly upfield in the ^{1}H NMR spectrum from 4.34 ppm for the iodide salt **2.2** to 2.84 for the tetraphenylborate salt **2.3**. The reason for this significant upfield shift is that with a weakly coordinating counterion there is less electron density in close proximity to the imidazole. As a result, the imidazolium protons become far more electropositive, **H**2 being the most electropositive as the positive charge can be delocalised between both nitrogen atoms of the imidazole.

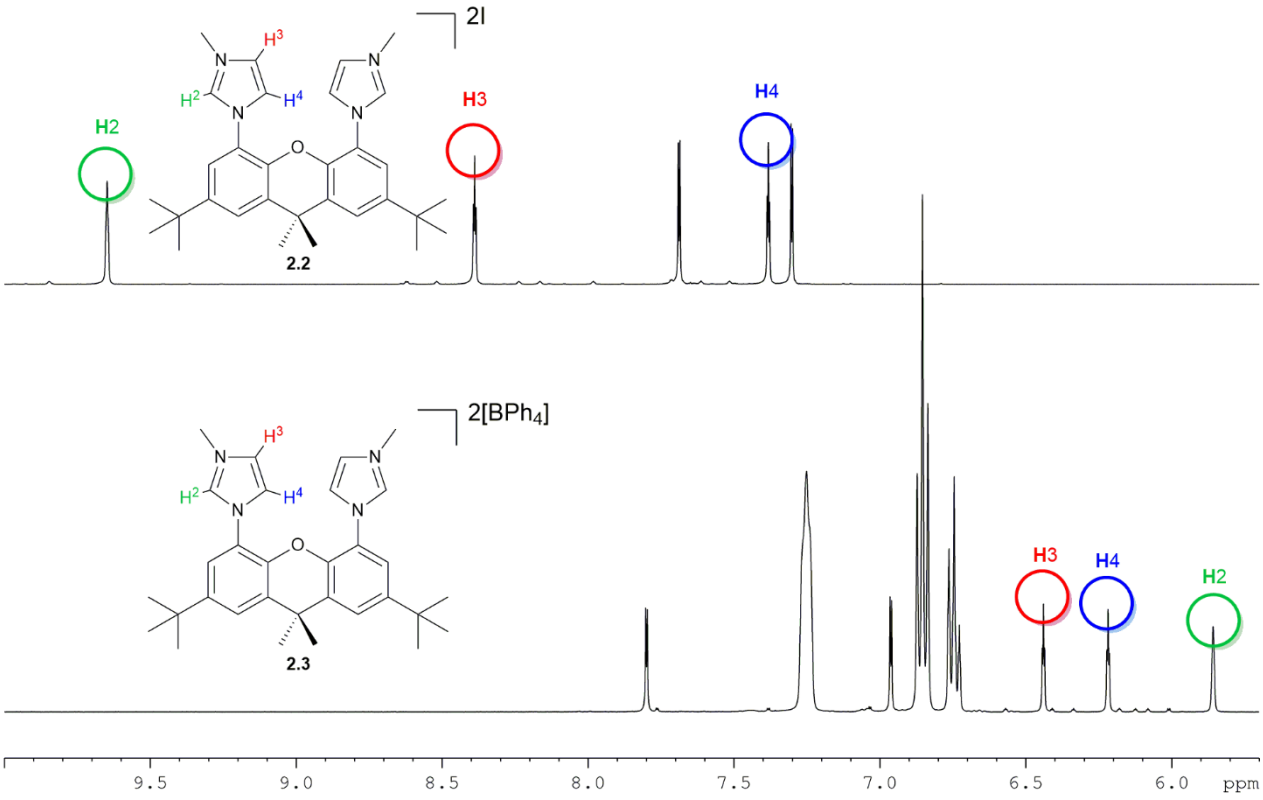

Figure 2.3: ^{1}H NMR (400 MHz, CD_2Cl_2, 25 °C) spectra of [(MeNHC)$_2$^{t}Xan]I_2 **2.2** and [(MeNHC)$_2$^{t}Xan][BPh_4]$_2$ **2.3** aromatic regions, illustrating the upfield shift in imidazolium proton resonances from the iodide salt **2.2** to the tetraphenylborate salt **2.3**.

2.2.3. Synthesis and Characterisation of [(BnNHC)$_2$^{t}Xan]Br_2 (2.4)

One of the major challenges in synthesising a bimetallic complex of the [(MeNHC)$_2$^{t}Xan] (**2.2** and **2.3**) pro-ligand is the free-rotation about the C-N bond of the imidazole to the xanthene scaffold. The only previous work with a bis(NHC)xanthene ligand system, to the best of our knowledge, reported the synthesis of monometallic silver(I) and rhodium(I) complexes of the ligand with the single metal centre bound to both NHC ligand substituents (Figure 2.4).[57] In addition to the use of two molar equivalents of metal to pro-ligand, pro-ligands with a bulkier substituents on the imidazolium nitrogen were designed in order to avoid the formation of the monometallic complex

through steric hindrance. It was intended that the bulkier substituents on the imidazole group would prevent the rotation of the imidazole groups so that the carbene units do not point inwards and bind to the same metal centre in a manner which is illustrated by the example in Figure 2.4.

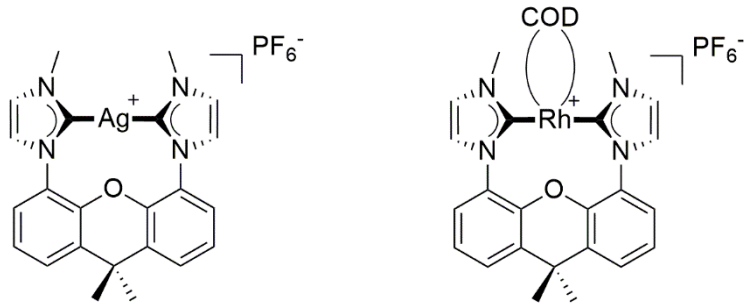

Figure 2.4: Bis-NHC complexes synthesised by Saito and colleagues.[57]

In the first instance, the aim was to attach a benzyl substituent to the imidazole units of the binucleating ligand. This type of benzyl-substituted NHC pro-ligand still formed a monometallic complex with a single metal centre bound simultaneously to both carbenes on the scaffold in the study by Saito *et al.* (Figure 2.4).[57] However, Saito and colleagues used only half an equivalent of metal precursor to ligand, and used both silver and rhodium which are far smaller metal centres than iridium. A benzyl substituted pro-ligand, combined with the use of excess iridium(I) precursor and a larger metal, could lead to the preferential formation of a binuclear complex over a mononuclear complex.

To this end, [(BnNHC)$_2$^{t}Xan]Br$_2$ (**2.4**) was synthesised *via* the same S$_N$2 substitution reaction of **2.1** as the methyl substituted pro-ligand with exactly the same reaction conditions, the only exception being that benzyl bromide was used as the alkyl halide in place of iodomethane (Scheme 2.5).

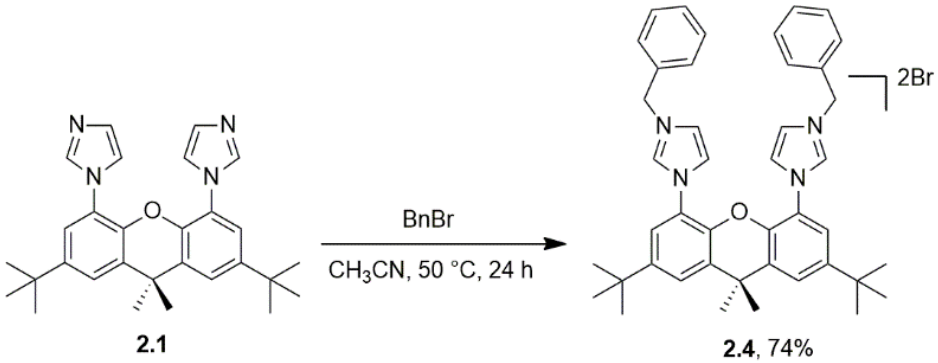

2.1 **2.4**, 74%

Scheme 2.5: S$_N$2 halide substitution of **2.1** with benzyl bromide to form [(BnNHC)$_2$^{t}Xan]Br$_2$ **2.4**.

The ^{1}H and ^{13}C NMR spectra of **2.4** were fully assigned, with the formation of the imidazolium salt causing a downfield shift of the imidazolium proton from 7.02 ppm in the starting material **2.1** to 10.00 ppm in **2.4**. **2.4** was isolated in 74% yield, which is significantly lower than the yield of **2.2**

with a methyl substituent (98%), and generally low for an S_N2 reaction. The lower yield in this reaction with benzyl bromide could possibly be due to the fact that bromine is a less efficient leaving group than iodine of the iodomethane used for the methyl substituent. Therefore, an *in situ* Finkelstein reaction could potentially increase the yield as it involves the addition of sodium iodide which exchanges iodine for the bromine on the alkyl halide, making it more reactive towards the S_N2 reaction.[58]

2.3. Attempted Synthesis of Additional Bulky Pro-Ligands

In addition to the synthesis of a pro-ligand with benzyl substituents, the synthesis of three other pro-ligands with bulky alkyl substituents was attempted (Figure 2.5). The addition of *n*-butyl, *iso*-butyl, and *tert*-butyl substituents was intended through the reaction of the appropriate alkyl bromide with **2.1** under the same reaction conditions as used for the reaction in the previous section with benzyl bromide (Scheme 2.5).

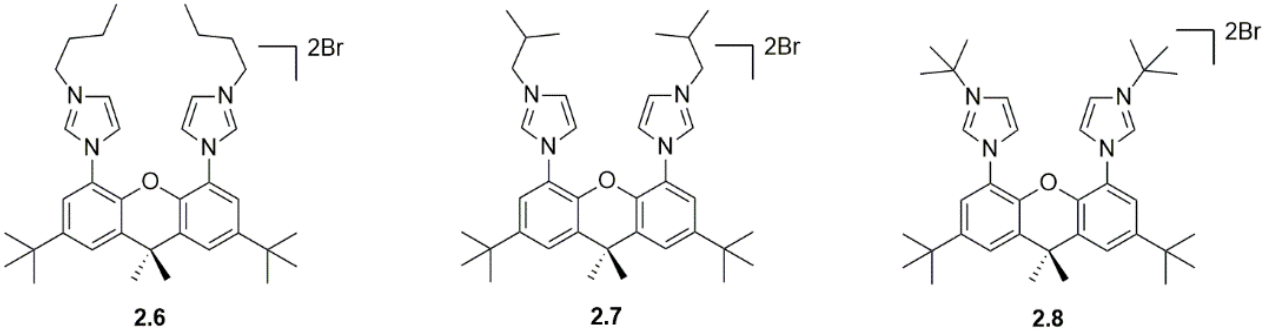

2.6 **2.7** **2.8**

Figure 2.5: Target pro-ligands: [(*n*-BuNHC)$_2$^{t}Xan]Br$_2$ **2.6**; [(*i*-BuNHC)$_2$^{t}Xan]Br$_2$ **2.7**; and [(*t*-BuNHC)$_2$^{t}Xan]Br$_2$ **2.8**.

The attempted synthesis of the *n*-butyl and *tert*-butyl derivatives (**2.6** and **2.8**) resulted in the possible protonation of the imidazolium nitrogen instead of the addition of the alkyl group of the alkyl bromide, forming the pro-ligand [(HNHC)$_2$^{t}Xan]Br$_2$ **2.9** (Figure 2.6). This was evidenced by the characteristic down field shift in the of the imidazolium proton (**H**2) that was observed in the ^{1}H NMR spectrum, confirming the formation of an imidazolium salt (Figure 2.6). However, the appearance of resonances corresponding to the protons of alkyl chains on the imidazolium nitrogen were absent. Instead, in those spectra that were taken in wet NMR solvent, a slight broadening and down field migration of the water peak is observed. This is likely to be caused by a proton on the imidazolium nitrogen (**H**1). The source of the proton could be water in the solvent used for the reaction, however this was not investigated further.

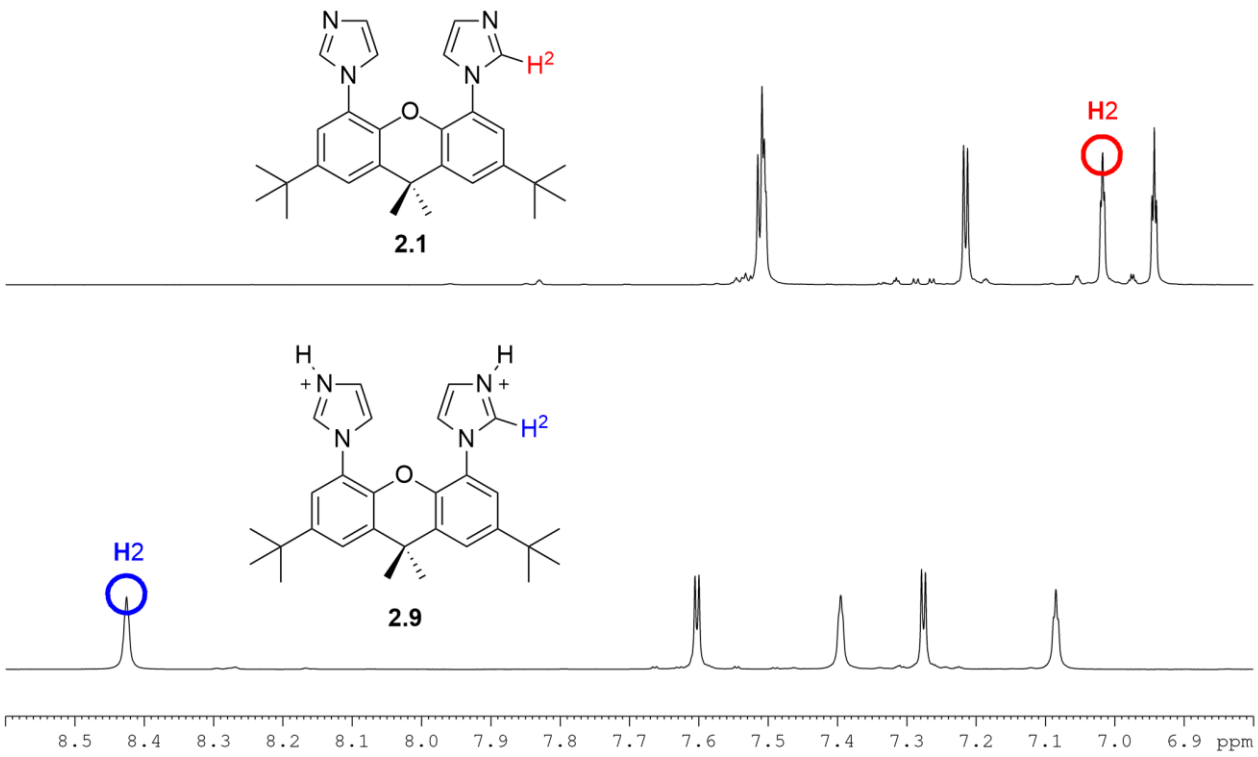

Figure 2.6: ^{1}H NMR spectra (400 MHz, CD_2Cl_2, 25 °C) of **2.1** and [(HNHC)$_2$^{t}Xan]Br_2 **2.9** illustrating the down field shift of the imidazolium proton **H**2.

The reduced reactivity of *tert*-butyl bromide in this reaction is not surprising as the carbon to be substituted is a tertiary carbon and is therefore not amenable to S_N2 substitution reactions. To take an alternative approach to this reaction, a microwave reactor was employed in a method adapted from work described by Librando and Creencia for the substitution reaction of **2.1** with *tert*-butyl bromide.[59] The reaction was performed neat at 100 °C for 20 minutes and in acetonitrile at 150 °C for 20 minutes. Both sets of conditions again resulted in the protonated compound **2.9** instead of the desired *tert*-butyl substituted pro-ligand **2.8**. A last attempt was made to synthesise [(*t*-BuNHC)$_2$^{t}Xan]Br_2 **2.8** using an adapted method from Braunstein and colleagues.[60] **2.1** and *tert*-butyl bromide were stirred in toluene at 170 °C for 18 hours, but this also resulted in the formation of the protonated compound **2.9**. At this stage, the attempt to synthesise more bulky alkyl-substituted pro-ligands was abandoned due to time constraints, as well as success in synthesising a bimetallic iridium(I) complex of the pro-ligand [(MeNHC)$_2$^{t}Xan]I_2 **2.2** (as discussed in Section 3.2.1), rendering the pursuit of sterically bulky pro-ligands unnecessary for the purposes of forming a bimetallic complex.

Chapter 3 : Complex Synthesis

3.1. Introduction

This chapter describes the synthesis and characterisation of two novel iridium(I) bimetallic complexes of a binucleating NHC-xanthene ligand (**3.3** and **3.4**). These bimetallic complexes were designed as an analogue of two monometallic iridium(I) catalysts bearing NHC ligands that had previously been prepared and studied for their catalytic activity in the Messerle group (**3.1** and **3.2**, Figure 3.1).[49] These particular monometallic iridium(I) complexes have been proven to be highly active catalysts for alkyne activation reactions such as the hydroamination of alkynyl amines and dihydroalkoxylation of alkyne diols. Combining this and the fact that bimetallic complexes have often been shown to substantially enhance catalytic activity, the use of these motifs in a bimetallic system was postulated to lead to interesting catalysts.

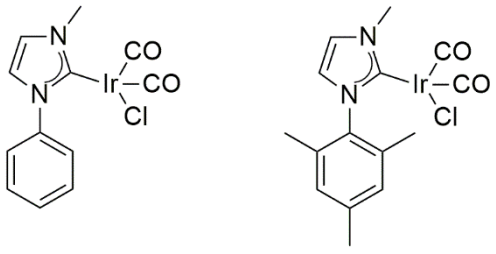

3.1 **3.2**

Figure 3.1: Monometallic Ir NHC complexes [Ir(CO)$_2$Cl(PhNHC)] (**3.1**) and [Ir(CO)$_2$Cl(MesNHC)] (**3.2**) (unpublished results from Messerle group).[49]

3.2. Synthesis of Homobimetallic Ir(I) Complexes of Binucleating NHC Ligands

The homobimetallic Ir(I) complexes [Ir$_2$((MeNHC)$_2$^{t}Xan)(COD)$_2$Cl$_2$] (**3.3**) and [Ir$_2$((MeNHC)$_2$^{t}Xan)(CO)$_4$Cl$_2$] (**3.4**) were synthesised and characterised.

3.2.1. Synthesis and Characterisation of [Ir$_2$((MeNHC)$_2$^{t}Xan)(COD)$_2$Cl$_2$] (3.3)

[Ir$_2$((MeNHC)$_2$^{t}Xan)(COD)$_2$Cl$_2$] (**3.3**) was synthesised by two different methods, the first of which was a silver transmetallation reaction and the second was *via* deprotonation with potassium carbonate (Scheme 3.1). Initially, the silver transmetallation route was utilised, however there were difficulties in removing the residual silver salts from the product, hence the reaction that involved deprotonation was the preferred approach to obtaining pure product in quantity. Both synthetic routes toward the production of [Ir$_2$((MeNHC)$_2$^{t}Xan)(COD)$_2$Cl$_2$] (**3.3**) are outlined in Scheme 3.1.

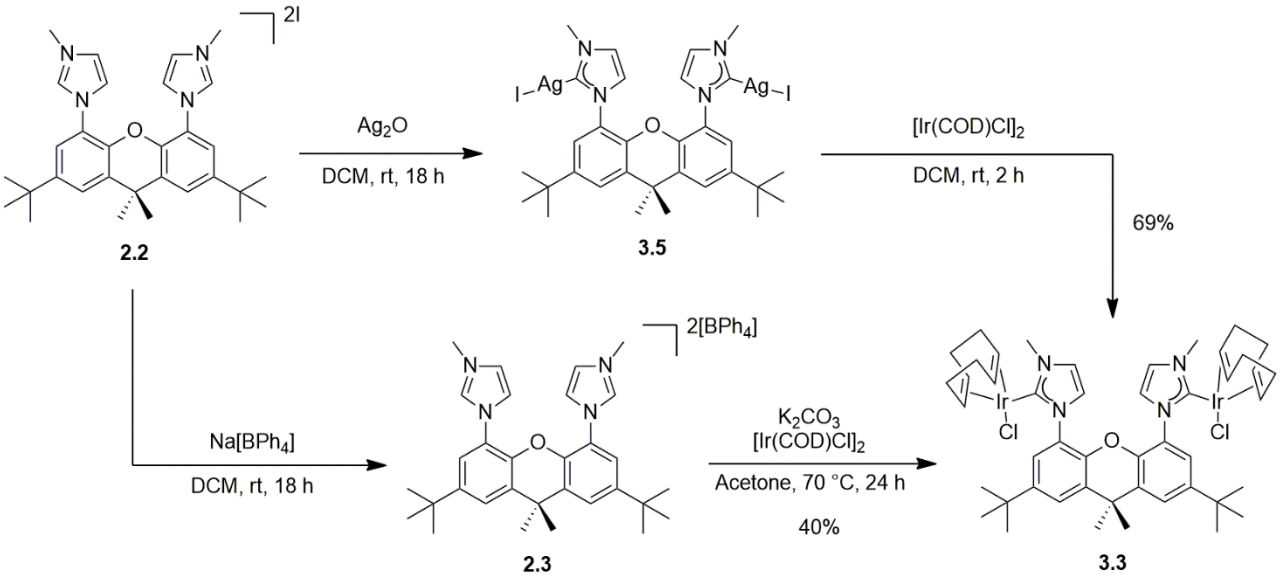

Scheme 3.1: Synthesis of $[Ir_2((MeNHC)_2{}^tXan)(COD)_2Cl_2]$ (**3.3**) *via* silver transmetallation (top route), and *via* deprotonation (bottom route).

The silver(I) complex **3.5** was generated *in situ* through the reaction of one and a half molar equivalents of silver(I) oxide with one molar equivalent of the iodide salt pro-ligand **2.2** in dichloromethane at room temperature for 18 hours. The silver complex **3.5** was not isolated. Instead, the mixture containing **3.5** was filtered through a Celite® pad to remove any excess silver salts. One molar equivalent of the metal precursor, $[Ir(COD)Cl]_2$, relative to the substrate was then added to the reaction mixture and the mixture stirred for another two hours at room temperature. The bimetallic Ir(I) complex **3.3** was obtained from this reaction in 69% yield. The removal of silver salts from the product was attempted first using column chromatography, however the iridium product **3.3** decomposed on the silica. The majority of silver salts were successfully removed by slow addition of *n*-hexane to a solution of the crude mixture in dichloromethane. Both the silver salts and the Ir(I) complex **3.3** precipitate upon addition of *n*-hexane, however the silver salts do so at a faster rate. Thus, the precipitation and filtration had to be repeated multiple times by removal of the solvent under reduced pressure and redissolving the product in dichloromethane. This was laborious, resulted in the loss of some product each time, and still did not completely remove all of the silver salts. Therefore, an alternative synthetic route was sought.

The use of potassium carbonate to deprotonate an imidazolium salt pro-ligand was the alternate and ultimately best route towards the formation of a metal-NHC bond. The use of such a weak base to abstract an imidazolium proton requires the imidazolium salt to possess a weakly coordinating anion (such as tetraphenylborate), therefore the pro-ligand $[(MeNHC)_2{}^tXan][BPh_4]_2$ (**2.3**) was used in this reaction. One molar equivalent of $[(MeNHC)_2{}^tXan][BPh_4]_2$ (**2.3**) was refluxed

in acetone with an excess of potassium carbonate and one molar equivalent of the metal precursor $[Ir(COD)Cl]_2$. The removal of $[BPh_4]^-$ salt from the final product was achieved by filtration through a Celite® pad and $[Ir_2((MeNHC)_2{}^tXan)(COD)_2Cl_2]$ (**3.3**) was obtained in 40% yield. The product was pure and could be used for catalysis work without further purification.

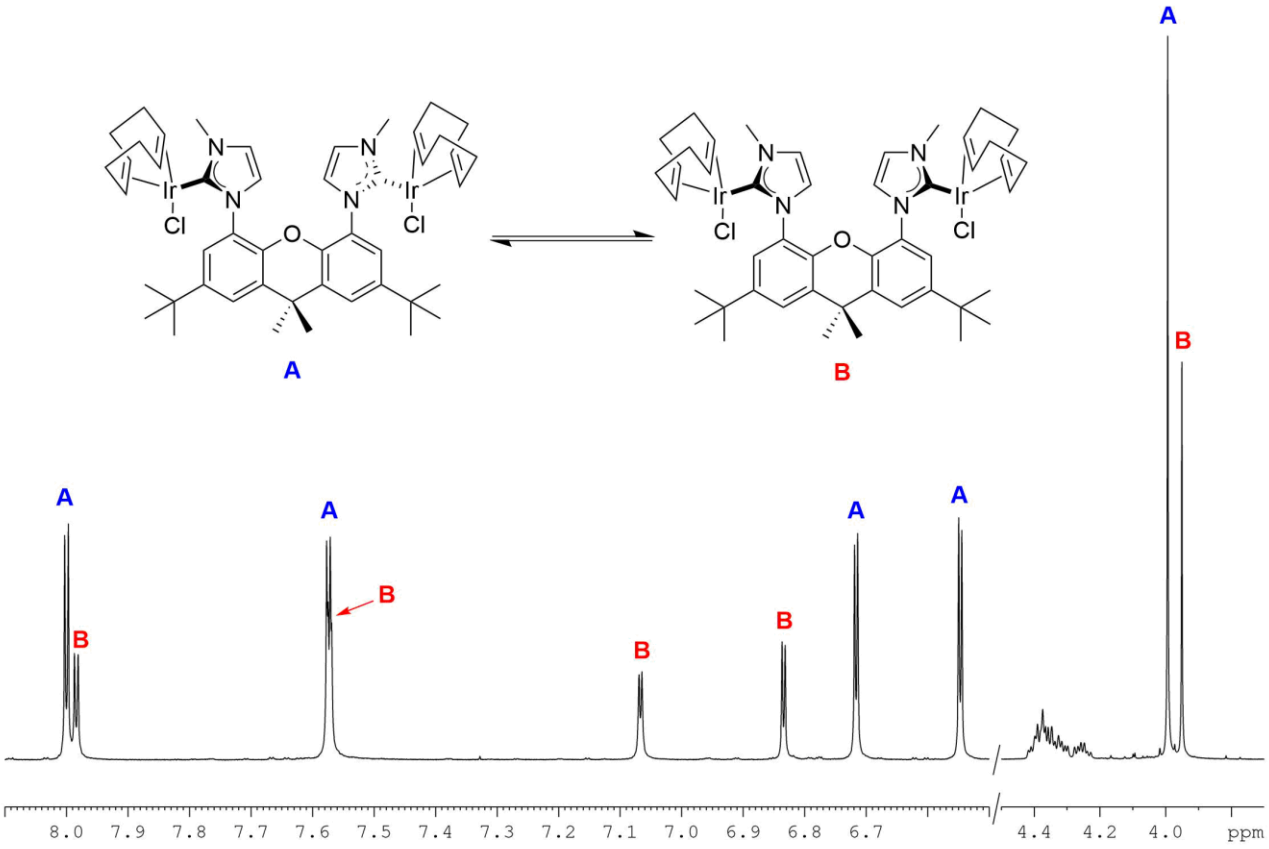

Figure 3.2: ^1H NMR spectrum (400 MHz, CD_2Cl_2, 25 °C) of $[Ir_2((MeNHC)_2{}^tXan)(COD)_2Cl_2]$ (**3.2**) depicting the appearance of two separate postulated conformations.

The ^1H NMR spectrum of **3.3** revealed what appeared to be resonances derived from two distinct products in an approximately 1:2 molar ratio (Figure 3.2). This was initially thought to be a mixture of the desired bimetallic complex **3.3** and a monometallic complex where the metal was bound to both NHCs (similar to the complexes synthesised by Saito *et al.*[57] as seen in Figure 2.4). Due to overlapping resonances from the 1,5-cyclooctadiene (COD) co-ligands in the ^1H NMR spectrum, it was not possible to determine whether the two species were a monometallic and the bimetallic **3.3** based on integration of the co-ligand resonances. After attempting various purification techniques such as column chromatography and recrystallisation, as well as changing reaction conditions such as the solvent, temperature and duration, the molar ratio of the two observed species always remained the same. This was an indication that the two sets of resonances actually originated

from a single product existing as a mixture of two conformational isomers, rather than originating from two separate molecules (Figure 3.2).

To confirm this, a ^{1}H-^{1}H NOESY experiment was conducted using NMR spectroscopy. Two-site exchange between pairs of protons was observed as positive phase correlations between the resonances due to the protons of one of the observed species and the resonances due to the protons of the other (Figure 3.3). This was evidence that the two observed sets of peaks were derived from conformational isomers of the bimetallic complex [Ir_2(($MeNHC)_2{}^t$Xan)$(COD)_2Cl_2$] (**3.3**). Hindered rotation around the C-N bond between the NHC and the scaffold would force the complex to adopt specific conformations that could undergo exchange.

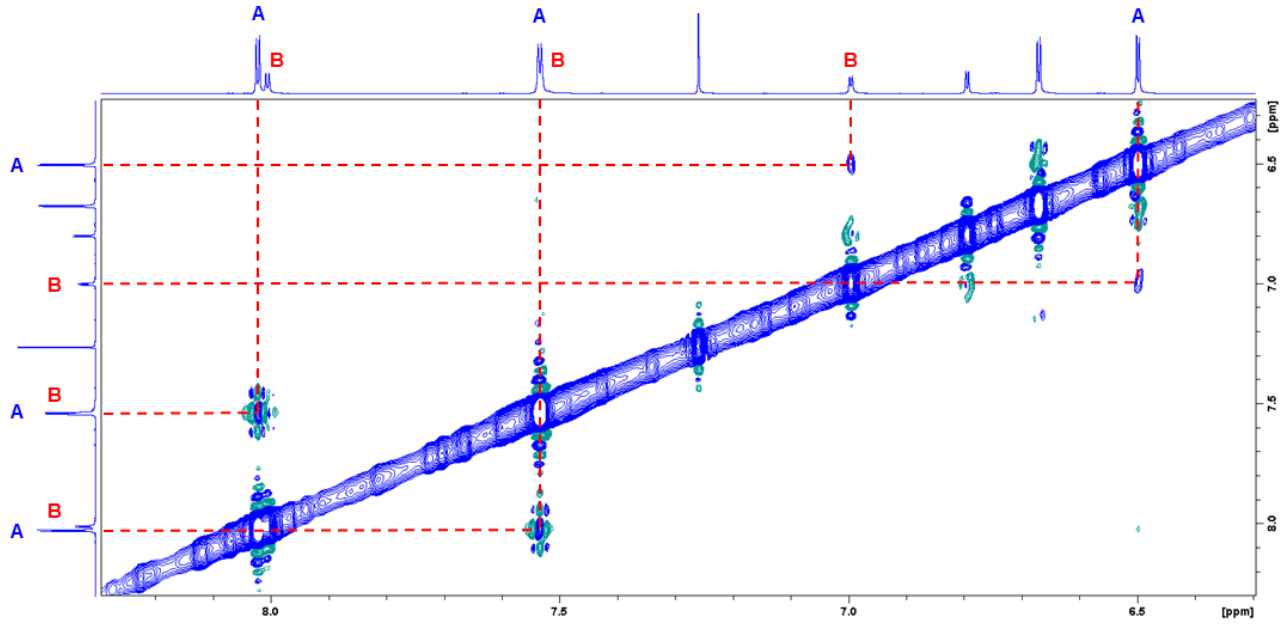

Figure 3.3: NOESY spectrum (400 MHz, $CDCl_3$, 25 °C) of [Ir_2(($MeNHC)_2{}^t$Xan)$(COD)_2Cl_2$] (**3.3**) demonstrating exchange between the resonances corresponding to the aromatic protons of the xanthene scaffold from the two different conformational isomers **A** and **B**.

^{1}H NMR spectra of **3.3** were collected at temperatures ranging from -55 °C to 105 °C in an attempt to resolve the resonances into those of a single isomer for the purpose of characterisation. However, neither of these extreme temperatures resulted in the observation of a single set of resonances. Therefore, the resonances corresponding to the major conformational isomer of **3.3** (**A** in Figure 3.3) in the ^{1}H and ^{13}C NMR spectra were fully assigned, indicating the formation of one of the conformational isomers of the desired complex **3.3**.

To further confirm that either of the two sets of resonances observed in the ^{1}H NMR spectrum are not just a similar complex with a single iridium metal centre bound, HR-ESI-MS (High Resolution Electro-Spray Ionisation Mass Spectrometry) was performed. The major peak obtained corresponded

to m/z $[M+Na]^+$ = 1177.3433, which is the predicted mass of the desired bimetallic complex **3.3**. The isotope splitting pattern of the molecular ion, which can be used as a finger print for a bimetallic iridium complex, was compared to a prediction using predictive software which demonstrated that the product was a bimetallic iridium complex, rather than a monometallic iridium complex (Figure 3.4).

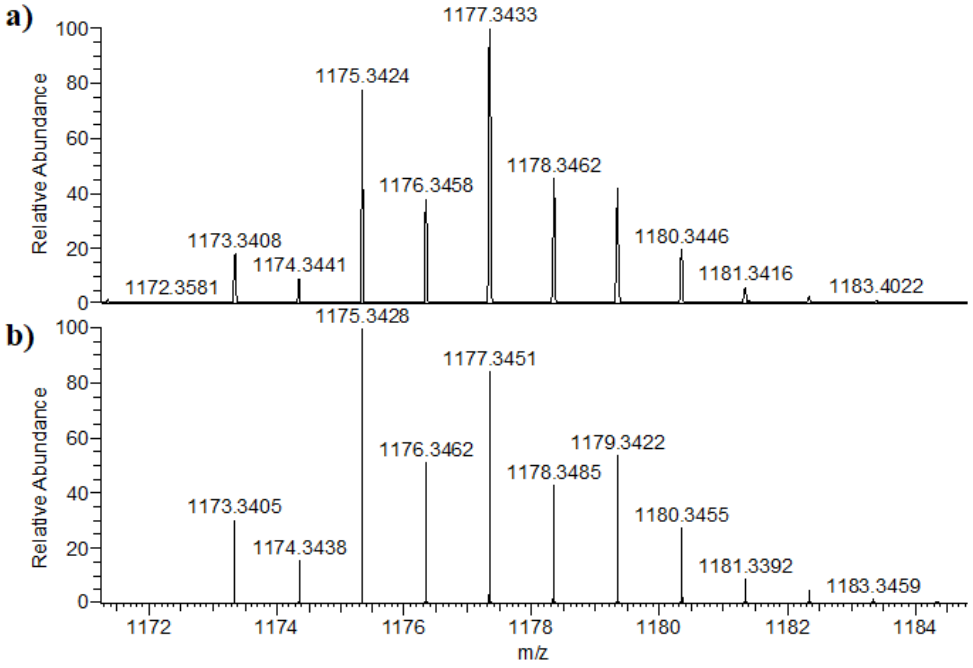

Figure 3.4: $[M+Na]^+$ peak of $[Ir_2((MeNHC)_2{}^tXan)(COD)_2Cl_2]$ (**3.3**) depicting the isotopic splitting pattern from **a)** the high-resolution mass spectrum, **b)** the predicted spectrum.

3.2.2. Synthesis and Characterisation of $[Ir_2((MeNHC)_2{}^tXan)(CO)_4Cl_2]$ (3.4)

The bimetallic iridium(I) complex $[Ir_2((MeNHC)_2{}^tXan)(CO)_4Cl_2]$ (**3.4**) was synthesised by reaction of the analogous 1,5-cyclooctadiene complex $[Ir_2((MeNHC)_2{}^tXan)(COD)_2Cl_2]$ (**3.3**) with gaseous carbon monoxide (CO) (Scheme 3.2). A solution of **3.3** in dichloromethane was thoroughly degassed through three cycles of the freeze-pump-thaw method before the atmosphere of the Schlenk flask was replaced with carbon monoxide from a balloon whilst the solution was still frozen. Once the solution had thawed and begun stirring under the CO atmosphere it rapidly turned from a deep yellow to a pale yellow/green colour, indicating the exchange of the 1,5-cyclooctadiene co-ligands with carbonyl co-ligands. **3.4** displayed high thermal stability and was stable in air both as a solid and in solution (dichloromethane and chloroform).

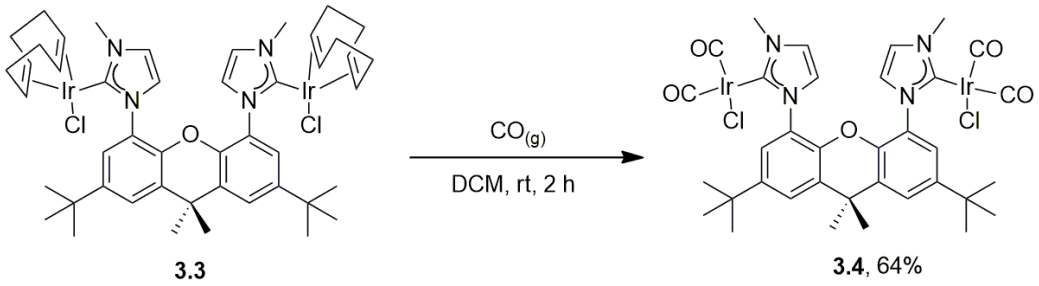

3.3 **3.4**, 64%

Scheme 3.2: Synthesis of $[Ir_2((MeNHC)_2{}^tXan)(CO)_4Cl_2]$ (**3.4**) *via* carbonylation of $[Ir_2((MeNHC)_2{}^tXan)(COD)_2Cl_2]$ (**3.3**).

The bimetallic complex **3.4** was fully characterised by NMR spectroscopy (^{1}H and ^{13}C), mass spectrometry (HR-ESI-MS), infrared (IR) spectroscopy, and elemental analysis. Unlike $[Ir_2((MeNHC)_2{}^tXan)(COD)_2Cl_2]$ (**3.3**), there was only one set of resonances for the carbonylated complex **3.4** in the ^{1}H NMR spectrum, which therefore did not appear as two separate conformational isomers (Figure 3.5). An interesting feature in the ^{1}H NMR spectrum of **3.4** is the slight broadening of the resonance corresponding to **H**4, which appeared as a sharp doublet in the analogous 1,5-cyclooctadiene complex **3.3** but appears as slightly broad singlet in the dicarbonyl complex **3.4**. This broadening observed for complex **3.4** could be attributed to a change in orientation Ir(I)-NHCs relative to the xanthene scaffold so that **H**4 may have a stronger interaction with the oxygen of xanthene and undergo a more rapid relaxation that **H**4 of complex **3.3**. The adjacent imidazole proton (**H**3) resonance still appears as a sharp doublet with the same coupling constant in the ^{1}H NMR spectrum of **3.4** as it did in the ^{1}H NMR spectrum of the analogous 1,5-cyclooctadiene complex **3.3**. In the ^{13}C NMR spectrum of **3.4**, two resonances corresponding to the carbons of the carbonyl co-ligands were present, indicating that the carbonyls are in a *cis* conformation around the square planar iridium(I) metal centre. If they adopted a *trans* configuration, only one resonance corresponding to the carbon of a carbonyl would be expected as the carbonyl co-ligands would be magnetically and chemically equivalent. HR-ESI-MS also confirmed the identity of the complex **3.4** with major peak obtained corresponded to *m/z* $[M+Na]^+$ = 1073.1338 and an isotope splitting pattern of the molecular ion consistent with a bimetallic iridium species.

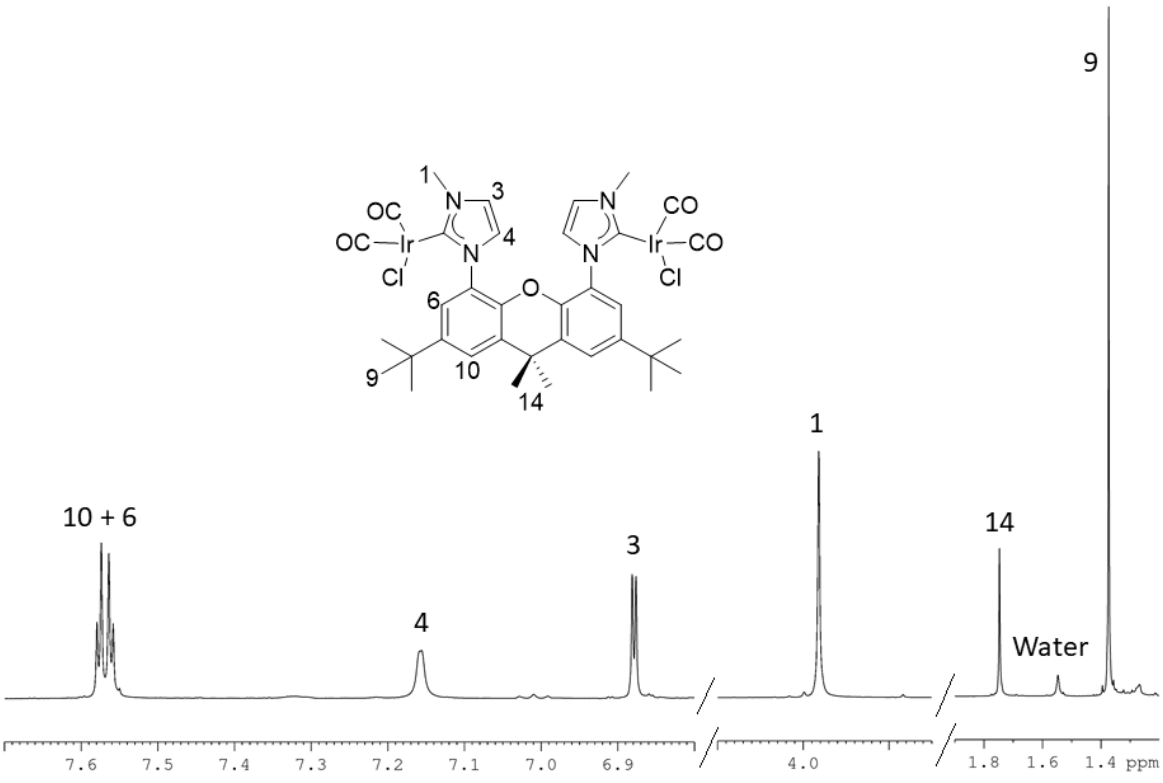

Figure 3.5: ^{1}H NMR spectrum (400 MHz, CD_2Cl_2, 25 °C) of $[Ir_2((MeNHC)_2{}^{t}Xan)(CO)_4Cl_2]$ (**3.4**).

During an attempted synthesis of **3.4**, after 2 hours of stirring the solution had turned a dark blue colour. The solvent volume was reduced and the product was precipitated as a dark blue (nearly black) solid from excess *n*-hexane. By ^{1}H NMR spectroscopy, the dark blue product was indistinguishable from the regular pale yellow/green iridium(I) complex. After a week of standing, the blue species slowly turned completely black. A possible explanation could be the oxidation of iridium(I) to iridium(II) by a small amount of unremoved oxygen in the reaction, and another could be the formation of a radical species. However, neither of these are likely explanations, given that both the Ir(II) species and the radical species are highly unstable and the blue colour would have disappeared much faster than was observed. Further investigation was not possible or necessary as the blue colour did not reoccur in any subsequent reactions.

Chapter 4 : Catalysis

4.1. Introduction

Having successfully synthesised $[Ir_2((MeNHC)_2{}^tXan)(CO)_4Cl_2]$ (**3.4**), the efficiency of the complex as a catalyst for a series of organic transformations was assessed. The efficiency of **3.4** was then compared with the monometallic catalysts $[Ir(CO)_2Cl(PhNHC)]$ (**3.1**) and $[Ir(CO)_2Cl(MesNHC)]$ (**3.2**) (Figure 3.1) that were discussed in Section 1.5. The aim was to establish if bimetallic complex **3.4** exhibits an enhanced efficiency as a catalyst resulting from the two metal centres being held together in close proximity relative to that of the monometallic complexes. The existence and degree of catalytic enhancement was determined in two classes of alkyne activation reactions, the hydroamination and dihydroalkoxylation of alkynes. The data and conditions for the catalysis reactions using the monometallic catalysts (**3.1** and **3.2**) were established by Dr. Mark Gatus.[49,54] The reaction conditions (*i.e.* catalyst loading, temperature and solvent) were chosen to match the data previously acquired for the monometallic catalysts (**3.1** and **3.2**) in order to achieve an accurate comparison. This includes the addition of sodium tetrakis[3,5-bis(trifluoromethyl)phenyl]borate ($Na[BAr^F{}_4]$). $Na[BAr^F{}_4]$ acts as a weakly coordinating anion that allows the chloride co-ligand of the catalyst **3.4** to vacate an orbital on the iridium metal centre, leaving it as a vacant coordination site for activation of the substrate to take place. It has also been demonstrated previously that $Na[BAr^F{}_4]$ alone will not catalyse the hydroamination or dihydroalkoxylation reactions that were investigated in this project.[34,46,61] Each of the catalysis reactions using **3.4** as the catalyst were monitored by ^1H NMR spectroscopy from which a reaction profile of the percentage conversion of substrate to product versus reaction time was constructed.

4.2. Iridium(I)-Catalysed Intra- and Intermolecular Hydroamination

Hydroamination reactions of alkynes result in the formation of either heterocyclic imines or aliphatic imines depending on whether the reaction is performed intramolecularly using alkynyl amines or intermolecularly with alkynes and amines. Imines and *N*-heterocycles are important functional groups that are common in bulk chemicals and in many important pharmaceuticals.[50] The performance of the bimetallic iridium(I) complex **3.4** as a catalyst for the intramolecular hydroamination of alkynyl amines to form cyclic imines and the intermolecular hydroamination of an alkyne with a primary amine to generate a secondary ketimine was investigated. This investigation focussed on how the bimetallic catalyst **3.4** behaves in the hydroamination reaction using the following substrates: 4-pentyn-1-amine (**4.1a**), 5-phenyl-4-pentyn-1-amine (**4.2a**), and phenylacetylene (**4.3a**) and aniline (**4.3b**). The efficiency of the bimetallic complex **3.4** as a catalyst

for the intermolecular reaction with phenylacetylene (**4.3a**) and aniline (**4.3b**) is of particular interest as intermolecular hydroamination reactions are generally slower and more difficult to catalyse than their intramolecular counterparts.

4.2.1. Catalysed Hydroamination of 4-Pentyn-1-amine (4.1a)

The catalysed hydroamination of 4-pentyn-1-amine (**4.1a**) was conducted using 1 mol% of the Ir(I) bimetallic complex **3.4** and 2 mol% of Na[BAr^F_4] at 100 °C in toluene-d_8, resulting in the formation of the product, 2-methyl-1-pyrroline (**4.1b**) (Scheme 4.1).

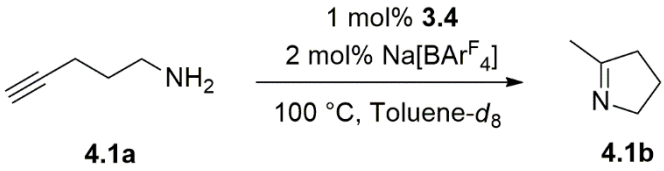

Scheme 4.1: Catalysed intramolecular hydroamination of 4-pentyn-1-amine (**4.1a**).

The bimetallic complex **3.4** catalysed the hydroamination of 4-pentyn-1-amine (**4.1a**) with a fast initial reaction rate, as reflected by its turnover frequency (TOF) of 1682 h^{-1} which was calculated at the time of 50% conversion of substrate to product (Figure 4.1). The reaction rate began to decrease at around 60% conversion and plateaued as it reached >95% conversion after 45 minutes.

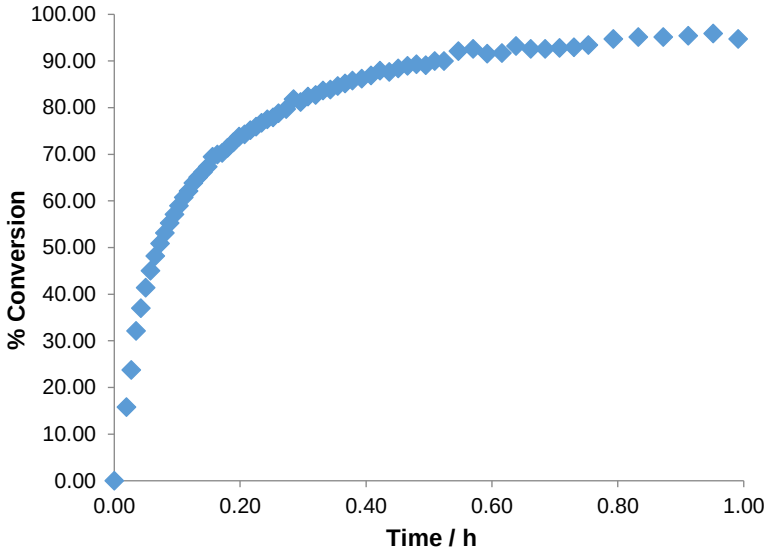

Figure 4.1: Reaction profile for the intramolecular hydroamination of **4.1a** catalysed by **3.4**.

4.2.2. Catalysed Hydroamination of 5-Phenyl-4-pentyn-1-amine (4.2a)

The progress of the catalysed intramolecular hydroamination reaction of 5-phenyl-4-pentyn-1-amine (**4.2a**) to form 2-benzyl-1-pyrroline (**4.2b**) was investigated using **3.4** as a catalyst (1 mol%) and Na[BAr^F_4] (2 mol%) as an additive (Scheme 4.2).

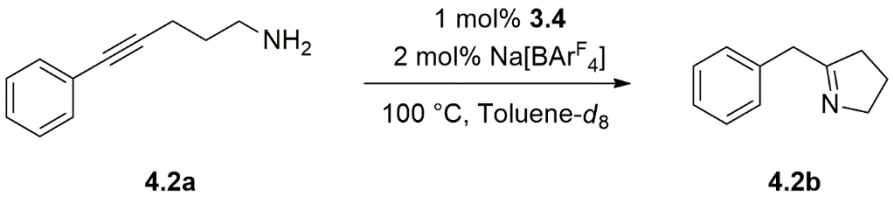

Scheme 4.2: Catalysed hydroamination of 5-pheny-4-pentyn-1-amine (**4.2a**).

The TOF for the hydroamination of **4.2a** at 100 °C in toluene-d_8 using the bimetallic catalyst was 112 h^{-1} as the reaction rate began to slow at about 40% conversion after a moderate initial reaction rate (Figure 4.2). After 4.5 hours the reaction was seemingly coming to an end at >70% conversion, thus consistent monitoring by ^{1}H NMR spectroscopy was stopped. However, heating of the reaction in an oil bath was continued for two days and a subsequent ^{1}H NMR spectra revealed that the reaction had reached >95% conversion to product after approximately 70 hours.

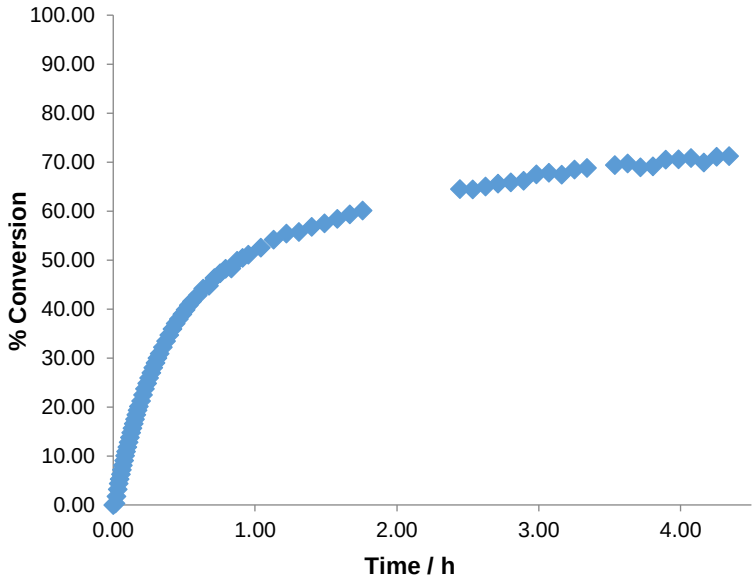

Figure 4.2: Reaction profile for the intramolecular hydroamination of **4.2a** catalysed by **3.4**.

4.2.3. Catalysed Intermolecular Hydroamination of Phenylacetylene (4.3a) with Aniline (4.3b)

An intermolecular hydroamination reaction of phenylacetylene (**4.3a**) with aniline (**4.3b**) was investigated using the bimetallic complex **3.4** as a catalyst (1 mol%) and Na[BAr$^F_4$] (2 mol%) as an additive at 80 °C in toluene-d_8, generating (*E*)-*N*-(1-phenylethylidene)aniline (**4.3c**) as the ketimine product (Scheme 4.3).

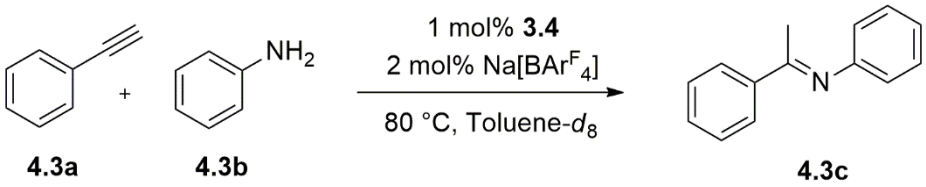

Scheme 4.3: Catalysed hydroamination of phenylacetylene (**4.3a**) with aniline (**4.3b**).

The intermolecular hydroamination reaction of **4.3a** with **4.3b** catalysed by the bimetallic complex **3.4** demonstrated a fast initial rate of reaction and a steadier decline in reaction rate than the two intramolecular hydroamination reactions (Figure 4.3). As a result, >95% conversion was achieved after 110 minutes and the TOF for the reaction using the bimetallic complex **3.4** as the catalyst was 331 h^{-1}.

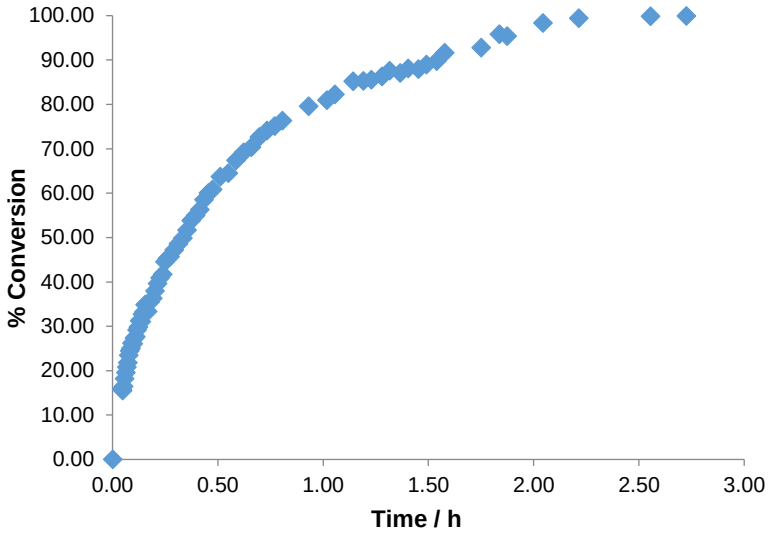

Figure 4.3: Reaction profile for the intermolecular hydroamination of phenylacetylene (**4.3a**) with aniline (**4.3b**) catalysed by **3.4**.

4.2.4. Comparison of 3.4 with Monometallic Catalysts 3.1 and 3.2

For the catalysed intramolecular hydroamination reactions and the catalysed intermolecular hydroamination reaction, the efficiency of the catalysts followed a consistent trend when assessed using the TOF values. In each case, the monometallic Ir(I) catalyst containing an NHC ligand substituent on a phenyl scaffold **3.1** achieved the greatest turnover number, followed by the bimetallic Ir(I) catalyst **3.4**, and lastly the monometallic Ir(I) catalyst with and NHC ligand substituent on a mesitylene scaffold **3.2** (*i.e.* **3.1** > **3.4** > **3.2**) (Table 4.1). As the TOF was calculated at the time of 50% conversion of substrate to product, this was used for comparison as a more reproducible measure of catalyst efficiency than the time to completion (>95%) of the reaction. This is because the time to

completion can be disproportionally skewed due to small changes in the reaction rate very near to the completion of the reaction.

Table 4.1: Comparison of catalysed hydroamination results (Schemes 4.1, 4.2, and 4.3) using an Ir(I) bimetallic complex (**3.4**, 1 mol%) and Ir(I) monometallic complexes (**3.1** and **3.2**, 2 mol%) with $Na[BAr^F{}_4]$ (2 mol%).

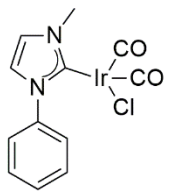

3.1

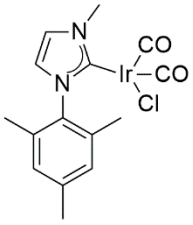

3.2

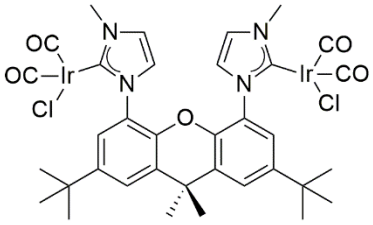

3.4

Hydroamination				
Substrate(s)	Product	Catalyst	TOF / h^{-1}	>95% conv. / min
4.1a 	**4.1b** 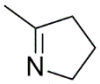	**3.1**	>2123	<0.6
		3.2	674	34.8
		3.4	1682	45.2
4.2a 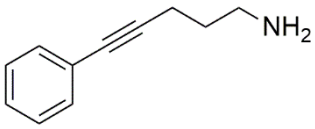	**4.2b** 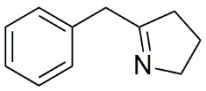	**3.1**	136	21.6
		3.2	73	180.0
		3.4	112	N/A
4.3a + 4.3b 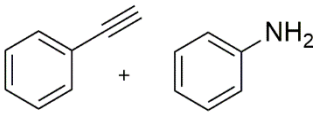	**4.3c** 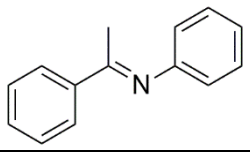	**3.1**	>1336	<1
		3.2	<30	N/A
		3.4	331	110.3

4.3. Iridium(I)-Catalysed Tandem Intramolecular Dihydroalkoxylation of Alkyne Diols

Spiroketals are useful natural products in the pharmaceutical industry, often employed as active ingredients in anti-inflammatory drugs and even in cancer-cell inhibitors.[51,52] However, traditional approaches to the formation of spiroketals often require the use of harsh reaction conditions and multiple steps.[62-64] Therefore, the one-pot, transition metal-catalysed intramolecular dihydroalkoxylation of alkyne diols provides a simple synthetic route towards the formation of spiroketals, as harsh reaction conditions can be avoided.[34,46-48,54] The bimetallic complex **3.4** was investigated as a catalyst for the intramolecular dihydroalkoxylation of 6-(2-(hydroxymethyl)phenyl)hex-5-yn-1-ol (**4.4a**), 1,8-dihydroxy-4-octyne (**4.5a**), and 5-(2-(hydroxymethyl)phenyl)pent-4-yn-1-ol (**4.6a**). The catalytic activity of the bimetallic complex **3.4** in

the dihydroalkoxylation reactions was compared to the results previously obtained in the Messerle research group using the monometallic complexes **3.1** and **3.2** as catalysts.[49]

4.3.1. Catalysed Dihydroalkoxylation Reaction of 6-(2-(Hydroxymethyl)phenyl)hex-5-yn-1-ol (4.4a)

The catalysed intramolecular dihydroalkoxylation of 6-(2-(hydroxymethyl)phenyl)hex-5-yn-1-ol (**4.4a**) to form the 6,6-spiroketal product (**4.4b**) was investigated using 0.5 mol% of the bimetallic complex **3.4** as a catalyst and 1 mol% Na[BAr^F_4] at 100 °C in 1,1,2,2-tetrachloroethane-d_2 (TCE-d_2) (Scheme 4.4).

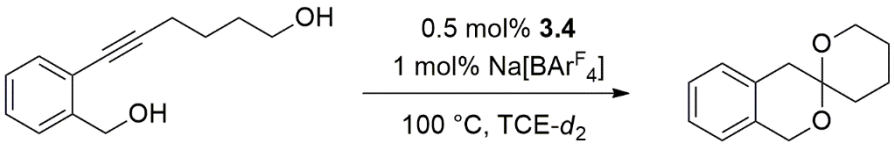

4.4a **4.4b**

Scheme 4.4: Catalysed dihydroalkoxylation of 6-(2-(hydroxymethyl)phenyl)hex-5-yn-1-ol (**4.4a**).

Interestingly, the dihydroalkoxylation reaction of **4.4a** catalysed by **3.4** underwent an induction period of approximately 7 minutes before the conversion of substrate to product began. The rate of reaction was steady until 70% conversion at which point the rate slowed steadily until it plateaued after 180 minutes when it reached >95% conversion (Figure 4.4). An induction period as observed in this reaction can often be attributed to the delayed formation of the active catalyst from the pre-catalyst in solution. Na[BAr^F_4] is poorly soluble in TCE-d_2, and therefore dissolution of the counterion in the solvent once it was heated up to 100 °C may be the cause of the observed induction period. It was particularly likely in this case as the reaction mixture was kept frozen until it was inserted into the NMR spectrometer to prevent the reaction from proceeding before measurements could be taken.

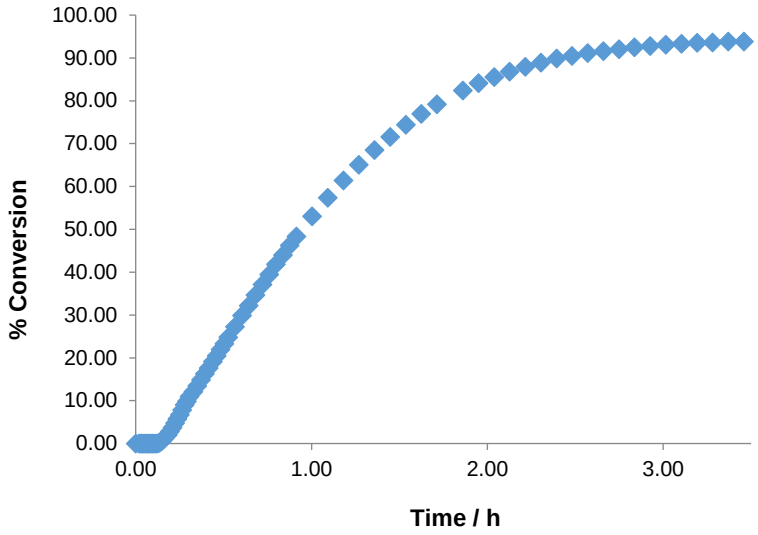

Figure 4.4: Reaction profile for the intramolecular dihydroalkoxylation of **4.4a** catalysed by **3.4**.

4.3.2. Catalysed Dihydroalkoxylation Reaction of 1,8-Dihydroxy-4-octyne (4.5a)

The progress of the dihydroalkoxylation reaction of 1,8-dihydroxy-4-octyne (**4.5a**) was tested using **3.4** as the catalyst (0.5 mol%) and Na[BAr$^F_4$] (1 mol%) as an additive at 60 °C in 1,1,2,2-tetrachloroethane-d_2, forming 1,6-dioxaspiro[4.5]decane (**4.5b**) as the spiroketal product (Scheme 4.5).

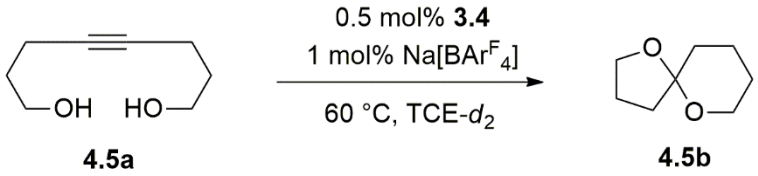

Scheme 4.5: Catalysed dihydroalkoxylation of 1,8-dihydroxy-4-octyne (**4.5a**).

The progress of the catalysed dihydroalkoxylation reaction of **4.5a** using the bimetallic catalyst **3.4** displayed a sigmoid reaction profile (Figure 4.5). The reaction proceeded at a slow rate that gradually increased from the time at 10% conversion until the time at approximately 60% conversion, and then slowed as the reaction reached full conversion after 33 minutes. The turnover frequency of the bimetallic iridium(I)-catalysed reaction was 676 h^{-1}. As discussed in Section 4.3.1, the slow dissolution of Na[BAr$^F_4$] in the solvent could lead to in the observation of a sigmoid curve such as the one depicted in Figure 4.5.

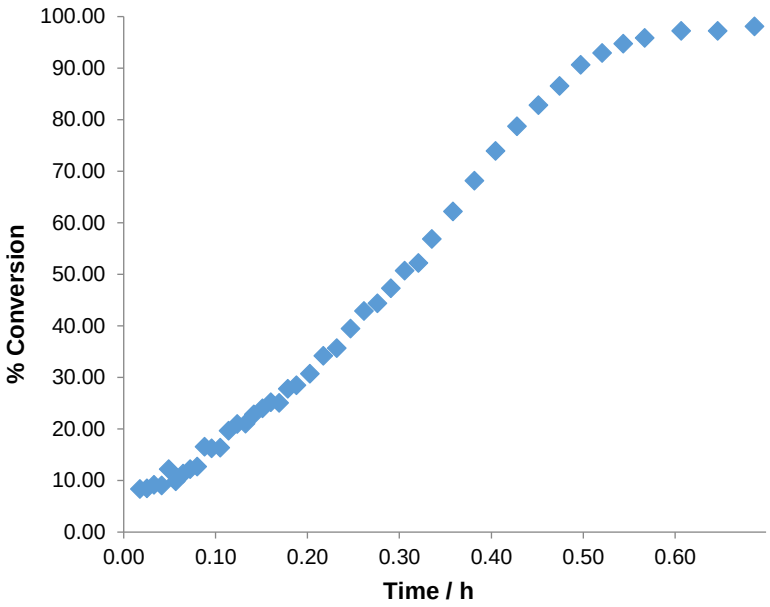

Figure 4.5: Reaction profile for the intramolecular dihydroalkoxylation of **4.5a** catalysed by **3.4**.

4.3.3. Catalysed Dihydroalkoxylation Reaction of 5-(2-(Hydroxymethyl)phenyl)pent-4-yn-1-ol (4.6a)

The catalysed dihydroalkoxylation reaction of 5-(2-(hydroxymethyl)phenyl)pent-4-yn-1-ol (**4.6a**) was investigated using 0.5 mol% of **3.4** as the catalyst and 1 mol% of Na[BAr^F_4] as an additive at 100 °C in TCE-d_2 (Scheme 4.6). This reaction results in the formation of two spiroketal products; 4,5-dihydro-3*H*-spiro[furan-2,3'-isochroman] (6,5-spiroketal, **4.6b**), and 3',4',5',6'-tetrahydro-3*H*-spiro[isobenzofuran-1,2'-pyran] (5,6-spiroketal, **4.6c**).

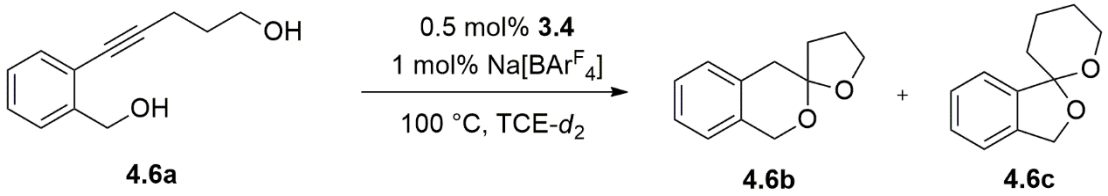

4.6a **4.6b** **4.6c**

Scheme 4.6: Catalysed dihydroalkoxylation of 5-(2-(hydroxymethyl)phenyl)pent-4-yn-1-ol (**4.6a**).

As with the previous dihydroalkoxylation reactions (Sections 4.3.1 and 4.3.2), the reaction profile of the catalysed dihydroalkoxylation reaction of **4.6a** appears sigmoidal in shape. However, the sigmoidal shape is less pronounced than in the dihydroalkoxylation of 1,8-dihydroxy-4-octyne (**4.5a**, Figure 4.5), possibly due to the fact that a higher temperature of 100 °C was used in this reaction (as opposed to 60 °C for the reaction with **4.5a**), resulting in better solubility of Na[BAr^F_4] in TCE-d_2. The TOF achieved by the bimetallic catalyst **3.4** for this reaction was 1360 h^{-1} with the reaction reaching >95% conversion in just over 16 minutes. The bimetallic complex **3.4** achieved a product selectivity of 2:1 favouring the 5,6-spiroketal (**4.6c**) over the 6,5-spiroketal (**4.6b**). The formation of

the product **4.6c** proceeds by a sequential two-step mechanism comprised of 5-exo-dig cyclisation, followed by an aliphatic 6-endo-dig hydroalkoxylation.[47] The selectivity for the 5,6-spiroketal product (**4.6c**) using the bimetallic catalyst **3.4** is equal to the highest selectivity that has previously been reported in the literature by Hashmi and colleagues using gold(I) catalysts with phosphite ligands.[65]

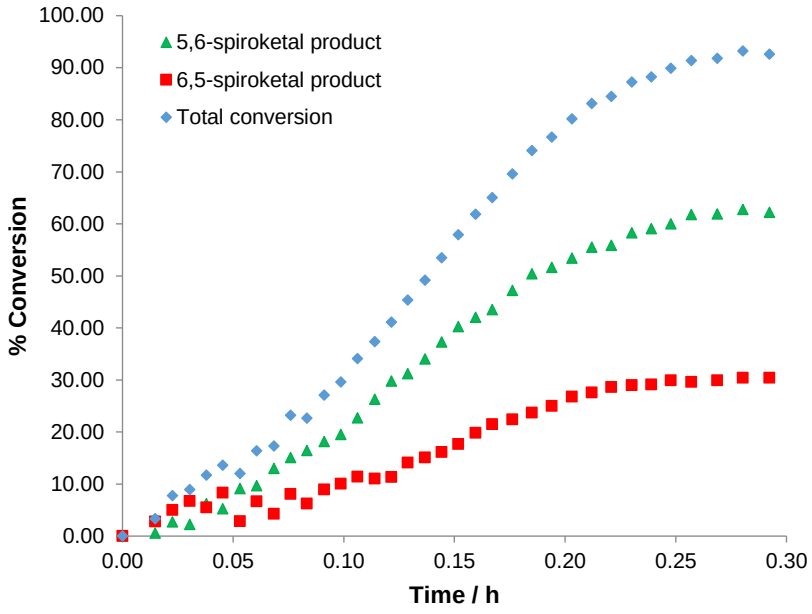

Figure 4.6: Reaction profile for the intramolecular dihydroalkoxylation **4.6a** catalysed by **3.4**.

4.3.4. Comparison of 3.4 with Monometallic Catalysts 3.1 and 3.2

The catalysed two-step dihydroalkoxylation reactions of **4.4a** and **4.5a** both demonstrated similar trends to those observed for the hydroamination reactions in terms of which catalyst was the most active. For both substrates **4.4a** and **4.5a**, the TOFs of the reactions catalysed by the bimetallic catalyst **3.4** were lower than the TOFs of the reactions catalysed by [$Ir(CO)_2Cl$(PhNHC)] (**3.1**) and higher than the TOFs of the reactions catalyst by [$Ir(CO)_2Cl$(MesNHC)] (**3.2**) (Table 4.2). For the dihydroalkoxylation reaction of **4.6a** however, the bimetallic catalyst **3.4** was less active than both of the monometallic analogues (**3.1** and **3.2**) (Table 4.2). This observation may be explained, not by a reduced activity of the bimetallic complex **3.4**, but by an increase in the activity of the monometallic complex **3.2** for the dihydroalkoxylation of this particular alkyne diol substrate (**4.6a**). Not only does the monometallic complex **3.2** demonstrate large activity in terms of reaction rate for the dihydroalkoxylation of **4.6a**, but it also exhibits an unprecedentedly large selectivity for the 5,6-spiroketal product (**4.6c**), yielding products **4.6b** and **4.6c** in a 1:14 ratio.[49]

Table 4.2: Comparison of catalysed dihydroalkoxylation results (Schemes 4.4, 4.5, and 4.6) using Ir(I) bimetallic complex (**3.4**, 0.5 mol%) and Ir(I) monometallic complexes (**3.1** and **3.2**, 1 mol%) with $Na[BAr^F{}_4]$ (1 mol%).

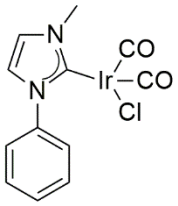

3.1

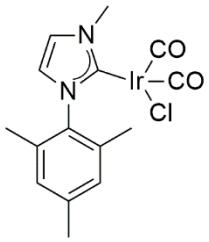

3.2

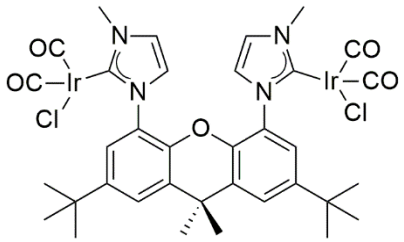

3.4

Dihydroalkoxylation				
Substrate	Product(s)	Catalyst	TOF / h^{-1}	>95% conv. / min
4.4a 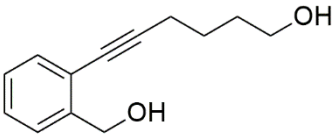	**4.4b** 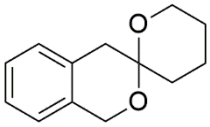	**3.1**	255	47.4
		3.2	132	42.0
		3.4	210	180.9
4.5a 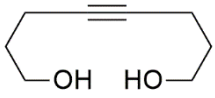	**4.5b** 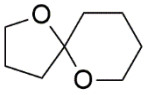	**3.1**	817	5.9
		3.2	647	7.4
		3.4	676	32.7
4.6a 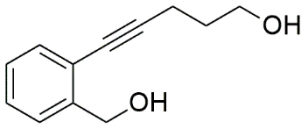	**4.6b + 4.6c** 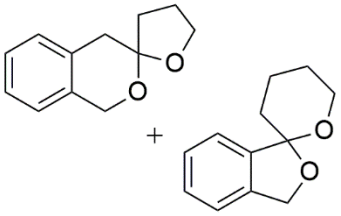	**3.1**	2950	4.2
		3.2	2143	3.0
		3.4	1360	16.8

4.4. Monometallic vs. Bimetallic Catalysts: Assessing Bimetallic Cooperativity

At first glance, it would seem that the bimetallic complex **3.4** does not exhibit bimetallic cooperativity as a catalyst for the hydroamination and tandem dihydroalkoxylation reactions investigated in this project. The turnover frequencies of each of the reactions catalysed by **3.4** are generally of a magnitude that lies between the TOFs of the reactions catalysed by the two analogous monometallic complexes (**3.1**, and **3.2**). The relative efficiencies of the three complexes for each reaction considered will be dependent on the specific mechanism of each reaction and the role of the catalyst. The differences between the activities of the catalysts will be due to electronic or structural differences of the active metal centre, or due to an additional cooperative effect in the case of the bimetallic complex. Structurally, the Ir(I)-NHC motif bound to the xanthene scaffold in the bimetallic complex **3.4** does not differ greatly to the Ir(I)-NHC motif bound to the mesitylene substituent of the

monometallic complex **3.2**, and differs only slightly to the Ir(I)-NHC motif bound to the phenyl substituent. The implications of this observation are that the major factors affecting the catalytic efficiency of the catalysts are likely to be electronic, and not merely steric as has been observed in previous bimetallic studies by the Messerle research group.[34,46,66]

To explore the possible electronic contributions to the differences in the catalytic efficiencies of the three complexes (**3.1**, **3.2**, and **3.4**), the differences in ^{13}C NMR spectroscopy chemical shifts and carbonyl stretches from the infrared (IR) spectra of the complexes were analysed for trends that matched the trends observed in the catalytic activity of the complexes. In the ^{13}C NMR spectra of the catalysts, the differences in chemical shift of the carbene (**C**2, Figure 4.7) matched the trend in catalytic activity of the complexes and are tabulated alongside the wavenumbers of the IR spectra carbonyl stretches in Table 4.3.

Table 4.3: Table of the infrared spectroscopy (IR) carbonyl stretches and the ^{13}C NMR spectroscopy chemical shifts of the carbene (**C**2) of $[Ir(CO)_2Cl(MesNHC)]$ (**3.2**), $[Ir_2((MeNHC)_2{}^tXan)(CO)_4Cl_2]$ (**3.4**), and $[Ir(CO)_2Cl(PhNHC)]$ (**3.1**).[49]

Catalyst	**3.2**	**3.4**	**3.1**
^{13}C NMR shift of **C**2	175.1 ppm	174.6 ppm	173.7 ppm
IR ν_{CO}	2054.45 cm^{-1} 1974.22 cm^{-1}	2056.39 cm^{-1} 1972.01 cm^{-1}	2066.86 cm^{-1} 1984.62 cm^{-1}

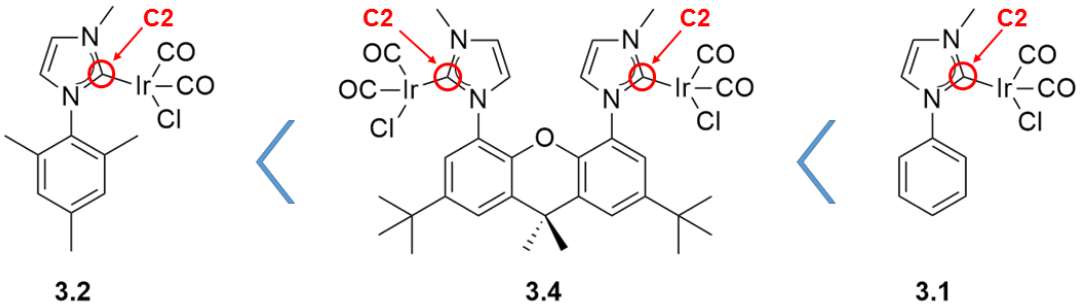

Figure 4.7: Catalysts **3.2**, **3.4**, and **3.1**, ranked in order of increasing activity observed in each of the hydroamination reactions and the dihydroalkoxylation reactions of **4.4a** and **4.5a**.

The trend in chemical shift of **C**2 for each complex mimics the trend in catalytic activity of the complexes, such that the further upfield the chemical shift of **C**2 is, the better the observed activity of the catalyst.[67] This correlates with a more electron poor iridium metal centre in the better performing catalysts. The observed carbonyl stretches in the IR spectra of the catalysts support this observation as the strongest C-O carbonyl bonds as determined by IR spectroscopy correlate with the most electron poor metal centres as inferred by the ^{13}C NMR spectroscopy data.[67]

Another consideration in the existence of bimetallic cooperativity present in **3.4** is, in terms of their electronic and steric properties, which of the monometallic complexes (**3.1** and **3.2**) is a closer analogue of **3.4**. The carbonyl stretches of the IR spectra would suggest that the mesitylene monometallic complex **3.2** is a much closer analogue to bimetallic complex **3.4** as the stretches only differ by approximately ± 2 cm^{-1} as opposed to the approximately 10 – 12 cm^{-1} difference between the bimetallic complex **3.4** and the phenyl monometallic complex **3.1**. Also, sterically both the mesitylene monometallic complex **3.2** and the bimetallic complex **3.4** contain a substituent *meta* to the NHC on the aromatic scaffold, whereas the phenyl monometallic complex **3.1** does not. Therefore, if the mesitylene monometallic complex **3.2** is a closer analogue of the bimetallic complex **3.4**, this could be evidence that a slight bimetallic cooperative enhancement has been observed for the alkyne activation reactions that were investigated. In addition, the better of the three catalysts, $[Ir(CO)_2Cl(PhNHC)]$ (**3.1**), may not be a close enough analogue of the bimetallic complex **3.4** to assess bimetallic cooperativity. However, more investigations would need to be performed, such as the design of more closely related monometallic analogues of the bimetallic complex **3.4**.

Chapter 5 : Conclusions and Future Directions

5.1. Conclusions

This work describes the synthesis of novel binucleating *bis*-*N*-heterocyclic carbene pro-ligands containing a *tert*-butyl substituted xanthene bridging scaffold (**2.2**, **2.3**, and **2.4**). The pro-ligand **2.2** was used in the synthesis and characterisation of iridium(I) bimetallic complexes (**3.3** and **3.4**). The efficiency of the bimetallic complex $[Ir_2((MeNHC)_2{}^tXan)(CO)_4Cl_2]$ (**3.4**) as a catalyst for the hydroamination of alkynyl amines and the tandem dihydroalkoxylation of alkyne diols to form spiroketals was evaluated by comparison to the efficiency of two previously examined analogous monometallic Ir(I) complexes (**3.1** and **3.2**) as catalysts for the same reactions.

The synthesis of the novel binucleating pro-ligands (**2.2** and **2.4**) was achieved through an Ullman-type coupling of imidazole to the brominated xanthene scaffold **2.5** to generate the precursor to the pro-ligand **2.1** in 78% yield. The pro-ligand precursor **2.1** was then alkylated in an S_N2 reaction with the appropriate alkyl halide to generate the pro-ligands $[(MeNHC)_2{}^tXan]I_2$ (**2.2**), and $[(BnNHC)_2{}^tXan]Br_2$ (**2.4**) in 98% and 74% yields respectively. An anion exchange was performed on **2.2** to generate a $[BPh_4]^-$ salt of the ligand (**2.3**) for the purpose of having a weakly coordinating anion that would allow deprotonation of the carbene proton using a weak base. Each of the pro-ligands (**2.2**, **2.3**, and **2.4**) were fully characterised by ^1H and ^{13}C NMR spectroscopy and mass spectrometry.

The bimetallic Ir(I) complex $[Ir_2((MeNHC)_2{}^tXan)(COD)_2Cl_2]$ (**3.3**) was synthesised by two separate methods. **3.3** was successfully synthesised from pro-ligand $[(MeNHC)_2{}^tXan][BPh_4]_2$ (**2.3**) *via* deprotonation of the imidazolium proton to form the carbene ligand and subsequent complexation with the Ir(I) precursor to generate the clean product **3.3** in 40% yield. A silver transmetallation reaction was employed with pro-ligand $[(MeNHC)_2{}^tXan]I_2$ (**2.2**) that generated **3.3** in 69% yield, however separation of the product **3.3** from the residual silver salt was difficult and in most cases unsuccessful. The bimetallic complex **3.3** was then carbonylated in a reaction with gaseous CO to form the bimetallic complex $[Ir_2((MeNHC)_2{}^tXan)(CO)_4Cl_2]$ (**3.4**) in 64% yield.

The bimetallic complex **3.4** was investigated for its efficiency as a catalyst for both the hydroamination of alkynes using amines and the tandem intramolecular dihydroalkoxylation of alkyne diols to form spiroketals. The efficiency of **3.4** as a catalyst was compared to the efficiency of two previously developed and tested analogous monometallic Ir(I) complexes (**3.1** and **3.2**) as catalysts for the same reactions. It was found that the bimetallic catalyst **3.4** was less efficient than **3.1** for each of the reactions tested, but more efficient than the monometallic analogue **3.2** for the

majority of the reactions. It was also observed that the trend in catalytic activity of the complexes was mimicked by the electron deficiency of the Ir(I) metal centre, such that a more electron poor metal centre correlates with greater catalyst activity. However, the monometallic complex **3.2** was found to be a much closer analogue to the bimetallic complex **3.4** both electronically and sterically, suggesting that bimetallic cooperative enhancement may have been observed for the bimetallic complex **3.4**.

5.2. Future Directions

The work described in this thesis has resulted in observations that will lead to new areas for investigation, as follows:

Firstly, the electronic and differences between the two monometallic complexes (**3.1** and **3.2**) and the bimetallic complex **3.4** were deemed to be the major factor in the difference in catalytic activity of the three complexes. Thus, the development of an analogous monometallic catalyst with the same electronic properties as the bimetallic complex **3.4** would provide a much better benchmark from which to assess the level of bimetallic cooperativity in **3.4**. Two of the proposed monometallic analogues (**5.1** and **5.2**) are shown in Figure 5.1.

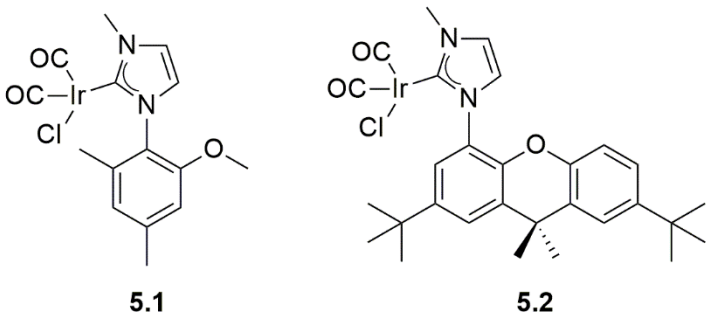

5.1 **5.2**

Figure 5.1: Proposed monometallic analogues of bimetallic complex **3.4**.

Considering the fact that the monometallic complex **3.1** out-performed both **3.2** and **3.4** as the catalyst for the chosen alkyne activation reactions, the development of a more closely analogous bimetallic complex of this catalyst would be a logical progression. Hence, we propose the synthesis of a bimetallic Ir(I) complex containing two monodentate NHC ligand substituents located on an anthracene scaffold. Homobimetallic Rh(I) complexes containing anthracene bridging scaffolds have previously been reported to have better efficiency as catalysts for the dihydroalkoxylation of alkyne diols.[34]

Lastly, the complexation of the ligands presented in this work with a different metal such as rhodium(I) or even the same metal in a different oxidation state (*i.e.* iridium(III)) could provide further comparisons for both bimetallic cooperativity and the effects of the electronic properties of the complex on its efficiency as a catalyst. A Rh(I) analogue of the monometallic complex **3.1** was previously investigated by Diachenko *et al.* for its efficiency as a catalyst for the dihydroalkoxylation of alkyne diols.[21] Thus, the development of a Rh(I) analogue of the bimetallic complex **3.4** on both xanthene and anthracene scaffolds could provide suitable comparisons of catalytic efficiency.

Chapter 6 : Experimental

6.1. General Experimental

All manipulations of air sensitive materials and metal complexes were performed using standard Schlenk or vacuum techniques.[68] For the purpose of manipulations involving air sensitive materials and metal complexes, solvents were either dried and distilled according to literature procedures[69] or dispensed from an LC Technology Solutions Inc. solvent purification system and stored in glass ampules with Youngs© Teflon valves under nitrogen gas. The compressed bulk gases nitrogen (>99.5%) and carbon monoxide (>99.5%) were purchased from British Oxygen Company.

Iridium(III) chloride hydrate ($IrCl_3.xH_2O$) was purchased from Precious Metals Online (PMO) P/L, and all other chemicals were purchased from Alfa-Aesar Inc. or Sigma-Aldrich Co. LLC and used as received. All deuterated NMR solvents were obtained from Cambridge Isotopes Laboratories (CIL) and used without further purification. $[Ir(COD)Cl]_2$,[70] $Na[BAr^F_4]$,[71] and 4-pentyn-1-amine (**4.1a**) [72,73] were synthesised by literature methods. Ligand precursor and substrates 4,5-dibromo-2,7-di-*tert*-butyl-9,9-dimethyl-9H-xanthene (**2.5**), 6-(2-(hydroxymethyl)phenyl)hex-5-yn-1-ol (**4.4a**), oct-4-yne-1,8-diol (**4.5a**), 5-phenylpent-4-yn-1-amine (**4.2a**) were provided by Dr. Mark Gatus. Substrate 5-(2-(hydroxymethyl)phenyl)pent-4-yn-1-ol (**4.6a**) was provided by Mr. Matthew Peterson.

The ^1H and ^{13}C NMR spectra were acquired on Bruker AVIIIHD 400 MHz and AVIIIHD 500 MHz spectrometers operating at 400 MHz and 500 MHz (^1H), or 100 MHz and 125 MHz (^{13}C). The spectra were acquired by the author at 25 °C unless stated otherwise. Chemical shifts (δ, quoted in ppm) are reported with uncertainties of ±0.01 ppm for ^1H and ±0.05 ppm for ^{13}C, and were referenced to residual solvent signals internally.[74] The typical uncertainty of reported coupling constants (J, reported in Hz) are ±0.05 Hz for ^1H-^1H couplings and ±0.5 Hz for ^{13}C-^{11}B couplings. The reported multiplicities for NMR resonances are abbreviated as follows: s, singlet; d, doublet; t, triplet; q, quartet; m multiplet; br, broad; and dd, doublet of doublets. Novel organic and organometallic compounds were assigned using one-dimensional ^1H, ^{13}C, and DEPT-135 (Distortionless Enhancement by Polarization Transfer with a pulse angle of 135°) NMR techniques as well as the following two-dimensional NMR techniques: Correlation Spectroscopy (COSY); Nuclear Overhauser Effect Spectroscopy (NOESY); Heteronuclear Single Quantum Coherence (HSQC); and Heteronuclear Multiple Bond Correlation (HMBC). Processing of NMR data was performed using either TopSpin™ (Bruker) or Mnova™ (Mestrelab Research).

Elemental microanalyses were carried out at the Chemical Analysis Facility in Macquarie University using a PerkinElmer Elemental Analyser, Model PE2400 CHNS/O with PC based data

system, PE Datamanager 2400 for Windows™ and a PerkinElmer AD-6 Ultra Micro Balance. Infrared spectra were recorded using a Nicolet iS10 FT-IR single beam spectrometer at a resolution of 4 cm^{-1}. OMNIC 8.2 Series software (Thermo Scientific) was used for FT-IR data collection, spectra processing and analysis.

Mass spectrometry was performed by Mr. Matthew Peterson at the BioAnalytical Mass Spectrometry Facility (BMSF), in the University of New South Wales using a Thermo LTQ Orbitrap XL (HR-ESI-MS, High Resolution Electro-Spray Ionisation Mass Spectrometry) and by Mr Raphael Lam at the Department of Molecular Sciences in Macquarie University using a Shimadzu LCMS-2010EV – Quadrupole Mass Spectrometer (ESI-LC/MS). $[M]^+$ is used to denote the molecular weight of the ionised compound of interest or cationic fragment in reporting of mass spectral data. Mass spectrometry prediction was performed using Thermo Xcalibur 2.2 Qual Browser software.

6.2. Synthesis of Ligands

6.2.1. 1,1'-(2,7-Di-*tert*-butyl-9,9-dimethyl-9H-xanthene-4,5-diyl)bis(1H-imidazole) (2.1)

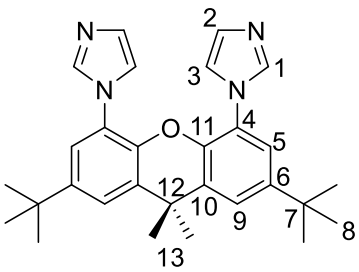

4,5-Dibromo-2,7-di-*tert*-butyl-9,9-dimethyl-9H-xanthene (**2.5**) (1.00 g, 2.09 mmol) was dissolved in a solution of imidazole (0.746 g, 11.0 mmol) and K_2CO_3 (1.53 g, 11.1 mmol) in dry DMF (100 mL). Copper(I) iodide (0.397 g, 2.09 mmol) was added and the stirring mixture was refluxed at 180 °C for 48 hours. The cloudy orange mixture was allowed to cool to room temperature, at which point the mixture turned dark green. The mixture was filtered through Celite® to remove the majority of the green solid. The reaction mixture was stirred in DCM (100 mL) and washed with a solution of ammonia (28%, 30 mL) in water (50 mL) three times. The ammonia/water solution was saturated with LiCl on the third wash to remove any remaining DMF. The organic layer was extracted and stirred in a saturated Na_2[EDTA] solution (100 mL) for 2 hours. The organic layer was separated, dried over $MgSO_4$ and filtered to afford a yellow solution. The solvent was removed under reduced pressure to afford an oily yellow residue. The oily residue was precipitated from the minimum amount of DCM in excess stirring hexane at 0 °C to yield 1,1'-(2,7-di-*tert*-butyl-9,9-dimethyl-9H-xanthene-4,5-diyl)bis(1H-imidazole) (**2.1**) as a beige powder.

Yield: 0.747 g (1.64 mmol), 78%.

^{1}H NMR (400 MHz, CD_2Cl_2): δ 7.51 (m, $^4J_{H\text{-}H}$ = 2.3 Hz, 2H, **H**9), 7.50 (m, $^3J_{H\text{-}H}$ = 1.2 Hz, 2H, **H**3), 7.22 (d, $^4J_{H\text{-}H}$ = 2.3 Hz, 2H, **H**5), 7.02 (t, $^4J_{H\text{-}H}$ = 1.1 Hz, 2H, **H**1), 6.94 (t, $^3J_{H\text{-}H}$ = 1.2 Hz, 2H, **H**2), 1.73 (s, 6H, **H**13), 1.35 (s, 18H, **H**8).

^{13}C{^{1}H} NMR (100 MHz, CD_2Cl_2): δ 147.4 (**C**6), 141.8 (**C**11), 137.5 (**C**3), 131.7 (**C**10), 129.5 (**C**1), 125.4 (**C**4), 122.8 (**C**9), 122.0 (**C**5), 120.7 (**C**2), 35.6 (**C**12), 35.0 (**C**7), 32.2 (**C**13), 31.5 (**C**8).

ESI-MS (CH_3OH), *m/z* (%): 455.3 (100) $[M]^+$ amu.

Anal. Found: C, 75.26; H, 6.81; N, 12.64. Calcd. for $C_{29}H_{34}N_4O$: C, 76.60; H, 7.55; N, 12.33%.

6.2.2. 1,1'-(2,7-Di-*tert*-butyl-9,9-dimethyl-9H-xanthene-4,5-diyl)bis(3-methyl-1H-imidazol-3-ium) iodide [(MeNHC)$_2$^{t}Xan]I$_2$ (2.2)

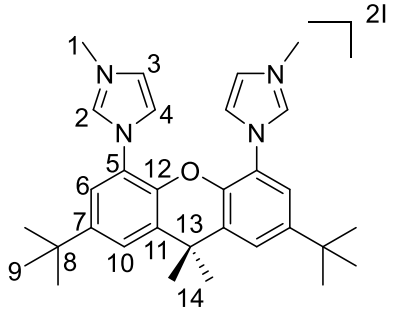

1,1'-(2,7-Di-*tert*-butyl-9,9-dimethyl-9H-xanthene-4,5-diyl)bis(1H-imidazole) (**2.1**) (0.200 g, 0.439 mmol) and iodomethane (0.7 mL, 11.5 mmol) were added to acetonitrile (15 mL) in a pressure flask. The mixture was stirred at 50 °C in the absence of light for 24 hours. The mixture was allowed to cool before the solvent was removed under reduced pressure to afford an oily yellow residue. The oily residue was precipitated from the minimum amount of DCM in excess stirring hexane to yield 1,1'-(2,7-di-*tert*-butyl-9,9-dimethyl-9H-xanthene-4,5-diyl)bis(3-methyl-1H-imidazol-3-ium) iodide (**2.2**) as a pale yellow powder.

Yield: 0.318 g (0.431 mmol), 98%.

^{1}H NMR (400 MHz, CD_2Cl_2): δ 9.65 (s, 2H, **H**2), 8.39 (t, $^4J_{H\text{-}H}$ = 1.7 Hz, 2H, **H**3), 7.69 (d, $^4J_{H\text{-}H}$ = 2.2 Hz, 2H, **H**10), 7.38 (t, $^4J_{H\text{-}H}$ = 1.7 Hz, 2H, **H**4), 7.30 (d, $^4J_{H\text{-}H}$ = 2.2 Hz, 2H, **H**6), 4.34 (s, 6H, **H**1), 1.78 (s, 6H, **H**14), 1.36 (s, 18H, **H**9).

^{13}C{^{1}H} NMR (100 MHz, CD_2Cl_2): δ 148.6 (**C**7), 140.9 (**C**12), 138.3 (**C**2), 131.8 (**C**11), 126.6 (**C**10), 125.2 (**C**3), 123.5 (**C**4), 122.5 (**C**6), 122.1 (**C**5), 37.9 (**C**1), 35.5 (**C**13), 35.3 (**C**8), 32.9 (**C**14), 31.4 (**C**9).

ESI-MS (CH_3OH), *m/z* (%): 612.2 (100) $[M - I]^+$ amu.

Anal. Found: C, 51.90; H, 6.70; N, 6.61. Calcd. for $C_{31}H_{40}I_2N_4O$: C, 50.41; H, 5.47; N, 7.59%.

6.2.3. 1,1'-(2,7-Di-*tert*-butyl-9,9-dimethyl-9H-xanthene-4,5-diyl)bis(3-methyl-1H-imidazol-3-ium) tetraphenylborate [(MeNHC)$_2$^{t}Xan][BPh$_4$]$_2$ (2.3)

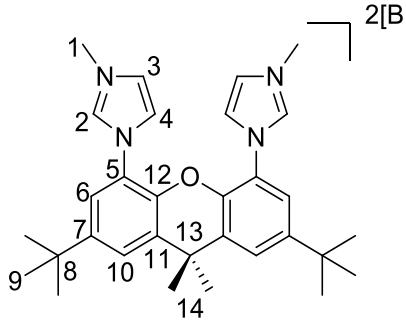

1,1'-(2,7-Di-*tert*-butyl-9,9-dimethyl-9H-xanthene-4,5-diyl)bis(3-methyl-1H-imidazol-3-ium) iodide (**2.2**) (0.305 g, 0.413 mmol) and sodium tetraphenylborate (0.285 g, 0.832 mmol) were added to DCM (50 mL) in a round bottom flask and the mixture was stirred at room temperature for 18 hours. The mixture was filtered through Celite® and then the solvent removed under reduced pressure to afford a clear colourless oil. The oil was precipitated from the minimum amount of DCM in excess stirring hexane to yield 1,1'-

(2,7-di-*tert*-butyl-9,9-dimethyl-9H-xanthene-4,5-diyl)bis(3-methyl-1H-imidazol-3-ium) tetraphenylborate (**2.3**) as a white powder.

Yield: 0.332 g (0.296 mmol), 72%.

^{1}H NMR (400 MHz, CD_2Cl_2): δ 7.80 (d, $^{4}J_{H\text{-}H}$ = 2.2 Hz, 2H, **H**10), 7.25 (s, 16H, *ortho*-C**H** of BPh_4) 6.96 (d, $^{4}J_{H\text{-}H}$ = 2.2 Hz, 2H, **H**6), 6.85 (m, $^{3}J_{H\text{-}H}$ = 7.2 Hz, 16H, *meta*-C**H** of BPh_4), 6.75 (m, $^{3}J_{H\text{-}H}$ = 7.2 Hz, 8H, *para*-C**H** of BPh_4) 6.44 (t, $^{4}J_{H\text{-}H}$ = 1.7 Hz, 2H, **H**3), 6.22 (t, $^{4}J_{H\text{-}H}$ = 1.7 Hz, 2H, **H**4), 5.86 (s, 2H, **H**2), 2.84 (s, 6H, **H**1), 1.85 (s, 6H, **H**14), 1.38 (s, 18H, **H**9).

^{13}C{^{1}H} NMR (100 MHz, CD_2Cl_2): δ 164.2 (q, $^{1}J_{B\text{-}C}$ = 49.2 Hz, *ipso*-**C** of BPh_4), 149.2 (**C**7), 140.5 (**C**12), 136.4 (**C**2), 136.2 (*ortho*-**C** of BPh_4), 131.8 (**C**11), 127.4 (**C**10), 126.2 (*meta*-**C** of BPh_4), 124.0 (**C**3), 123.2 (**C**6), 122.7 (**C**4), 122.5 (*para*-**C** of BPh_4), 121.2 (**C**5), 36.8 (**C**1), 35.5 (**C**13), 35.3 (**C**8), 33.4 (**C**14), 31.3 (**C**9).

ESI-MS (CH_3OH), *m/z* (%): 804.4 (100) $[M - BPh_4]^+$ amu.

Anal. Found: C, 84.02; H, 7.37; N, 4.97. Calcd. for $C_{79}H_{80}B_2N_4O$: C, 84.47; H, 7.19; N, 4.99%.

6.2.4. 1,1'-(2,7-Di-*tert*-butyl-9,9-dimethyl-9H-xanthene-4,5-diyl)bis(3-benzyl-1H-imidazol-3-ium) bromide [(BnNHC)$_2$^{t}Xan]Br$_2$ (2.4)

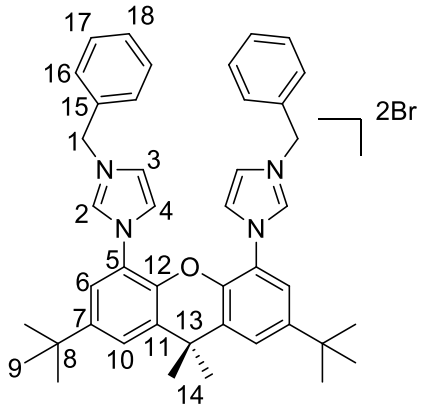

1,1'-(2,7-Di-*tert*-butyl-9,9-dimethyl-9H-xanthene-4,5-diyl)bis(1H-imidazole) (**2.1**) (0.199 g, 0.437 mmol) and benzyl bromide (1.2 mL, 10.5 mmol) were added to acetonitrile (25 mL) in a pressure flask. The mixture was stirred at 50 °C in the absence of light for 24 hours. The mixture was allowed to cool before the solvent was removed under reduced pressure to afford an oily yellow residue. The oily residue was precipitated from the minimum amount of DCM in excess stirring hexane to yield 1,1'-(2,7-di-*tert*-butyl-9,9-dimethyl-9H-xanthene-4,5-diyl)bis(3-benzyl-1H-imidazol-3-ium) bromide (**2.4**) as a fine white powder.

Yield: 0.258 g (0.324 mmol), 74%.

^{1}H NMR (400 MHz, $CDCl_3$): δ 10.00 (s, 2H, **H**2), 8.18 (s, 2H, **H**3), 7.74 (dd, $^{3}J_{H\text{-}H}$ = 7.7, $^{4}J_{H\text{-}H}$ = 1.7 Hz, 4H, **H**16), 7.61 (d, $^{4}J_{H\text{-}H}$ = 2.2 Hz, 2H, **H**10), 7.41 (m, 8H, **H**4, **H**17, **H**18), 7.12 (d, $^{4}J_{H\text{-}H}$ = 2.2 Hz, 2H, **H**6), 5.95 (s, 4H, **H**1), 1.76 (s, 6H, **H**14), 1.33 (s, 18H, **H**9).

^{13}C{^{1}H} NMR (100 MHz, $CDCl_3$): δ 148.3 (**C**7), 140.7 (**C**12), 137.3 (**C**2), 133.7 (**C**15), 131.4 (**C**11), 130.0 (**C**16), 129.7 (**C**18), 129.6 (**C**17), 126.2 (**C**10), 123.6 (**C**4), 123.6 (**C**3), 122.1 (**C**6), 122.0 (**C**5), 53.6 (**C**1), 35.2 (**C**13), 35.0 (**C**8), 33.1 (**C**14), 31.4 (**C**9).

Anal. Found: C, 62.58; H, 5.51; N, 6.79. Calcd. for $C_{43}H_{48}Br_2N_4O$: C, 64.82; H, 6.08; N, 7.03%.

6.3. Synthesis of Ir(I) Complexes

6.3.1. $[Ir_2((MeNHC)_2{}^tXan)(COD)_2Cl_2]$ (3.3)

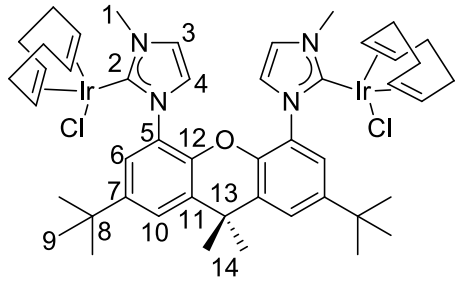

a) ***Via* Deprotonation of NHC:** 1,1'-(2,7-Di-*tert*-butyl-9,9-dimethyl-9H-xanthene-4,5-diyl)bis(3-methyl-1H-imidazol-3-ium) tetraphenylborate (**2.3**) (0.198 g, 0.177 mmol) and K_2CO_3 (0.250 g, 1.81 mmol) were dissolved in degassed acetone (30 mL) and stirred for 10 minutes. $[Ir(COD)Cl]_2$ (0.120 g, 0.179 mmol) was added to the mixture, which was subsequently refluxed at 70 °C in the absence of light for 24 hours. The solvent was then removed under reduced pressure to afford an oily residue. The oily residue was dissolved in DCM (25 mL) and filtered through Celite®, *n*-hexane (70 mL) was added, and the mixture was heated to 60 °C and filtered through Celite® whilst hot. The solvent was then removed under reduced pressure to yield $[Ir_2((MeNHC)_2{}^tXan)(COD)_2Cl_2]$ (**3.3**) as a yellow solid.

Yield: 0.082 g (0.071 mmol), 40%.

b) ***Via* Silver Transmetallation:** 1,1'-(2,7-Di-*tert*-butyl-9,9-dimethyl-9H-xanthene-4,5-diyl)bis(3-methyl-1H-imidazol-3-ium) iodide (**2.2**) (0.102 g, 0.138 mmol) and silver(I) oxide (0.044 g, 0.188 mmol) were dissolved in DCM (30 mL) and stirred at room temperature in the absence of light for 18 hours. The mixture was filtered through Celite®, $[Ir(COD)Cl]_2$ (0.102 g, 0.151 mmol) was added, and the mixture was stirred at room temperature for 2 hours in the absence of light. The mixture was filtered through Celite® and the solvent was removed under reduced pressure, resulting in a brown waxy solid. The waxy residue was precipitated from the minimum amount of DCM in excess stirring hexane to yield $[Ir_2((MeNHC)_2{}^tXan)(COD)_2Cl_2]$ (**3.3**) as a yellow powder.

Yield: 0.110 g (0.095 mmol), 69%.

^{1}H NMR (400 MHz, CD_2Cl_2): δ 8.00 (d, $^4J_{H\text{-}H}$ = 2.3 Hz, 2H, **H**6), 7.57 (d, $^4J_{H\text{-}H}$ = 2.3 Hz, 2H, **H**10), 6.71 (d, $^4J_{H\text{-}H}$ = 2.0 Hz, 2H, **H**3), 6.55 (d, $^4J_{H\text{-}H}$ = 2.0 Hz, 2H, **H**4), 3.99 (s, 6H, **H**1), 1.79 (s, 6H, **H**14), 1.40 (s, 18H, **H**9).

$^{13}C\{^1H\}$ NMR (100 MHz, CD_2Cl_2): δ 181.6 (**C**2), 146.5 (**C**7), 140.9 (**C**12), 129.6 (**C**11), 127.5 (**C**6), 127.2 (**C**5), 123.6 (**C**10), 122.2 (**C**4), 120.9 (**C**3), 37.7 (**C**1), 35.4 (**C**13), 35.1 (**C**8), 33.6 (**C**14), 31.5 (**C**9).

HR-ESI-MS (CH_3OH), *m/z* (%): 1177.3428 (100) $[M + Na]^+$ amu.

Anal. Found: C, 48.96; H, 5.08; N, 4.70. Calcd. for $C_{47}H_{62}Cl_2N_4OIr_2$: C, 48.89; H, 5.42; N, 4.85%.

6.3.2. $[Ir_2((MeNHC)_2{}^tXan)(CO)_4Cl_2]$ (3.4)

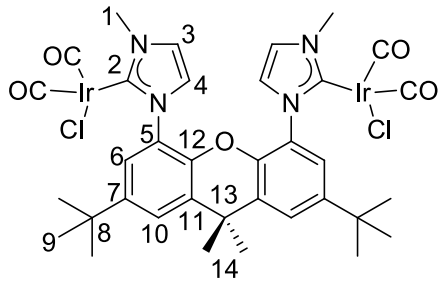

$[Ir_2((MeNHC)_2{}^tXan)(COD)_2Cl_2]$ (**3.3**) (49.5 mg, 0.043 mmol) was dissolved in degassed DCM (30 mL). The mixture was frozen and the headspace of the Schleck flask was evacuated, then filled with $CO_{(g)}$ *via* a balloon. The mixture was thawed and stirred at room temperature for 2 hours. The solvent was reduced to *ca*. 10 mL in volume and then *n*-hexane was added until a precipitate appeared. The solvent was removed under reduced pressure to afford $[Ir_2((MeNHC)_2{}^tXan)(CO)_4Cl_2]$ (**3.4**) as a pale yellow/green solid.

Yield: 29.0 mg (0.028 mmol), 64%.

IR (solid) ν_{co} = 2056, 1972 (s) cm^{-1}.

^1H NMR (400 MHz, CD_2Cl_2): δ 7.57 (d, $^4J_{H\text{-}H}$ = 2.3 Hz, 2H, **H**10), 7.56 (d, $^4J_{H\text{-}H}$ = 2.3 Hz, 2H, **H**6), 6.87 (d, $^4J_{H\text{-}H}$ = 2.0 Hz, 2H, **H**3), 7.16 (s, 2H, **H**4), 3.98 (s, 6H, **H**1), 1.75 (s, 6H, **H**14), 1.37 (s, 18H, **H**9).

$^{13}C\{^1H\}$ NMR (100 MHz, CD_2Cl_2): δ 181.9 (Ir-**C**O), 174.6 (**C**2), 168.7 (Ir-**C**O), 146.5 (**C**7), 140.1 (**C**12), 130.8 (**C**11), 126.0 (**C**6), 126.4 (**C**5), 124.2 (**C**10), 124.7 (**C**4), 121.8 (**C**3), 38.6 (**C**1), 35.4 (**C**13), 35.1 (**C**8), 32.6 (**C**14), 31.4 (**C**9).

HR-ESI-MS (CH_3OH), *m/z* (%): 1073.1338 (100) $[M + Na]^+$ amu.

Anal. Found: C, 40.39; H, 3.33; N, 4.83. Calcd. for $C_{35}H_{38}Cl_2N_4O_5Ir_2$: C, 40.03; H, 3.65; N, 5.34%.

6.4. General Procedure for Catalysed Hydroamination and Tandem Intramolecular Dihydroalkoxylation Reactions

The catalysed alkyne activation reactions (hydroamination and dihydroalkoxylation) were performed on a small scale in Youngs® NMR tubes. The substrate, catalyst and $Na[BAr^F{}_4]$ were weighed out into a small vial, followed by the solvent. The reaction mixture was then transferred into the NMR tube and the tube was immediately placed into a Dewar containing liquid nitrogen/acetone. The temperature of the NMR probe was calibrated using an Omega Microprocessor Thermometer (Model HH23) in neat ethylene glycol. The reaction mixture was briefly thawed and the NMR tube placed in the NMR spectrometer at heightened temperatures for up to 4 hours at which point heating was continued in an oil bath if necessary. ^1H NMR spectra were recorded at appropriate time intervals and the products were identified by comparison with previously reported ^1H NMR data. Integration of the product resonances in comparison to the substrate resonances in the ^1H NMR spectra at each time interval was the method used to determine the rate of conversion. The turnover frequency (TOF) was calculated at the time of 50% conversion of substrate to product by the number of moles of product(s) produced per mole of catalyst used per hour. Catalysis data can be found in Appendix B.

References

(1) Hartwig, J. F. *Organotransition Metal Chemistry: From Bonding to Catalysis*; University Science Books: Mill Valley, California, 2010.
(2) Atkins, P.; De Paula, J. *Physical Chemistry*; Oxford University Press: Oxford, 2010.
(3) Mankad, N. P. *Chem. Eur. J.* **2016**, *22*, 5822.
(4) Michon, C.; MacIntyre, K.; Corre, Y.; Agbossou-Niedercorn, F. *ChemCatChem* **2016**, *8*, 1755.
(5) Mudi, S. Y.; Usman, M. T.; Ibrahim, S. *Am. J. Chem. Appl.* **2015**, *2*, 151.
(6) Van Wyk, S. C.; Onani, M. O.; Ebbe, N. *Chem. Pap.* **2016**, *70*, 1003.
(7) Crabtree, R. H. *The Organometallic Chemistry of the Transition Metals*; 4th ed.; Wiley: Hoboken, NJ, USA, 2005.
(8) Stone, F. G. A.; West, R., Eds.; Academic Press, Inc: New York, 1975; Vol. 13.
(9) Grignard, F. A. V. *Comptes Rendus Chimie* **1900**, *130*, 1322.
(10) Housecroft, C. E. *Inorganic chemistry*; 4th ed. ed.; Pearson: Harlow, England New York, 2012.
(11) Fjermestad, T.; Ho, J. H. H.; Macgregor, S. A.; Messerle, B. A.; Tuna, D. *Organometallics* **2011**, *30*, 618.
(12) Franke, R.; Selent, D.; Börner, A. *Chem. Rev.* **2012**, *112*, 5675.
(13) Astruc, D. *New J. Chem.* **2005**, *29*, 42.
(14) César, V.; Zhang, Y.; Kośnik, W.; Zieliński, A.; Rajkiewicz, A. A.; Ruamps, M.; Bastin, S.; Lugan, N.; Lavigne, G.; Grela, K. *Chem. Eur. J.* **2017**, *23*, 1950.
(15) Samojłowicz, C.; Bieniek, M.; Grela, K. *Chem. Rev.* **2009**, *109*, 3708.
(16) Vougioukalakis, G. C.; Grubbs, R. H. *Chem. Rev.* **2010**, *110*, 1746.
(17) Wang, D.; Astruc, D. *Chem. Rev.* **2015**, *115*, 6621.
(18) Gray, K.; Page, M. J.; Wagler, J.; Messerle, B. A. *Organometallics* **2012**, *31*, 6270.
(19) Hua, C.; Vuong, K. Q.; Bhadbhade, M.; Messerle, B. A. *Organometallics* **2012**, *31*, 1790.
(20) Rumble, S. L.; Page, M. J.; Field, L. D.; Messerle, B. A. *Eur. J. Inorg. Chem.* **2012**, *2012*, 2226.
(21) Diachenko, V.; Page, M. J.; Gatus, M. R. D.; Bhadbhade, M.; Messerle, B. A. *Organometallics* **2015**, *34*, 4543.
(22) Busacca, C. A.; Fandrick, D. R.; Song, J. J.; Senanayake, C. H. *Adv. Synth. Catal.* **2011**, *353*, 1825.
(23) Shum, W. P.; Cannarsa, M. J.; John Wiley: New York, 1997.
(24) Blaser, H. U. *ChemInform* **2010**, *41*, no.
(25) Lee, J. M.; Na, Y.; Han, H.; Chang, S. *Chem. Soc. Rev.* **2004**, *33*, 302.
(26) Zanardi, A.; Corberan, R.; Mata, J. A.; Peris, E. *Organometallics* **2008**, *27*, 3570.
(27) Ramasamy, B.; Ghosh, P. *Eur. J. Inorg. Chem.* **2016**, *2016*, 1448.
(28) Housecroft, C. E.; Sharpe, A. G. *Inorganic Chemistry*; Pearson: New York, USA, 2012.
(29) van Den Beuken, E. K.; Feringa, B. L. *Tetrahedron* **1998**, *54*, 12985.
(30) Osborn, J. A.; Jardine, F. H.; Young, J. F.; Wilkinson, G. *Journal of the Chemical Society A: Inorganic, Physical, Theoretical* **1966**, 1711.
(31) Fagnou, K.; Lautens, M. *Chem. Rev.* **2003**, *103*, 169.
(32) Hartwig, J. F. *Nature* **2008**, *455*, 314.
(33) Ho, J.; Choy, S. W. S.; Macgregor, S. A.; Messerle, B. A. *Organometallics* **2011**, *30*, 5978.
(34) Timerbulatova, M. G.; Gatus, M.; Vuong, K.; Bhadbhade, M.; Agarra, A. G.; Macgregor, S. A.; Messerle, B. A. *Organometallics* **2013**, *32*, 5071.
(35) Vuong, K. Q.; Wong, C. M.; Bhadbhade, M.; Messerle, B. A. *Dalton Transactions* **2014**, *43*, 7540.
(36) Broussard, M. E.; Juma, B.; Train, S. G.; Peng, W. J.; Laneman, S. A.; Stanley, G. G. *Science (Washington, D. C., 1883-)* **1993**, *260*, 1784.
(37) Li, H.; Li, L.; Marks, T. J. *Angew. Chem., Int. Ed.* **2004**, *43*, 4937.
(38) Li, H.; Marks, T. J. *Proc. Natl. Acad. Sci.* **2006**, *103*, 15295.
(39) Guilard, R.; Gros, C. P.; Barbe, J.-M.; Espinosa, E.; Jérôme, F.; Tabard, A.; Latour, J.-M.; Shao, J.; Ou, Z.; Kadish, K. M. *Inorg Chem* **2004**, *43*, 7441.

(40) Guilard, R.; Burdet, F.; Barbe, J.-M.; Gros, C. P.; Espinosa, E.; Shao, J.; Ou, Z.; Zhan, R.; Kadish, K. M. *Inorg Chem* **2005**, *44*, 3972.
(41) Jerome, F.; P. Gros, C.; Tardieux, C.; Barbe, J.-M.; Guilard, R. *Chem. Commun.* **1998**, 2007.
(42) Kadish, K. M.; Frémond, L.; Ou, Z.; Shao, J.; Shi, C.; Anson, F. C.; Burdet, F.; Gros, C. P.; Barbe, J.-M.; Guilard, R. *J. Am. Chem. Soc.* **2005**, *127*, 5625.
(43) Fogg, D. E.; dos Santos, E. N. *Coord. Chem. Rev.* **2004**, *248*, 2365.
(44) Son, S. U.; Park, K. H.; Chung, Y. K. *J. Am. Chem. Soc.* **2002**, *124*, 6838.
(45) Zanardi, A.; Mata, J. A.; Peris, E. *J Am Chem Soc* **2009**, *131*, 14531.
(46) Ho, J. H. H.; Choy, S. W. S.; Macgregor, S. A.; Messerle, B. A. *Organometallics* **2011**, *30*, 5978.
(47) Ho, J. H. H.; Hodgson, R.; Wagler, J.; Messerle, B. A. *Dalton Trans.* **2010**, *39*, 4062.
(48) Choy, S. W. S.; Page, M. J.; Bhadbhade, M.; Messerle, B. A. *Organometallics* **2013**, *32*, 4726.
(49) Gatus, M.; Messerle, B. *Manuscript in preparation*.
(50) Hesp, K. D.; Stradiotto, M. *ChemCatChem* **2010**, *2*, 1192.
(51) Pettit, G. R.; Herald, C. L.; Cichacz, Z. A.; Gao, F.; Boyd, M. R.; Christie, N. D.; Schmidt, J. M. *Nat Prod Lett* **1993**, *3*, 239.
(52) Gouiffès, D.; Moreau, S.; Helbecque, N.; Bernier, J. L.; Hénichart, J. P.; Barbin, Y.; Laurent, D.; Verbist, J. F. *Tetrahedron* **1988**, *44*, 451.
(53) Hopkinson, M. N.; Richter, C.; Schedler, M.; Glorius, F. *Nature* **2014**, *510*, 485.
(54) Gatus, M. R. D.; McBurney, R. T.; Bhadbhade, M.; Messerle, B. A. *Dalton Trans.* **2017**, *46*, 7457.
(55) Zhang, S.; Yang, S.; Lan, J.; Yang, S.; You, J. *Chem. Commun.* **2008**, 6170.
(56) Alcalde, E.; Dinarès, I.; Rodríguez, S.; Garcia de Miguel, C. *Eur. J. Org. Chem.* **2005**, *2005*, 1637.
(57) Saito, S.; Kobayashi, T.; Makino, T.; Yamaguchi, H.; Muto, H.; Azumaya, I.; Katagiri, K.; Yamasaki, R. *Tetrahedron* **2012**, *68*, 8931.
(58) Magill, A. M.; McGuinness, D. S.; Cavell, K. J.; Britovsek, G. J. P.; Gibson, V. C.; White, A. J. P.; Williams, D. J.; White, A. H.; Skelton, B. W. *J. Organomet. Chem.* **2001**, *617–618*, 546.
(59) Librando, I. L.; Creencia, E. C. *Procedia Chem* **2015**, *16*, 299.
(60) Zuo, W.; Braunstein, P. *Organometallics* **2012**, *31*, 2606.
(61) Nair, A. G.; McBurney, R. T.; Gatus, M. R. D.; Binding, S. C.; Messerle, B. A. *Inorg Chem* **2017**, *56*, 12067.
(62) Bai, R.; Cichacz, Z. A.; Herald, C. L.; Pettit, G. R.; Hamel, E. *Mol Pharmacol* **1993**, *44*, 757.
(63) Doubský, J.; Streinz, L.; Šaman, D.; Zedník, J.; Koutek, B. *Org. Lett.* **2004**, *6*, 4909.
(64) Ghosh, S. K.; Hsung, R. P.; Liu, J. *J. Am. Chem. Soc.* **2005**, *127*, 8260.
(65) Blanco Jaimes, M. C.; Rominger, F.; Pereira, M. M.; Carrilho, R. M. B.; Carabineiro, S. A. C.; Hashmi, A. S. K. *Chem. Commun.* **2014**, *50*, 4937.
(66) Page, M. J.; Walker, D. B.; Messerle, B. A. In *Homo- and Heterobimetallic Complexes in Catalysis: Cooperative Catalysis*; Kalck, P., Ed.; Springer International Publishing: Cham, 2016, p 103.
(67) Field, L. D.; Sternhell, S.; Kalman, J. R. *Organic Structures from Spectra*; Wiley, 2008.
(68) Shriver, D. F.; Drezdon, M. A. *The Manipulation of Air Sensitive Compounds*; 2nd ed ed.; John Wiley & Sons: New York, 1986.
(69) Armarego, W. L. F.; Perrin, D. D. *Purification of laboratory chemicals*; 4th ed.; Butterworth Heinemann: Oxford ; Boston, 1996.
(70) Choudhury, J.; Podder, S.; Roy, S. *J. Am. Chem. Soc.* **2005**, *127*, 6162.
(71) Yakelis, N. A.; Bergman, R. G. *Organometallics* **2005**, *24*, 3579.
(72) Burling, S.; Field, L. D.; Messerle, B. A.; Rumble, S. L. *Organometallics* **2007**, *26*, 4335.
(73) Rumble, S., PhD, The University of New South Wales, 2005.
(74) Fulmer, G. R.; Miller, A. J. M.; Sherden, N. H.; Gottlieb, H. E.; Nudelman, A.; Stoltz, B. M.; Bercaw, J. E.; Goldberg, K. I. *Organometallics* **2010**, *29*, 2176.

Appendix A: Spectral Data

1,1'-(2,7-Di-*tert*-butyl-9,9-dimethyl-9H-xanthene-4,5-diyl)bis(1H-imidazole) (2.1)

^{1}H NMR spectrum (400 MHz, CD_2Cl_2, 298K)

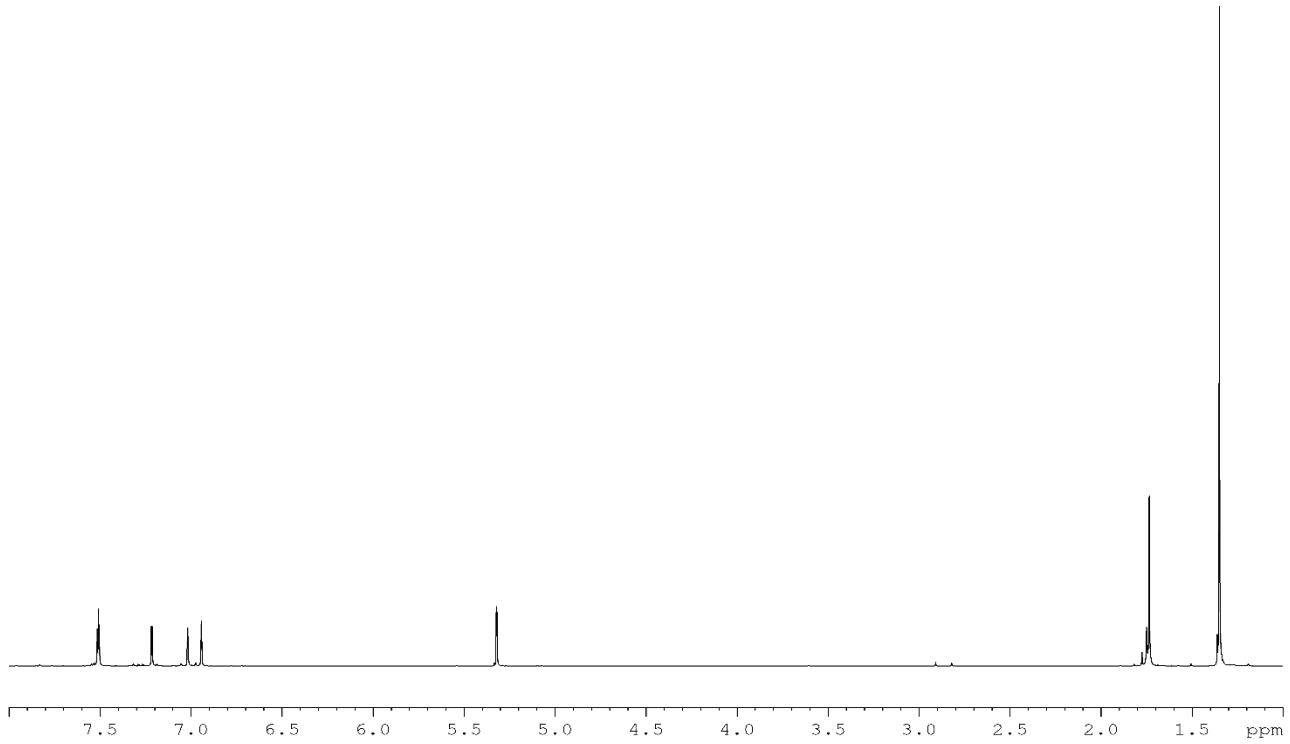

^{13}C NMR spectrum (100 MHz, CD_2Cl_2, 298K)

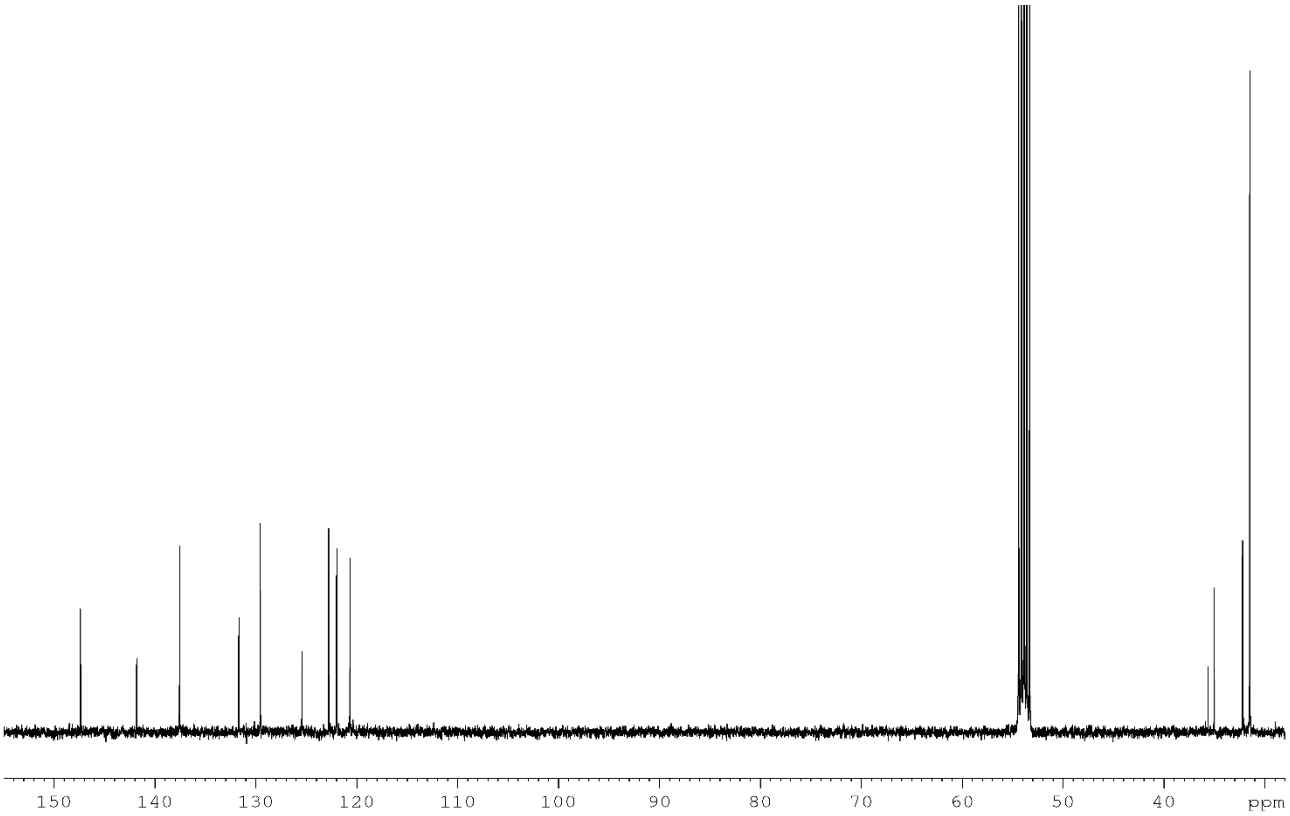

[(MeNHC)$_2$^{t}Xan][BPh$_4$]$_2$ (2.3)

^{1}H NMR spectrum (400 MHz, CD_2Cl_2, 298K)

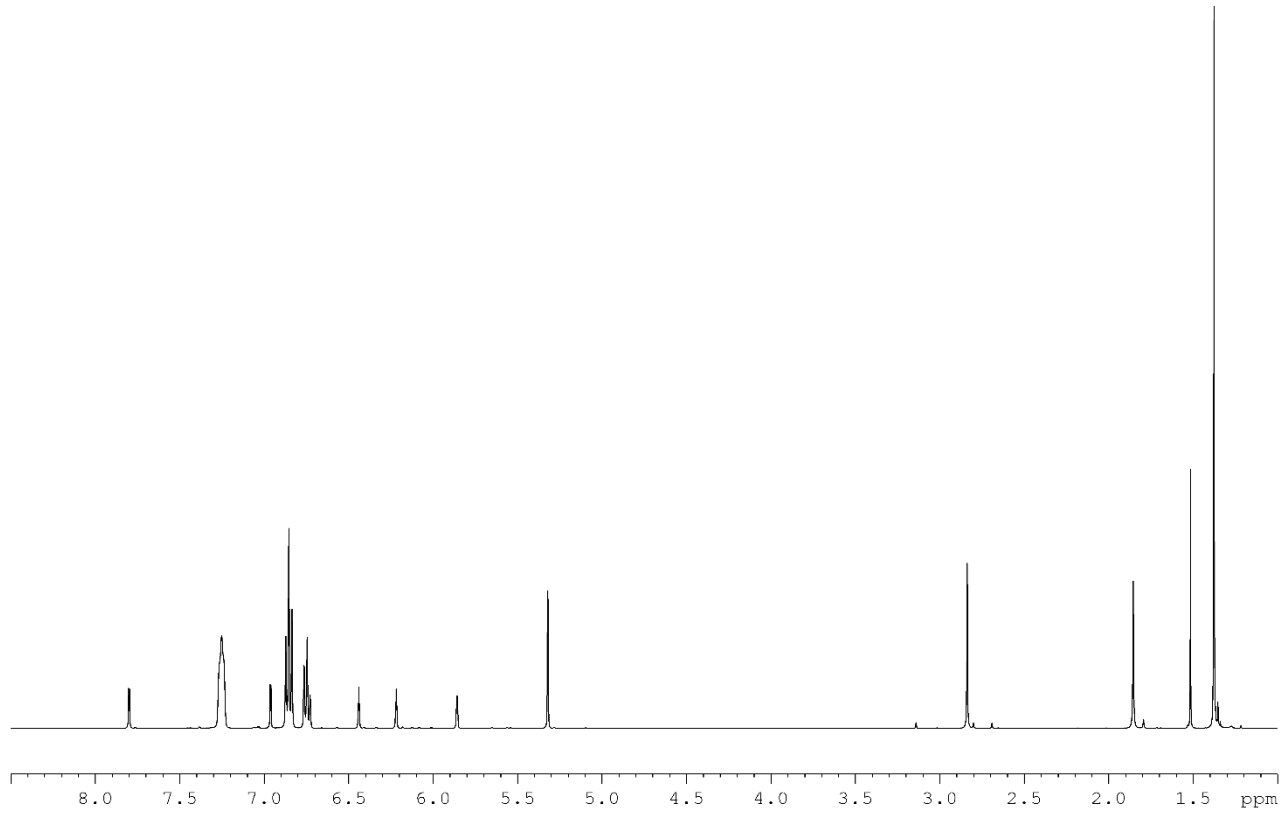

^{13}C NMR spectrum (100 MHz, CD_2Cl_2, 298K)

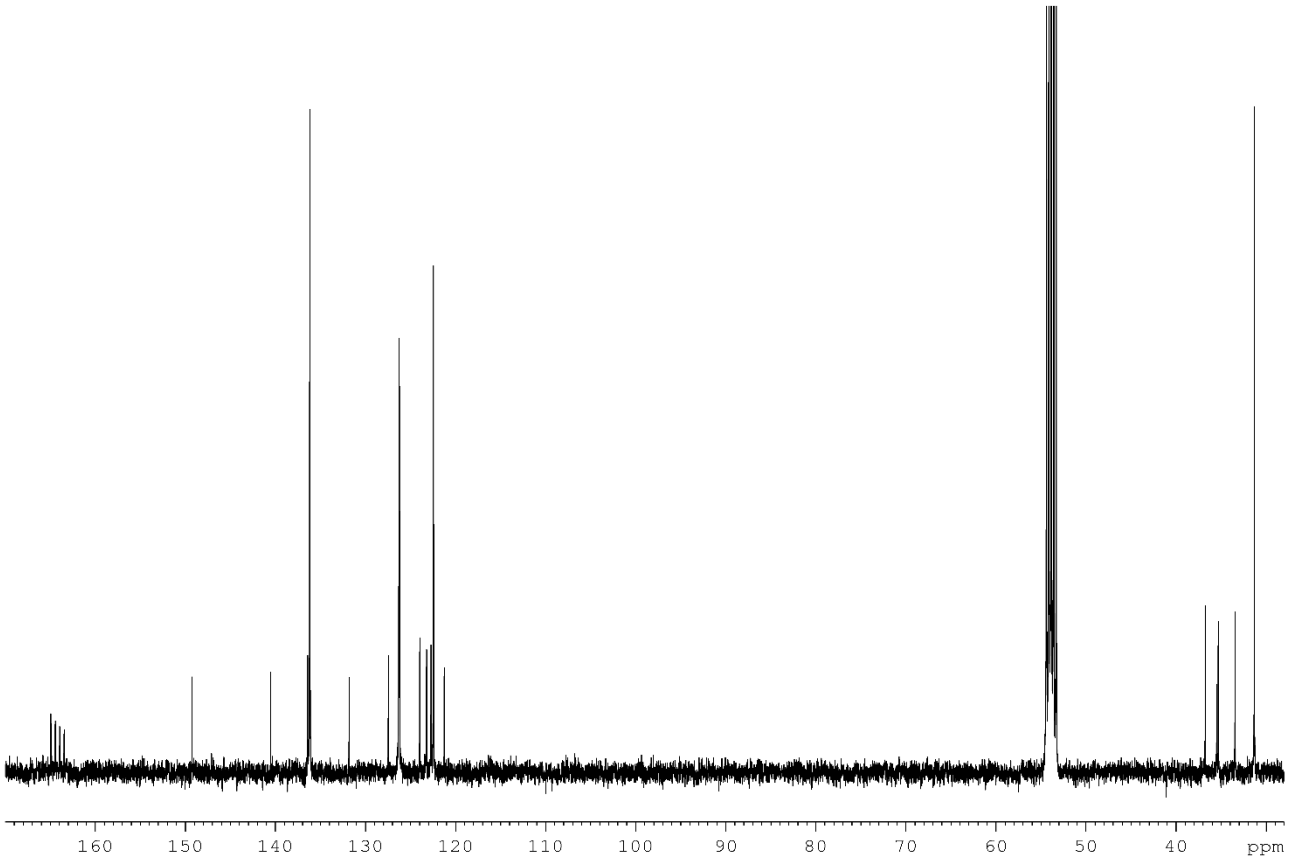

[Ir_2((^{t}MeNHC)$_2$Xan)(COD)$_2$$Cl_2$] (3.3)

^{1}H NMR spectrum (400 MHz, CD_2Cl_2, 298K)

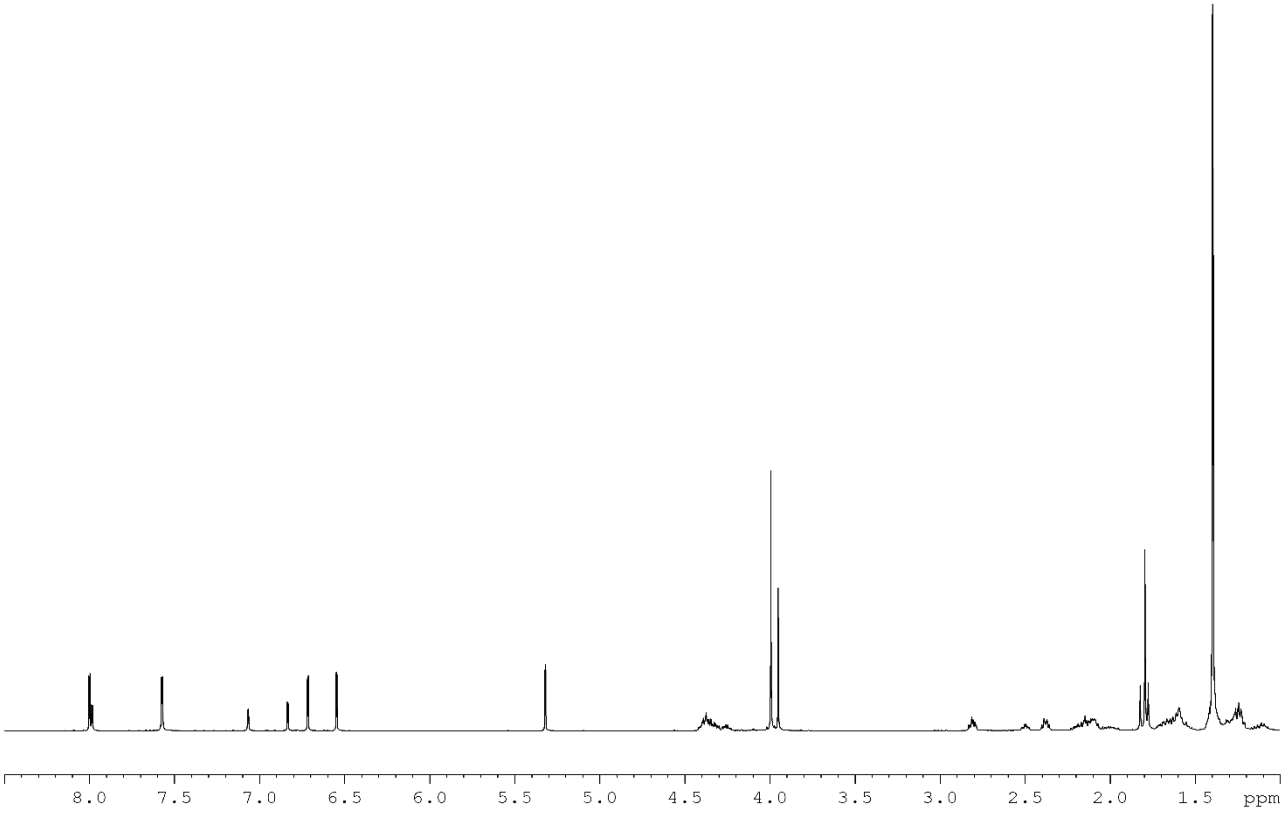

^{13}C NMR spectrum (100 MHz, CD_2Cl_2, 298K)

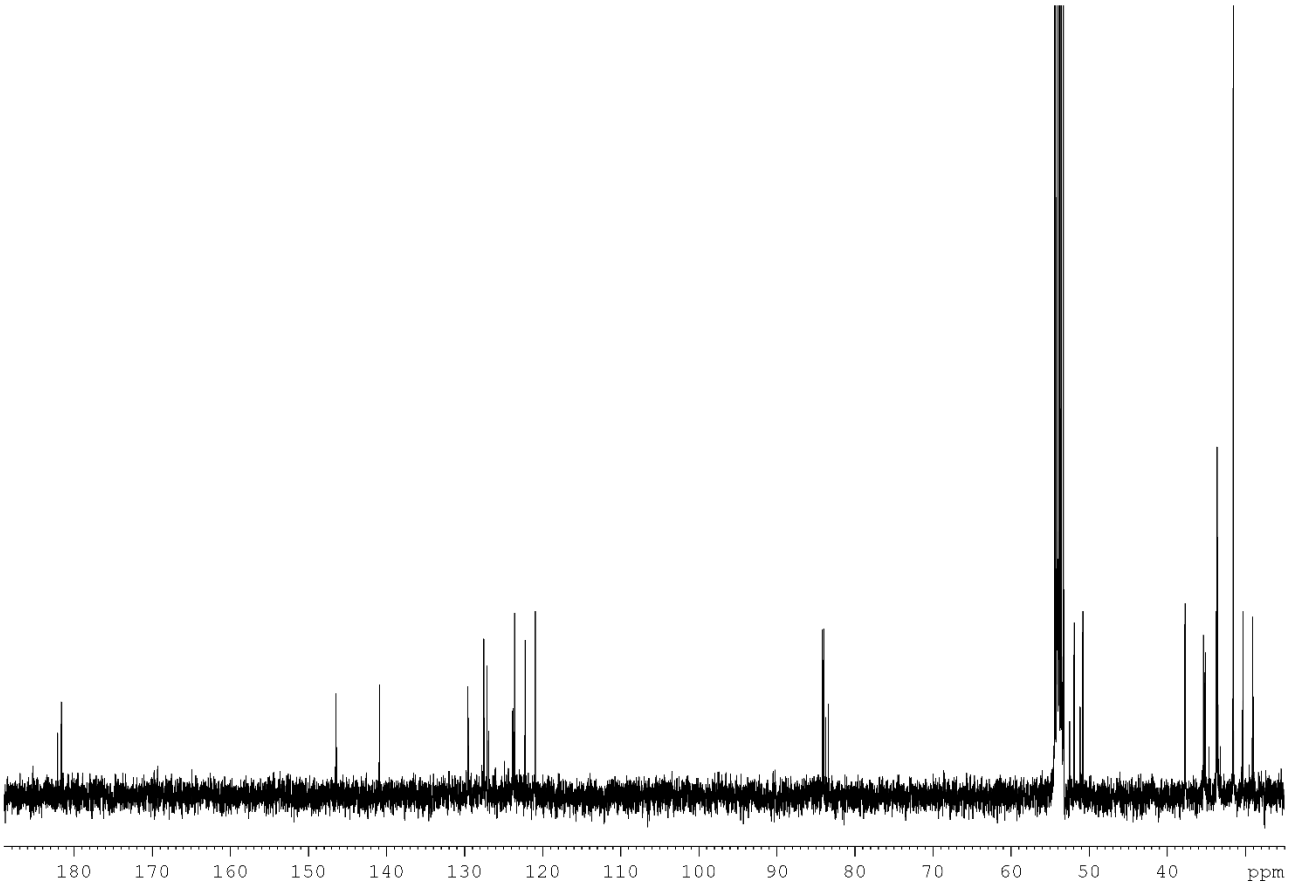

$[Ir_2((MeNHC)_2{}^tXan)(CO)_4Cl_2]$ (3.4)

^1H NMR spectrum (400 MHz, CD_2Cl_2, 298K)

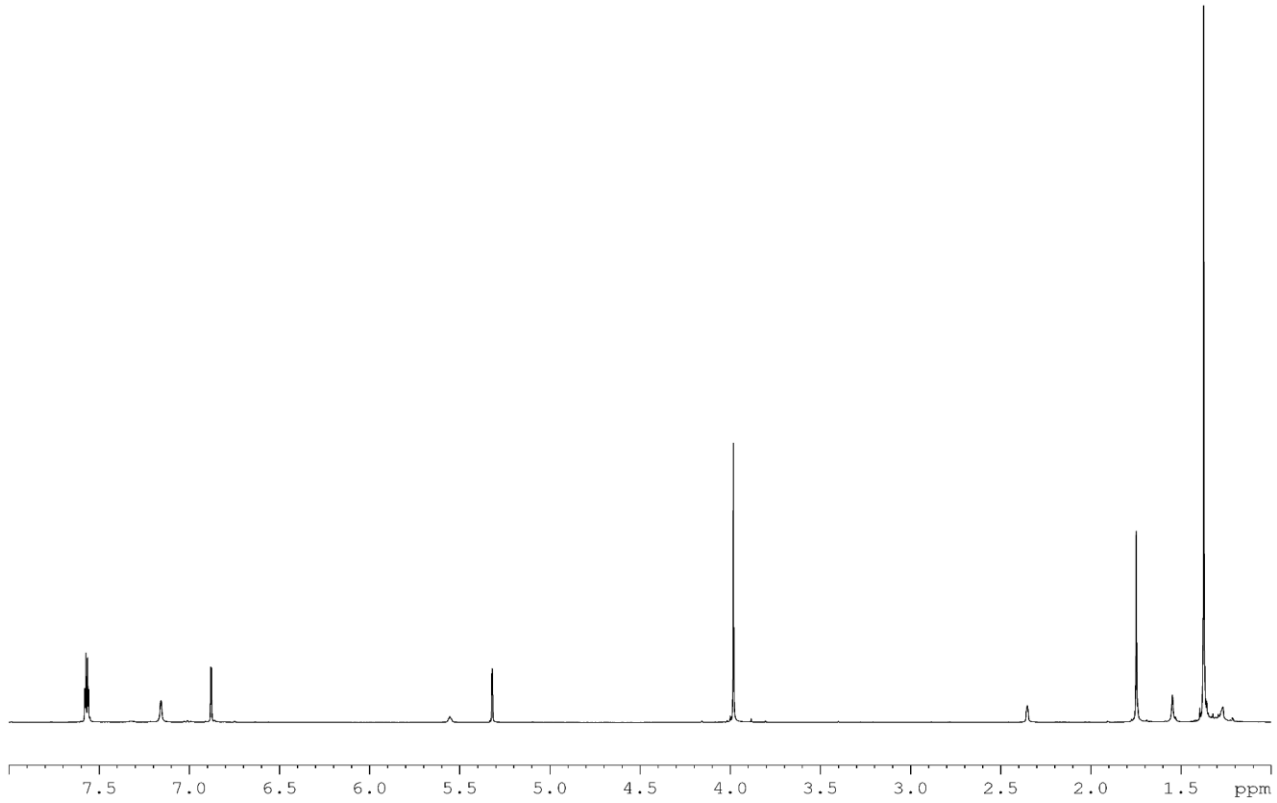

^{13}C NMR spectrum (100 MHz, CD_2Cl_2, 298K)

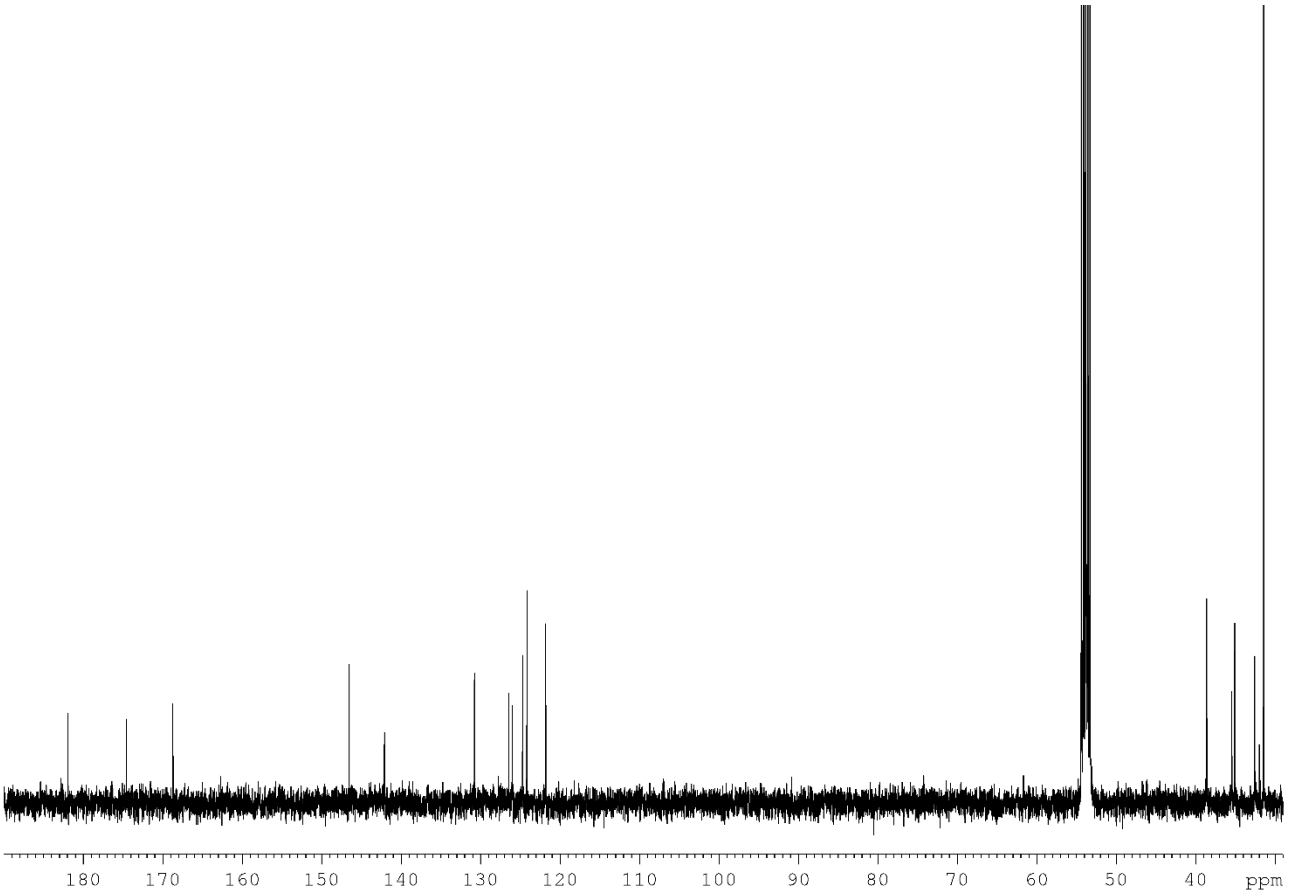

Appendix B: Catalysis Data

Hydroamination of 4-Pentyn-1-amine (4.1a)

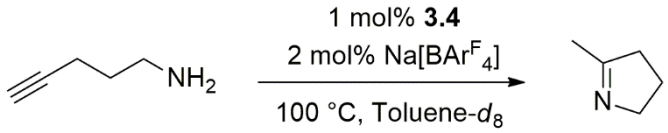

4.1a **4.1b**

Time / h	Conv. to **4.1b** / %	Time / h	Conv. to **4.1b** / %
0.00	0	0.45	88
0.02	16	0.47	89
0.03	24	0.48	89
0.03	32	0.49	89
0.04	37	0.51	90
0.05	41	0.52	90
0.06	45	0.55	92
0.07	48	0.57	93
0.07	51	0.59	92
0.08	53	0.62	92
0.09	55	0.64	93
0.10	57	0.66	93
0.10	59	0.68	93
0.11	61	0.71	93
0.12	62	0.73	93
0.13	64	0.75	93
0.13	65	0.79	95
0.14	66	0.83	95
0.15	67	0.87	95
0.16	69	0.91	95
0.16	70	0.95	96
0.17	70	0.99	95
0.18	71	1.03	95
0.19	73	1.07	96
0.20	74	1.11	95
0.21	74	1.15	96
0.22	75	1.24	95
0.23	76	1.33	96
0.23	77	1.42	96
0.24	78	1.51	96
0.25	78	1.60	96
0.26	79	1.69	95
0.27	80	1.78	95
0.28	82	1.87	96
0.30	81	1.96	96
0.31	82	-	-
0.32	83	-	-
0.33	84	-	-
0.34	84	-	-
0.36	85	-	-
0.37	85	-	-
0.38	86	-	-
0.39	86	-	-
0.41	87	-	-
0.42	88	-	-
0.44	88	-	-

Hydroamination of 5-Phenyl-4-pentyn-1-amine (4.2a)

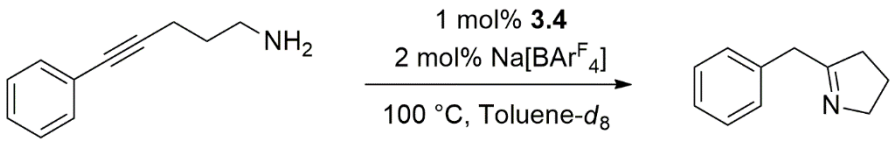

4.2a **4.2b**

Time / h	Conv. to **4.2b** / %	Time / h	Conv. to **4.2b** / %
0.00	0	0.75	47
0.01	0	0.79	48
0.02	2	0.83	48
0.03	3	0.87	50
0.04	4	0.91	50
0.05	5	0.95	51
0.05	6	1.04	53
0.06	7	1.13	54
0.07	8	1.22	55
0.08	9	1.31	56
0.08	10	1.40	57
0.09	11	1.49	58
0.10	12	1.58	58
0.11	13	1.67	59
0.12	14	1.76	60
0.13	15	2.44	65
0.14	16	2.53	64
0.14	17	2.62	65
0.15	17	2.71	66
0.16	18	2.80	66
0.17	19	2.89	66
0.18	20	2.98	67
0.19	21	3.07	68
0.21	22	3.16	67
0.22	24	3.25	68
0.24	25	3.34	69
0.25	26	3.54	69
0.27	27	3.63	70
0.28	28	3.72	69
0.30	29	3.80	69
0.31	30	3.89	70
0.33	31	3.98	71
0.35	32	4.07	71
0.37	33	4.16	70
0.39	35	4.25	71
0.42	36	4.34	71
0.44	37	70.09	93
0.46	38	-	-
0.49	39	-	-
0.51	40	-	-
0.53	41	-	-
0.55	42	-	-
0.59	43	-	-
0.63	44	-	-
0.67	45	-	-
0.71	46	-	-

Hydroamination of Phenylacetylene (4.3a) and Aniline (4.3b)

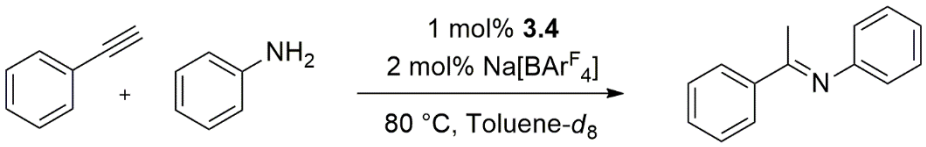

4.3a **4.3b** **4.3c**

Time / h	Conv. to **4.3c** / %	Time / h	Conv. to **4.3c** / %
0.00	0	0.66	70
0.04	16	0.70	73
0.05	16	0.73	74
0.05	16	0.77	75
0.06	18	0.81	76
0.06	20	0.93	80
0.07	21	1.02	81
0.07	22	1.19	85
0.08	23	1.28	86
0.08	24	1.37	87
0.09	25	1.45	88
0.09	26	1.54	90
0.10	26	1.06	82
0.10	27	1.14	85
0.11	28	1.23	86
0.12	29	1.32	88
0.12	30	1.40	88
0.13	31	1.49	89
0.14	31	1.58	92
0.14	33	1.75	93
0.15	33	1.84	96
0.15	35	1.87	95
0.17	33	2.04	98
0.18	36	2.21	99
0.19	36	2.55	100
0.20	38	2.72	100
0.21	40	-	-
0.23	41	-	-
0.24	42	-	-
0.25	45	-	-
0.26	45	-	-
0.27	46	-	-
0.29	47	-	-
0.31	49	-	-
0.33	50	-	-
0.35	52	-	-
0.37	54	-	-
0.39	55	-	-
0.41	56	-	-
0.43	58	-	-
0.45	60	-	-
0.47	61	-	-
0.51	64	-	-
0.55	64	-	-
0.59	67	-	-
0.62	69	-	-

Dihydroalkoxylation of 6-(2-(Hydroxymethyl)phenyl)hex-5-yn-1-ol (4.4a)

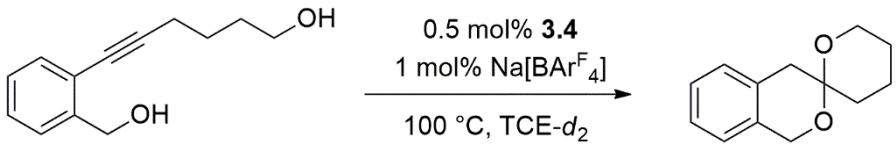

4.4a **4.4b**

Time / h	Conv. to **4.4b** / %	Time / h	Conv. to **4.4b** / %
0.00	0	0.72	37
0.02	0	0.76	39
0.03	0	0.80	42
0.03	0	0.84	44
0.04	0	0.88	46
0.05	0	0.91	48
0.05	0	1.00	53
0.06	0	1.09	57
0.07	0	1.18	61
0.07	0	1.27	65
0.08	0	1.36	69
0.09	0	1.45	72
0.09	0	1.54	74
0.10	0	1.62	77
0.11	0	1.71	79
0.12	0	1.86	82
0.13	0	1.95	84
0.14	0	2.04	86
0.14	0	2.13	87
0.15	1	2.22	88
0.16	1	2.30	89
0.17	1	2.39	90
0.18	2	2.48	90
0.20	3	2.57	91
0.21	4	2.66	92
0.22	5	2.75	92
0.24	6	2.84	93
0.25	7	2.93	93
0.26	8	3.01	93
0.28	9	3.10	93
0.29	10	3.19	94
0.30	11	3.28	94
0.33	12	3.37	94
0.35	13	3.46	94
0.37	15	3.55	94
0.39	16	3.82	94
0.42	18	3.91	94
0.44	19	3.99	94
0.46	20	4.08	94
0.48	22	4.17	94
0.50	23	4.26	94
0.53	25	4.35	94
0.56	27	4.44	94
0.60	30	4.53	94
0.64	32	4.62	94
0.68	35	-	-

Dihydroalkoxylation of 1,8-Dihydroxy-4-octyne (4.5a)

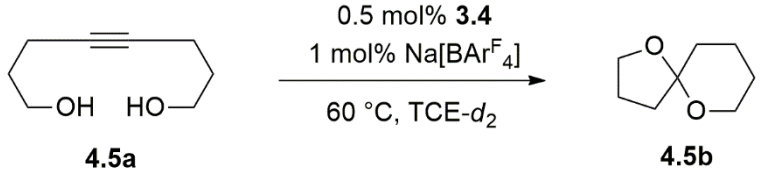

4.5a **4.5b**

Time / h	Conv. to **4.5b** / %	Time / h	Conv. to **4.5b** / %
0.00	0	0.77	98
0.02	8	0.81	98
0.03	9	0.85	98
0.03	9	0.89	98
0.04	9	0.93	98
0.05	12	0.97	98
0.06	10	1.06	98
0.07	11	1.15	98
0.07	12	1.24	98
0.08	13	1.33	99
0.09	17	1.42	98
0.10	16	1.51	98
0.11	16	1.60	98
0.12	20	1.69	98
0.12	21	1.77	98
0.13	21	2.35	99
0.14	23	-	-
0.15	24	-	-
0.16	25	-	-
0.17	25	-	-
0.18	28	-	-
0.19	29	-	-
0.20	31	-	-
0.22	34	-	-
0.23	36	-	-
0.25	40	-	-
0.26	43	-	-
0.28	44	-	-
0.29	47	-	-
0.31	51	-	-
0.32	52	-	-
0.34	57	-	-
0.36	62	-	-
0.38	68	-	-
0.41	74	-	-
0.43	79	-	-
0.45	83	-	-
0.48	87	-	-
0.50	91	-	-
0.52	93	-	-
0.54	95	-	-
0.57	96	-	-
0.61	97	-	-
0.65	97	-	-
0.69	98	-	-
0.73	99	-	-

Dihydroalkoxylation of 5-(2-(Hydroxymethyl)phenyl)pent-4-yn-1-ol (4.6a)

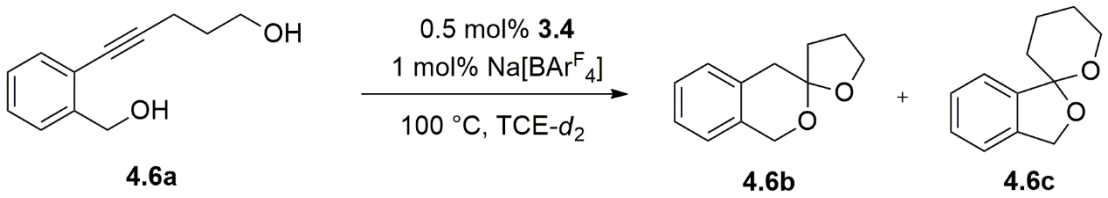

4.6a **4.6b** **4.6c**

Time / h	Conv. to **4.6b** / %	Conv. to **4.6c** / %	Total Conv. / %
0.00	0	0	0
0.01	1	3	3
0.02	3	5	8
0.03	2	7	9
0.04	6	5	12
0.05	5	8	14
0.05	9	3	12
0.06	10	7	16
0.07	13	4	17
0.08	15	8	23
0.08	16	6	23
0.09	18	9	27
0.10	20	10	30
0.11	23	11	34
0.11	26	11	37
0.12	30	11	41
0.13	31	14	45
0.14	34	15	49
0.14	37	16	53
0.15	40	18	58
0.16	42	20	62
0.17	44	22	65
0.18	47	22	70
0.19	50	24	74
0.19	52	25	77
0.20	53	27	80
0.21	56	28	83
0.22	56	29	84
0.23	58	29	87
0.24	59	29	88
0.25	60	30	90
0.26	62	30	91
0.27	62	30	92
0.28	63	30	93
0.29	62	30	93
0.30	62	31	93
0.32	63	30	93
0.33	63	30	93
0.34	61	31	92
0.35	63	31	93
0.36	62	31	94
0.37	62	31	93
0.39	63	31	95
0.40	63	31	94
0.42	63	31	94
0.43	64	31	94
0.45	63	31	94

0.46	63	31	93
0.48	62	32	94
0.49	63	30	93
0.51	62	31	93
0.52	62	31	93
0.54	62	31	94
0.57	62	30	93
0.59	61	32	93
0.61	62	31	94
0.63	63	31	94
0.66	62	31	93
0.68	61	32	93
0.70	62	32	93
0.73	62	31	93
0.75	61	32	93
0.79	62	32	93
0.83	62	31	93
0.87	62	32	94
0.91	62	32	94
0.95	61	32	93
0.99	62	32	94
1.03	60	32	92
1.07	61	32	93

Appendix C: List of Numbered Compounds

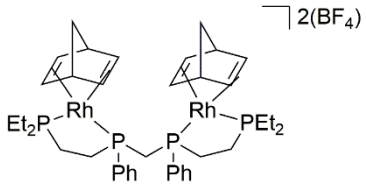

1.1

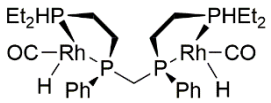

1.2

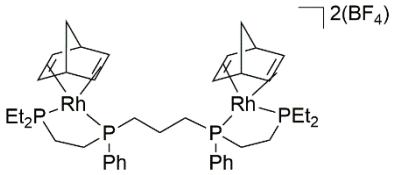

1.3

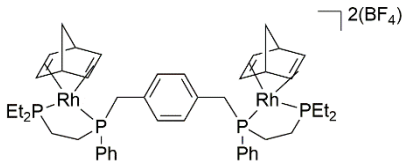

1.4

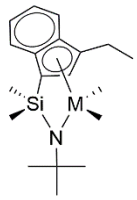

1.5a, M = Zr
1.5b, M = Ti

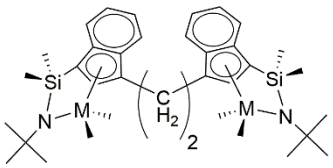

1.6a, M = Zr
1.6b, M = Ti

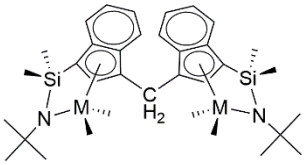

1.7a, M = Zr
1.7b, M = Ti

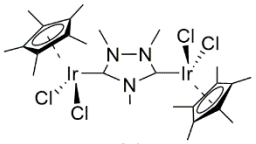

1.8

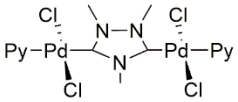

1.9

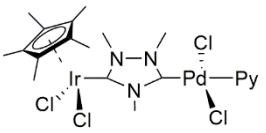

1.10

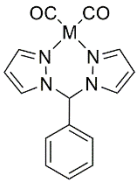

M = Rh, Ir

1.11

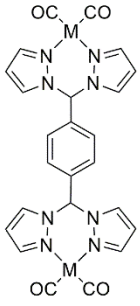

M = Rh, Ir

1.12

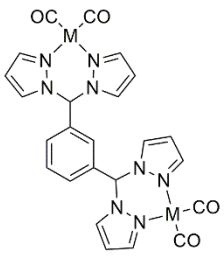

M = Rh, Ir

1.13

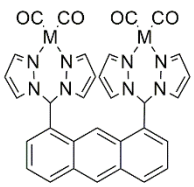

M = Rh, Ir

1.14

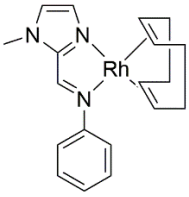

1.15

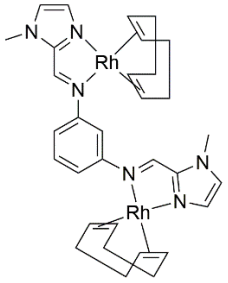

1.16

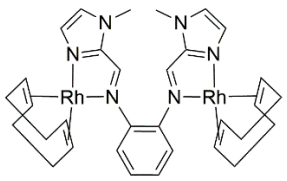

1.17

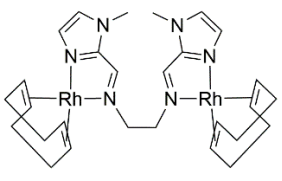

1.18

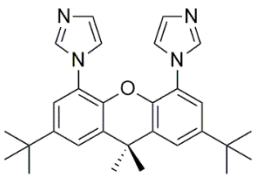

2.1

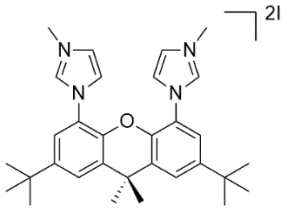

2.2

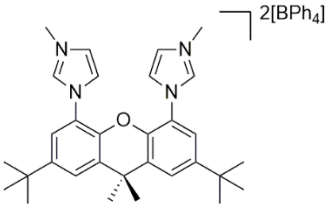

2.3

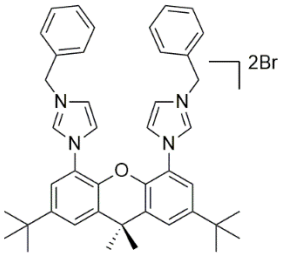

2.4

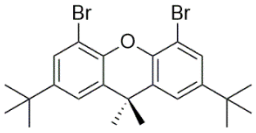

2.5

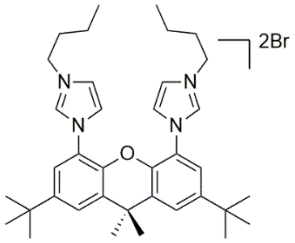

2.6

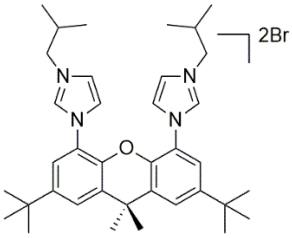

2.7

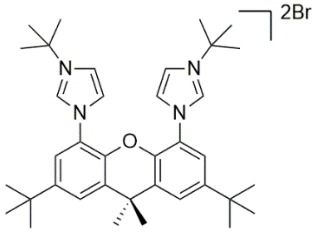

2.8

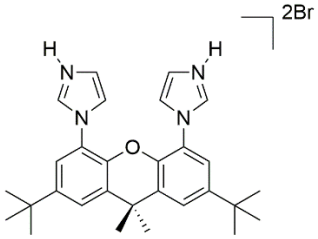

2.9

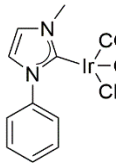

3.1

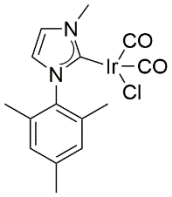

3.2

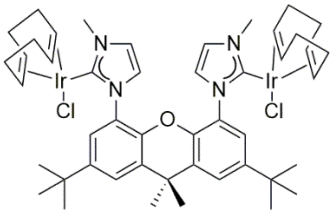

3.3

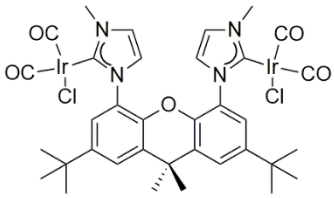

3.4

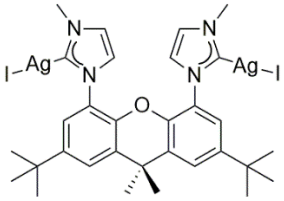

3.5

4.1a

4.1b

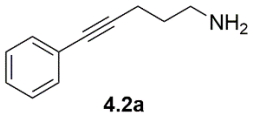

4.2a

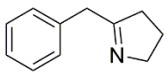

4.2b

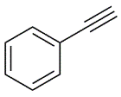

4.3a

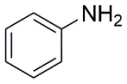

4.3b

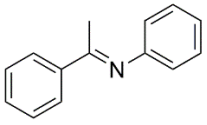

4.3c

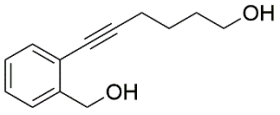

4.4a

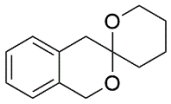

4.4b

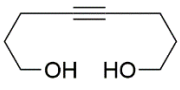

4.5a

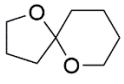

4.5b

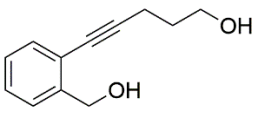

4.6a

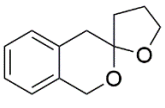

4.6b

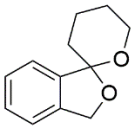

4.6c

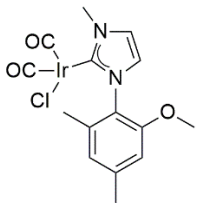

5.1

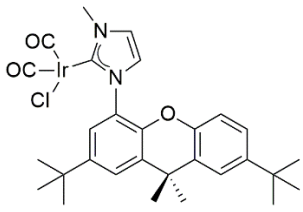

5.2